CRWR Online Report 08-06

Porous Friction Course: A Laboratory Evaluation of Hydraulic Properties

by

Remi M. Candaele, M.S.E.

Michael E. Barrett, Ph.D.

Randall J. Charbeneau, Ph.D.

May 2008

Center for Research in Water Resources

The University of Texas at Austin

J.J. Pickle Research Campus

Austin, TX 78712-4497

This document is available online via the World Wide Web at

http://www.crwr.utexas.edu/online.shtml

ACKNOWLEDGMENTS

This research was funded by the Texas Department of Transportation under project number 0-5220, "Investigation of Stormwater Quality Improvements Utilizing Permeable Pavement and/or the Porous Friction Course (PFC)".

TABLE OF CONTENTS

Contents

LIST OF TABLES

LIST OF FIGURES

1. OVERVIEW OF THE POROUS FRICTION COURSE PROJECT

1.1. OBJECTIVES

Porous Friction Course or open-graded friction course (OGFC) is commonly known as porous asphalt. The porous pavement is commonly used in Europe and the United States. The pavement consists in a porous overlay allowing rainwater to flow down to the bottom the overlay and then to drain on the edges of the pavement. The safety benefits from Permeable Friction Course (PFC) are well known, but the porous structure of the asphalt also may result into a significant reduction of pollutants associated with stormwater. Two preliminary aspects compose this project. On one hand, a study has been conducted by Christina Stanard on the in-situ monitoring of stormwater in terms of water quality and runoff quantifications. For this purpose, two sites located on Loop 360 near Bull Creek in Austin are being monitored. Another aspect of the project is the characterization of the hydraulic properties of the porous asphalt. Determining the porosity and the hydraulic conductivity of the pavement is motivated by two facts:

- The clogging phenomenon is persistent within PFC. Once the pores of the PFC become plugged, then runoff will begin flowing on the surface of the pavement and all the benefits, both in terms of safety and water quality, will be lost.
- The actual methods utilized to determine the hydraulic parameters are strongly dependent on the vertical hydraulic conductivity and the assumed isotropy of the flow. The hydraulic conductivity of samples of PFC is usually tested by constant or falling head permeameter (Appendix A: Permeameters & Measuring EAV Contents). EAV defines the effective air void content a porous media.

Facing these two facts, the laboratory experimentations are focused on determining porosity and hydraulic conductivity of a series of cylindrical PFC samples extracted at

three different locations around Austin on March 14, 2007. The results of the experiments will help us to determine:

- The rate at which pavement gets clogged. Another series of samples were extracted at the same locations on February 27th, 2008 and will be tested using the same procedure. A quantification of the clogging phenomenon will be established.
- The characteristics of the vertical and radial flow within the samples.

The purpose of determining the vertical and radial components of the flow within the samples is to develop in a later study a hydraulic model predicting the movement of water within the porous asphalt. At turn, this information will be useful in the evaluation of the effects of cross slope, highway width, curves, and superelevations on the flow within the pavement. This information will be valuable for supporting the development of guidelines for the appropriate use of PFC.

1.2. LOCATIONS OF STUDY

The Texas Department of Transportation utilizes the benefits of porous asphalt in terms of safety and water quality at sites around the Austin area. Six different sections of PFC overlay have been installed on I-35 Southbound, 183 North, Loop 360 near Bull Creek, RM 1431 and RM 620. The length of the sections varies approximately from a half-mile to a couple of miles. Most sections were installed during the years 2004 and 2005 on the highways. Figure 1 gives an overview of the location of the different porous asphalt sections in the Austin area. The PFC sections are represented by the blue color while the conventional pavement ones are represented in red and rose colors.

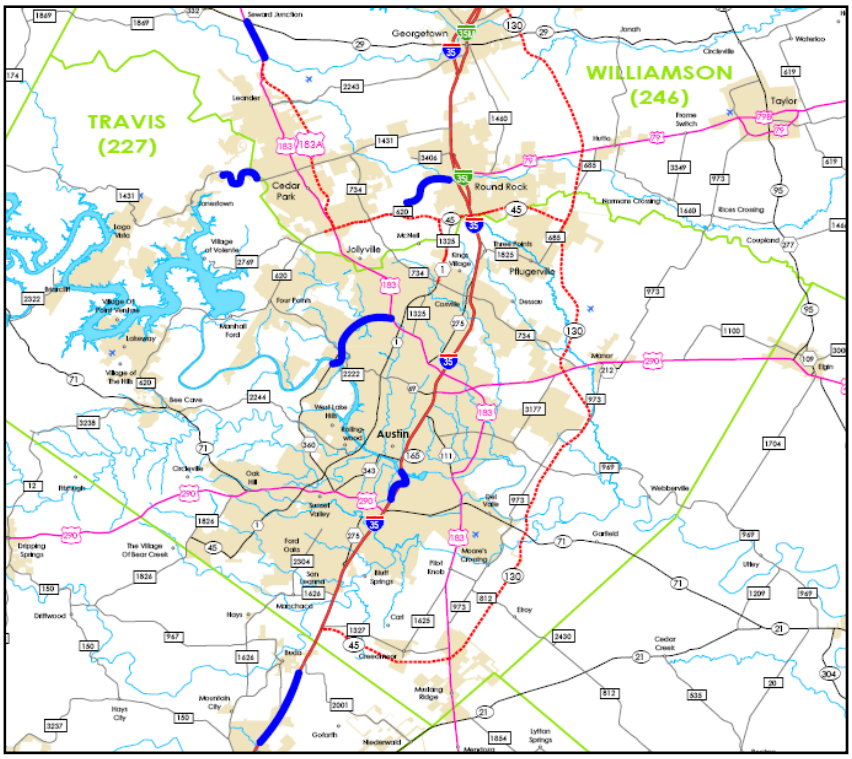

Figure 1 - Overview of the PFC locations in the Austin area.

From all these sections, three locations were chosen to be studied according to safety, traffic factors and the compatibility with in-situ measurements. On March 14th, 2007 a TxDOT crew drilled cylindrical samples at these three sites:

- Loop 360 near Bull Creek,
- RM 1431,
- RM 620.

At each site, four core samples were extracted. All samples were taken from between the tire tracks on the roadway. Figure 2 shows each coring location.

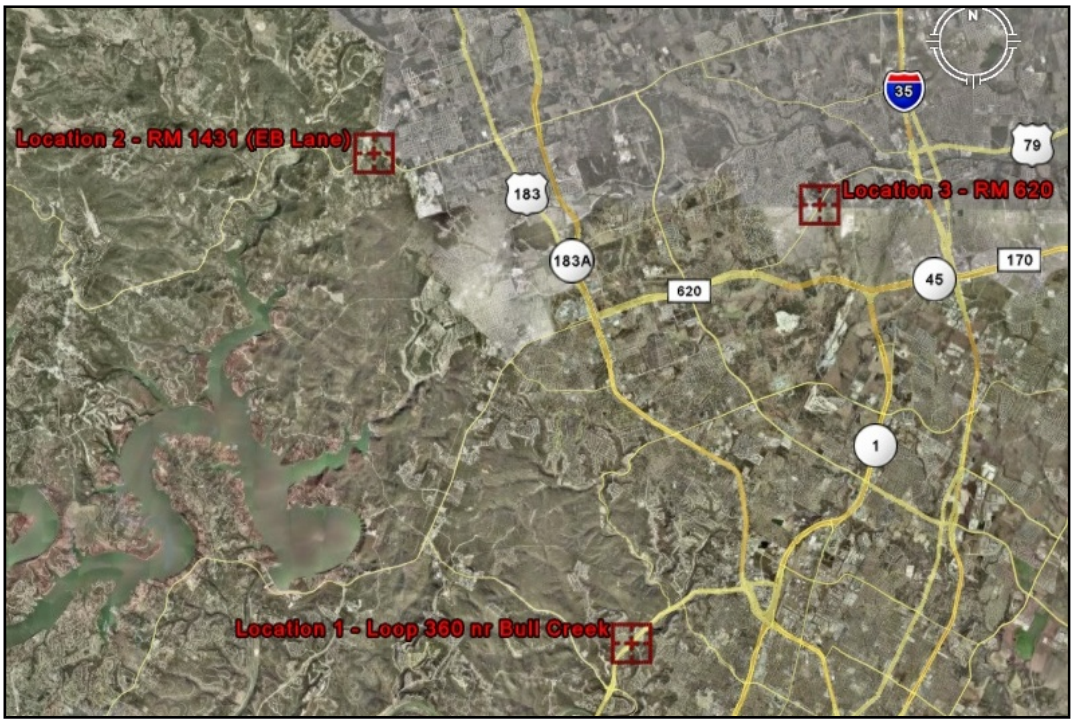

Figure 2 -Location of the three extraction sites – Photo Courtesy of Google Earth

Some more information is given below for each site in order to visualize the situation and the type of the road. Some traffic data is given and corresponds to a study headed by TxDOT. The Annual Average Daily Traffic Counts (AADT) are comprised of a mathematical computation where the counts are made over a given period-of-time and the high and low counts are removed. "The counts are done during the non-summer weeks; excluding Fridays, Saturdays, Sundays, and Holidays. The AADT counts are what could be expected during a normal workday of a given week." (Texas Department of Transportation, 2005)

Site 1 – Northbound Loop 360 near Bull Creek

The first site is positioned at the following geographic coordinates:

$$\begin{cases} 30° 22' 22" N \\ 97° 47' 03" W \end{cases}.$$

Figure 3 shows the exact location of the extracted samples on a map; cores were extracted northbound just of the bridge over Bull Creek.

Figure 3 - Northbound Loop 360 near Bull Creek Extraction Site – Photo Courtesy of Google Earth

The pavement was installed in October 2004. The statistics show an average daily traffic of 45,000 vehicles per day for the last seven years between Spicewood Springs Rd. and RM 2222. In 2005, the daily traffic reached 48,000 vehicles per day.

Loop 360 at this location consists of a two lane highway in each direction. The two roads are separated by a large V- shape median.

The proximity of the in-situ monitoring site of the location to the extraction site is an advantage because hydraulic properties determined from the extracted cores can be compared to the hydrographs obtained from the runoff analysis.

Site 2 – Eastbound RM 1431

The second site is positioned with the following geographic coordinates:

$$\begin{cases} 30°31'00"N \\ 97°52'20"W \end{cases}.$$

Figure 4 shows the exact location of the extracted samples on a map; cores were indeed extracted eastbound near the Industrial park Hur of Cedar Park.

Figure 4 - Eastbound RM1431 Extraction Site – Photo Courtesy of Google Earth

The PFC was installed in February 2004. The statistics show an average daily traffic that has been slightly increasing since 2001 from 14,000 to 18,200 in 2005 between Nameless

Road and Lime Creek Road on RM1431. Two lanes in each direction are separated by a double yellow line at this site on RM1431.

Site 3 – Northbound RM 620

The third extraction site is positioned with the following geographic coordinates:

$$\begin{cases} 30°\,30'\,06''\,N \\ 97°\,43'\,12''\,W \end{cases}.$$

Figure 5 shows the exact location of the extracted samples on a map; cores were extracted northbound on RM 620 at the intersection with Connor Road.

Figure 5 - Northbound RM 620 Extraction Site – Photo Courtesy of Google Earth

The PFC overlay was installed in June 2004. The statistics show that the average daily traffic has been fluctuating over the last 5 years of data (from 2001 to 2005). In 2001, the traffic reached a count of 50,000 vehicles per day but was 38,000 vehicles per day in

2005. The section of RM620 corresponding to our site is the one between FM 734 (Parmer Lane) and Lake Creek Pkwy.Two lanes in each direction are separated by a double yellow line at this site on RM620.

1.3. EXTRACTION OF CORES

Four cores were drilled and extracted for each location. The extraction was organized by Gary Lantrip of TxDOT. The operation was realized under extreme precaution since cores were drilled from between the tire track on the right lane of double lanes roads. Two signalization trucks closed the right lane about 400 yards before the extraction site and most locations were chosen after an intersection in order to avoid traffic accidents.

An asphalt engineering company was contracted by TxDOT for the day. Cylindrical samples composed of different layers of asphalt were extracted using a drill press attached to the truck's bed. A core pin of inner diameter 6-inches was connected to the drill press. Figure 6 was taken on RM 620, the large cylinder rotating is the core pin. On the left to the pin, a 6 inch diameter hole stands open on the road after a first core was drilled.

Figure 6 - Drill Press on RM 620 - March 14, 2007

The four extracted cylindrical cores at each location are principally composed of two layers. The lower one is a 10-15 cm thick impervious asphalt layer which acts as a rigid and impermeable base. The upper layer is a 5 cm thick porous asphalt layer. Figure 7shows two extracted cores on RM 620.

Figure 7 - Extracted Cores on RM 620 - March 14, 2007

The holes on the road were refilled with a quick pavement mixture, which consists in standard impervious repair asphalt (Figure 8).

Figure 8 - Quick pavement filling holes on RM 620 - March 14, 2007

In order to conduct experiments on the layer of porous asphalt itself, the last operation required separating the PFC overlay from the impervious layer. This separation was done at the TxDOT Asphalt Laboratory in Cedar Park by Byron Kneipfel. Figure 9 shows the operation of separation of the two layers using a circular saw.

Figure 9 - Separation of the overlay – April 09, 2007

All cores were stored in a cold room in order to preserve the properties of the binders. For each site, the four cores were classified by alphabetical order:

- A and B would be tested as are for their porosity by the water displacement method and for their hydraulic conductivity,
- C would be sliced in two halves and its porosity would be determined by the method of image analysis,
- D would be preserved in the cold room for possible later experiments.

1.4. OUTLINE OF THESIS

In order to answer the defined objectives, the present thesis will develop and analyze the results of porosity and hydraulic conductivity measurements conducted on the extracted cores. In the first part, the present methods for determining the hydraulic properties of porous asphalt but also the preponderant need of maintenance will be developed as a summary of the scientific literature. The thesis will then focus on the porosity experiments either by the water displacement or image analysis methods. An interpretation of the results on porosity will be given at this point. In a third part, the thesis will precisely look at the analytical and experimental characteristics of the methodology for determining the hydraulic conductivity of the sample. The results on hydraulic conductivities will be analyzed and verified: an interpretation of the results on the general patterns but also for every site will conclude the analysis. A discussion on potential uncertainties and recommendations will conclude this thesis.

2. POROUS ASPHALT AND HYDRAULIC PROPERTIES IN LITERATURE

The widely-accepted advantages of PFC are the road safety improvements in wet conditions as well as the noise reduction from the roadway. The safety benefits during rain events include reduced hydroplaning, greater skid resistance at high speeds, less spray and light reflection from the roadway due to the improved drainage, and therefore, better visibility. In addition to these benefits, PFC has been found to reduce pollutant concentrations in stormwater runoff (Pagotto et al., 2000).

These advantages come with greater initial and maintenance costs and sometimes shorter service lives than conventional pavement. Cost-benefit analyses (van der Zwan, 1990) have shown that even with a greater yearly maintenance cost and shorter service life, the benefits outweigh the increased costs. Also, recent improvements in mix designs have increased the expected service life of these types of pavements. Other commonly noted disadvantages are reduced performance over time due to clogging of the pavement and the winter maintenance requirements. The literature review focuses on the hydraulic properties, water quality benefits and common maintenance practices for porous pavements. The majority of the cited articles are from online databases or journals. The search for articles focused on recent publications with relevant experiments and results or discussion. Part of this chapter utilizes the "State of Practice of Porous Friction Course (2007)", written in collaboration with Christina Stanard.

2.1. MEASURE OF POROSITY AND METHODS

As stated, the drainage capacity of PFC depends greatly on the porosity, or void content. Studies on different mix designs are used to improve the durability and strength of new mix designs, and also to decrease issues associated with clogging. Based on experiences with mixes with different void contents, a study in Spain (Ruiz et al., 1990) found that pavements with greater than 20% void content are more durable than ones with less than 20% void content.

Regimand et al. (2004) developed a method for evaluating air void contents for compacted materials. This method determines the effective air void (EAV) content of a porous sample which is a subset of the total void content. The EAV content includes the voids that are accessible by water and other environmental fluids and excludes the portion of voids that will not be reached by liquid during the compacted material's use. The EAV parameter is beneficial since it strongly correlates to mixture permeability. To determine the EAV, a compacted material sample is encased in a sealant material of known weight and air is evacuated from the encasement. The vacuum-sealed material is weighed both in air and then under water. After weighing the sealed sample in water, the seal is opened to allow water to contact the compacted sample. Since the volume of the bag is non-negligible, the dimensions of both the sample and the sample in the bag should also be recorded. With these recorded values, Equation 1 can be used to calculate the EAV parameter.

Equation 1

$$EAV = \left(\frac{\rho_2 - \rho_1}{\rho_2} \right) \cdot 100$$

where ρ_1 = the density of the vacuum sealed compacted material sample

ρ_2 = the density of the vacuum sealed sample after opening the seal under water

Illustrations of the techniques and methods of measuring the EAV content of porous asphalt can be seen in Appendix A: Permeameters & Measuring EAV Contents.

In 1999, researchers in Denmark used samples from test sections of porous asphalt surfacing to conduct porosity measurements with image analysis (Bendsten et al., 2002). The Danish Road Institute has been using the image analysis method since the early 1980s. This method of analyzing thin sections was developed to detect clogged pores sooner than would otherwise be possible. Other benefits of image analysis besides porosity and clogging of pores include the observation of the size of voids and their distribution. The surfaces of the plane sections are impregnated with a florescent epoxy that fills all of the void space in the section. Porous stones exposed in the thin sections are marked with black ink to avoid any confusion in the analysis. The void content number is determined by looking at the plane section under ultraviolet light. Bendsten et al. (2002) obtained air void contents of 0.182 to 0.224 depending on the size of the aggregates.

2.2. MEASURE OF HYDRAULIC CONDUCTIVITY

Permeability is a measure of a materials ability to transmit fluids. Measured values for permeability, hydraulic conductivity, and infiltration rate vary widely in the literature. While these terms are often used interchangeably, they do not represent the same quantity. In this thesis, hydraulic conductivity is used as the permeability coefficient which relates the volumetric flux and the hydraulic gradient. Its units are length per time.

Nearly every reported value is derived from a different test, thus preventing a direct comparison. However, the test methods do share some similarity in that many utilize a falling head apparatus to achieve a sense of the flow capacity of the pavement. The test documents the time required for a certain amount of water to drain into the pavement, which can be converted to a flow rate measurement. One problem with this test is that the water surfaces around the apparatus rather than flowing through the pavement. Thus, the data from such tests do not accurately represent a theoretical quantity.

Bear (1972) describes the methods commonly used in determining the hydraulic conductivity of a porous media. The experiments consist of characterizing the unsteady or steady flow in the vertical or horizontal direction through a cylindrical specimen with an instrument called a permeameter. The two types of permeameters can be distinguished.

The constant head permeameter applies a constant head loss ΔH over a porous media of height L, and cross-sectional area A. The measured discharge Q flows through the sample, and the hydraulic conductivity is computed according to Equation 2:

$$K = \frac{QL}{A\Delta H}$$

Equation 2

Several runs are necessary in order to reduce the uncertainty. In France, the standardized test consists in a constant head of 1.50 meters of water (Di Benedetto et al., 1996).

The falling head permeameter measures a percolation velocity (v_p) through a specimen of porous media of height L and cross section A. Initially, a standpipe of section *a* constrains the sample to a fixed volume of water V. The time T for the water level to drop in the standpipe from heights H_i to H_f is recorded and the hydraulic conductivity is computed with Equation 3 (Terzaghi et al., 1996):

$$K = \frac{aL}{AT} \ln\left(\frac{H_i}{H_f}\right)$$

Equation 3

Experimental data is needed to calibrate both permeameters. Standardized diagrams for these two types of permeameters can be seen in Appendix A.

Isenring et al. (1990) discuss the testing apparatus used to measure the drainage potential of porous asphalt in Switzerland. The Institute for Transportation, Traffic, Highway and Railway Engineering (IVT) of the Swiss Federal Institute of Technology developed the "IVT permeameter". A cylindrical tube with putty around the bottom is used to time how long it takes for 2.27 L of water to flow into the porous pavement, or "drainage potential". It is extremely similar to TxDOT's cylindrical field permeameter, specified in Tex-246 (TxDOT, 2004). The tested pavements had void contents ranging from 11 to 22% and layer thicknesses of 28 to 50 mm. The average measured discharge through this new porous asphalt was 3.4 L/min.

Isenring et al. point out that a single point measurement does not represent the true flow rate since the porous mixture is not homogeneous. Nonetheless, it does allow for

comparison of the porous asphalt over time. As expected, the project in Switzerland found that the drainage potential decreased with time at all of the testing locations. The greatest reduction in the results was found in the years directly following construction of the overlay. The measurements from multiple sites of two types of porous asphalt (maximum aggregate sizes of 10 mm and 16 mm) from this project are shown in Figure 10.

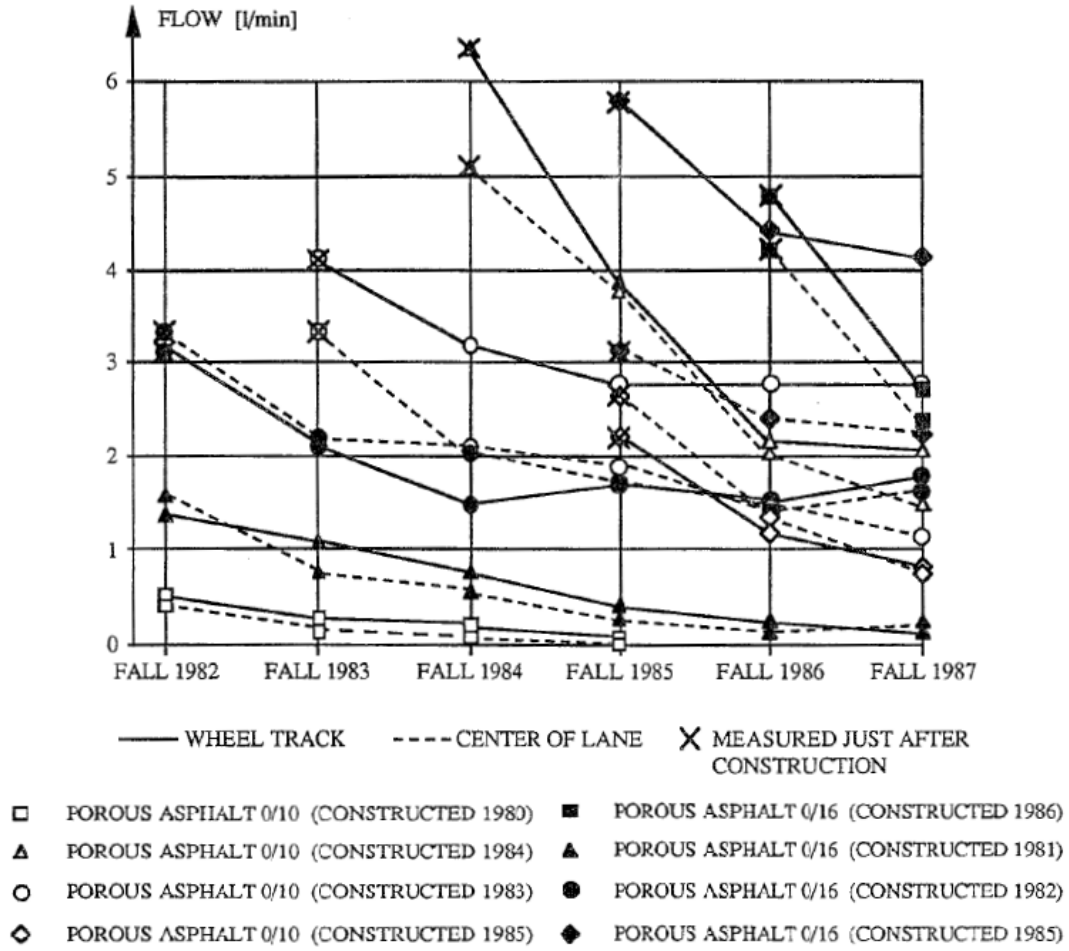

Figure 10 - Drainage potential over time (Isenring et al., 1990)

Ruiz et al. (1990) also perform similar testing on porous asphalt mixtures in Spain. Using an "LCS Drainometer", the time to drain 1.735 L of water is recorded. This test

includes a large plate around the bottom of the tube in an effort to prevent the water from surfacing. The drainage time (T) is related to the hydraulic head gradient (H) by Equation 4, which was developed with laboratory tests.

Equation 4

$$H = \frac{58.6}{T^{0.305}}$$

The drainometer test was conducted on porous mixes with void contents less than 20% and mixes with void contents greater than 20%. The mixes with the lower void content experienced a larger decrease in drainage capacity over time. Overlays with initial air voids of 16% and heavy traffic had clogged up after only two years according to the drain time. Other mixes totally clogged at different times up to nine years. Clogged overlays are defined as having a drainage time from the LCS drainometer greater than 600 seconds. The mixes with the void content above 20% had initial drainage times in the range of 15 to 25 seconds. These mixes had longer drainage times after many years of service and did not totally clog or deteriorate. After 9 years, drainage times were still under 300 seconds.

In Denmark, porous asphalt is characterized with a similar instrument called "Becker's Tube" as described by Bendtsen et al. (2002). Measurements taken immediately after construction and over time, before and after cleaning, were compared to cleaning guidelines for Dutch porous asphalt surfaces from Van Leest et al. (1997), which are shown in Table 1. Once the outflow time gets too high, the porous asphalt is considered clogged and cannot be flushed clean.

Table 1 - Cleaning guidelines from Van Leest et al. (1997)

Degree of Clogging of Porous Asphalt	Outflow time (seconds)	Permeability Class
New	30	High
Partly Clogged	50	Medium
Clogged	75	Low

A study on pervious pavement in Germany by Stotz and Krauth (1994) evaluated the drainage capacity of a highway section based on the percentage of rainfall that ran off the highway. The porous asphalt was 40 mm thick with a porosity of 19%. Comparison of values in the summer and winter revealed that the infiltration rate was approximately 50% larger in the winter than in the summer. Since Germany has cold and damp winters, it is assumed that the greater conductivity is due to fewer losses from high temperatures and dry pavements.

The Georgia DOT uses open-graded friction course as the overlay on all interstate projects. Watson et al. (1998) compare the three different types of OGFC mix designs that have been developed by GDOT: conventional, modified and European. The conventional mix has a maximum aggregate size of 9.5 mm, while the modified and European mixtures have a max aggregate size of 12.5 mm. The air voids percentage of the mixes ranges from 10-20 %. A falling head permeameter is used by GDOT to determine the hydraulic conductivity of the mixes. The conventional mix had the smallest hydraulic conductivity of all of the mixes with an average value of 39 m/day

(0.045 cm/s). The European mix, with coarser gradation and largest thickness of 32 mm, had the greatest drainage capacity of approximately 100 m/day (0.116 cm/s).

Birgisson et al. (2006) evaluated the use of OGFC in Florida. Field tests were performed to analyze the latest PFC design. A falling head permeameter was used to measure the hydraulic conductivity of test sections of porous pavement. Hydraulic conductivity tests in and between the wheel paths gave values of 0.81 cm/s and 0.74 cm/s respectively. The hydraulic conductivity was greater in the wheel path even only 2 months after construction. Part of the test section was repaved with lower design asphalt content and similar field tests were again performed two months later. The permeability of the PFC increased overall, and the permeability between the wheel paths was greater with a value of 1.27 cm/s.

Kandhal and Mallick (1999) compared four OGFC mixes with different gradations using Florida DOT's laboratory falling head permeameter. The results show that the mixes with the smallest percentage of fine aggregates (4.75 mm) have the largest hydraulic conductivity. The reported values are shown in Table 2. For comparison, the values found in the literature are presented in Table 3.

Table 2 - Summary of conductivity data from Kandhal and Mallick (1999)

Gradation (percent passing 4.75 mm sieve)	Hydraulic Conductivity (m/day)	Hydraulic Conductivity (cm/s)
15	117	0.135
25	88	0.102
30	28	0.032
40	21	0.024

Table 3 - Literature Values for PFC Characterization

Location	Age of Pavement	Flowrate	Hydraulic Conductivity (cm/s)	Void Content	Layer Thickness	Max Agg. Size	Source
Switzerland	Initial	3.4 L/s	-	11-22%	28-50 mm	10 mm	Isenring et al. 1990
Spain	Initial	-	-	>20%	40 mm	10 mm	Ruiz et al. 1990
Belgium	Design Spec	< 1.4 L/s	-	19-25%	40 mm	-	Van Heystraeten et al. 1990
Germany	3 years	-	0.047 – 0.11	19%	40 mm		Stotz and Krauth 1994
Netherlands	Design Spec	-	-	> 20%	50 mm	11 mm	Van der Zwan et al. 1990
Georgia	Design Spec	-	0.116	10-20%	30 mm	12.5 mm	Watson et al. 1998
Florida	2 months		1.2		1.4”		Birgisson et al. 2006
Oregon	Design Spec	-	-		50 mm	19 mm	Moore et al. 2001
Florida	Design Spec	-	0.78	18-22%	32 mm	10 mm	Bjorn et al. 2006

2.3. LIMITATION OF DARCY’S LAW

In a porous media, the hydraulic conductivity K represents the specific discharge per unit hydraulic gradient, which means that the coefficient depends on both matrix and fluid

properties (Bear, 1972). From a dimensional analysis, the hydraulic conductivity can be derived as (Nutting, 1930):

Equation 5

$$K = \frac{k \cdot g}{\nu}$$

Where k is the intrinsic permeability, v the kinematic viscosity and g the gravity acceleration. The intrinsic permeability is only a function of the matrix composing the porous media and its characteristics such as grain size distribution, tortuosity and porosity. For porous media, the Reynolds number (Re) can be defined as (Charbeneau, 2000):

Equation 6

$$\mathrm{Re} = \frac{q \cdot d}{\nu}$$

Where q is Darcy's velocity and d is the average grain diameter or d10 of the size distribution profile of the porous media. Experiments have shown that Darcy's law remains valid as long as the Reynolds number doesn't exceed a value between 1 to 10 (Venkataraman, 1999). As the Reynolds number doesn't exceed this value, the flow remains laminar and is governed by viscous forces. However the inertial forces start to govern the flow through the porous media in transitional flow when Re becomes higher than the transition value. As the Reynolds number continues to increase, the flow becomes turbulent at some point (Bear, 1972).

A quadratic model was suggested by Forchheimer (1901) in order to describe the inertial effects in the relationship between the hydraulic gradient and the flowrate:

Equation 7

$$\tilde{\mathrm{I}} = -\Delta H = \alpha \cdot Q + \beta \cdot Q^2$$

Where α and β are experimental coefficients depending respectively on the properties of the fluid and the matrix. Using a dimensional analysis, Ward (1964) derived analytical expressions for both coefficients:

Equation 8

$$\alpha = \frac{\nu}{k \cdot g} = \frac{1}{K}$$

And

Equation 9

$$\beta = \frac{C}{\sqrt{k} \cdot g}$$

Where C is a characteristic constant of the porous media. The first term is attributed to the viscous forces, or Darcy's linear relationship. The second term quantifies the inertial effects within the porous media. The characteristic length was reported by Ward as the square root of the intrinsic permeability.

Another approach was based on drag forces (Rumer, 1966). The drag coefficient is a function of both the Reynolds number and the shape of the grains. When the flow becomes non-laminar, the drag resistance is not proportional to Darcy's velocity anymore.

2.4. MAINTENANCE OF POROUS ASPHALT

The service life of porous asphalt depends not only on the deterioration of the overlay, but also the drainage capacity (Fwa et al., 1999). Only a few studies have been

conducted on the long-term behavior of porous pavements which are necessary to help determine the functional life of PFC. Since the pores in the overlay collect particles and are susceptible to clogging, some transportation authorities perform regular maintenance on the porous overlays (FHWA, 2005). This section discusses the causes of deterioration and commonly used maintenance procedures.

Causes of Deterioration

Graff (2006) discusses different aspects of asphalt pavement preservation, in particular the most common causes of deterioration. Asphalt is made from by-products of refining crude oil. Over the past few decades, overall asphalt quality has declined due to better refining of crude oil. To offset the decreasing quality of asphalt, it is now common to add materials to asphalt mixes in order to improve the properties of the asphalt.

According to Graff (2006), two main physical factors lead to the aging of asphalt: ultraviolet (UV) light and heat. The surface or the chip seal of overlay ages first because of their exposure to UV light and heat. Porous asphalt allows more light penetration, which results in faster aging than regular asphalt. The high temperature that porous asphalt is manufactured and placed under also contributes to a shorter service life.

All pavements are also subject to stresses that cause failure in the form of cracking or raveling. Thermal expansion causes internal stresses in porous asphalt since the coefficients of expansion are different for the aggregates and the asphalt. Traffic loading and expansive soils also cause internal stresses. As the asphalt ages, it cannot handle these stresses as well as new asphalt. Water in the pores of the pavement, combined with

traffic loading and temperature changes, also creates extreme internal pressures on the pavement. (Graff, 2006)

Clogging

Since porous asphalt allows surface runoff to flow within it, particles in the runoff are often collected by the pores of the pavement. The particles are generally sand particles or debris released from tires (Fwa et al., 1999). The drainage capacity of the pavement can be drastically affected by the clogging of the pores (Van Heystraeten and Moraux, 1990). Therefore, clogging of the pores will decrease the benefits of wet weather traction and noise reduction. Regular maintenance is often required to ensure adequate drainage capabilities over time.

In many locations, porous asphalt is only used on high-speed roadways to help avoid clogging problems. The tires push water into the voids and suck it back out as they drive over the surface. At high speeds, this helps to clean the pores at the surface. For this reason, it is not recommended to use porous asphalt on low-volume or slow-traffic roadways (Van Heystraeten and Moraux, 1990). Also, less traffic results in more debris on the roadway since there is not enough wind created by the cars to keep the roadway clean (NCHRP, 2000).

Fwa et al. (1999) performed laboratory testing on porous asphalt samples to evaluate the clogging potential. The testing involved manually clogging the porous samples with soil and measuring the permeability of the sample throughout the clogging process. The permeability coefficient (k) in this experiment was calculated with an equation based on

Darcy's law. The results consistently showed that the permeability coefficient decreased quickly in the beginning of the test and then asymptotically approached a terminal value, as shown in Figure 11.

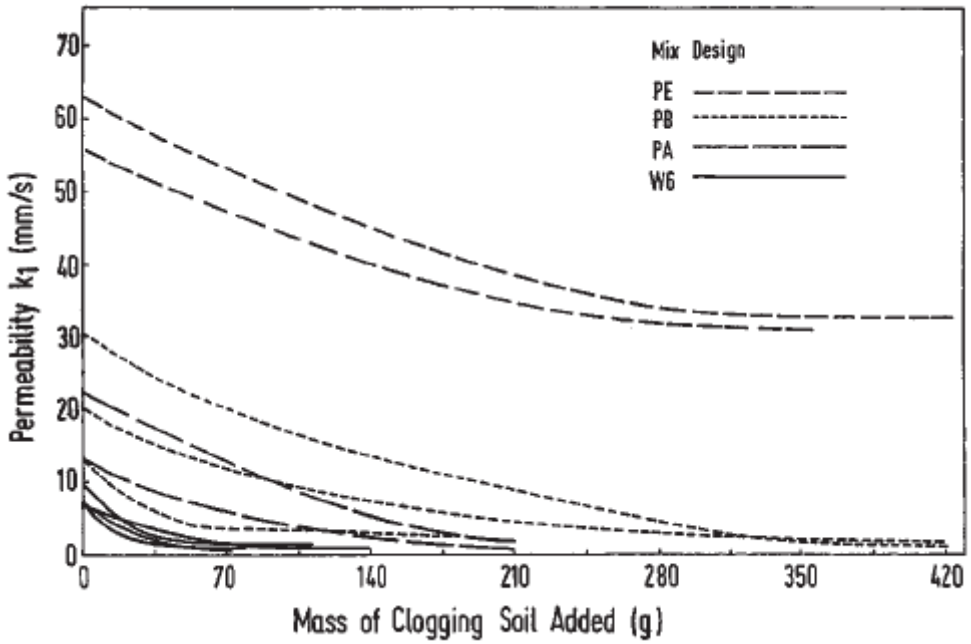

Figure 11 - Deterioration of Permeability Coefficient k (Fwa et al., 1999)

The curves for the deterioration of k are comparable with an average of 33 mm/s overall reduction of k from the different initial values. This information could be used in design to establish a required initial permeability depending on the expected terminal value.

According to NCHRP (2000), larger aggregate sizes are being specified since they create larger air voids. Larger voids are less likely to clog because they are cleaned by the pressure from traffic during rain events.

Cleaning Machines

Different techniques are used to clean porous pavement around the world. One major and recurrent technique is the use of cleaning machines. The most common type of these cleaning machines spray water at high-pressures into the overlay and then vacuum out the resulting sludge. This process is referred to as "captive hydrology". According to Newcomb and Scofield (2004), pressure cleaning is recommended on fine-graded open-graded overlays in Europe once or twice a year. Bäckström and Bergstrom (2000) recommend cleaning the porous asphalt every 2 to 4 years with this high-pressure water cleaning.

The stormwater quality study in Israel (Pacific Water Resources, 2004) tested the performance of a cleaning machine which used the "captive hydrology" technique. The cleaning machine used in Israel was supplied by Netivey Hamifratz Ltd. (NH). It was tested on its pick-up performance by cleaning a test area with a known weight of soil applied over it. The NH machine was found to have very high pick-up performance of 99.7%.

A report from the Public Work Research Institute (PWRI, 2005) in Japan gives some insight on porous asphalt cleaning machines. The first types of machines developed in Japan, similar to ones in Europe, had to clean at very slow speeds (1 km/hr) and attempted to fully recover the pavement. The newer machines can run at greater speeds (10-20 km/hr) and are designed to be used more frequently to maintain the function of the pavement.

One machine, the "Spec-keeper", sprays water into the pavement and creates high pressure air around the cleaning area to push the water back out of the pavement with the collected particles. The water and particles are then separated so the water can be reused. A schematic of the Spec-keepers cleaning process is shown below in Figure 12 and a picture of the machine is shown in Figure 13.

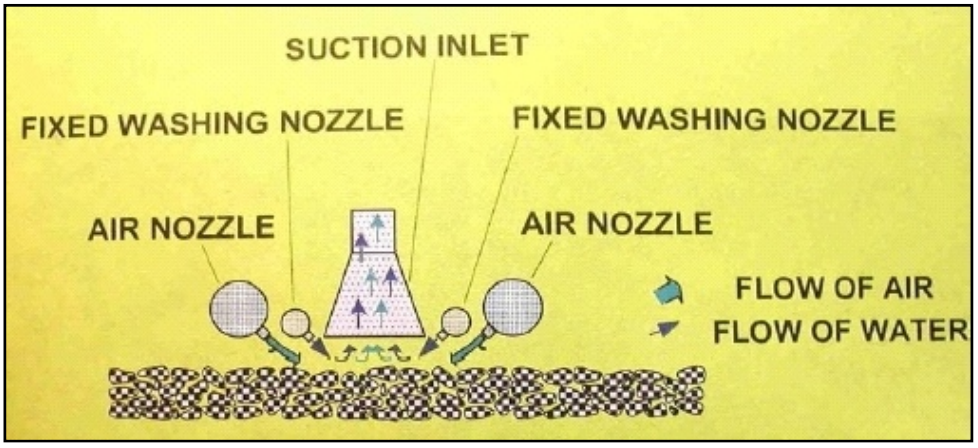

Figure 12 - The cleaning process of the Spec-keeper cleaning machine (PWRI, 2005)

Figure 13 - The Spec-Keeper cleaning machine in Japan from PWRI (2005)

Another machine uses high pressure air only to loosen the clogging particles. The particles are then vacuumed up. The machine blows air from both sides of the pavement and a vacuum in the middle collects the dirt and dust from the pavement. This machine runs at an average speed of 20 km/hr. Experiments on the frequency of use of this machine found that cleaning should be conducted as often as possible to maintain the most effective function of the pavement. The machine is shown in Figure 14.

Figure 14 - Cleaning Machine with High Pressure Air only from PWRI (2005)

Upon comparison of the different types of machines, the original slow-speed machines collected the most mass of particles per area and had to be used with the lowest frequency. However, the cleaning costs were much greater. The high-pressure water and air machines had lower efficiencies but were much more cost effective. An overview in effectiveness and costs of the three types of cleaning machines is given in Table 4.

Table 4 - Cleaning Machine Summary from Japan at PWRI (2005)

Cleaning Machine	Collected mass/cycle (g/m^2)	Frequency (times/year)	Cleaning Costs ($/m^2)	Cleaning Costs ($/m^2/year)
Conventional slow speed	100	3	8.55	25.65
High speed with high-pressure water	10	30	0.27	8.18
High-pressure air blow	6	50	0.10	4.96

A study was conducted by the Federal Highway Administration (FHWA, 2005) to learn more about common practices with noise-reducing pavements in European countries that have more experience with porous pavements. Different general and winter maintenance methods are used according to the policy priorities and environment conditions. In most countries, porous pavements are cleaned in order to maintain a certain acoustic ability (noise reduction) affected by clogging. A summary of each country's policy is given below.

In Denmark, porous asphalt is cleaned with high pressure water spray (125 psi) followed by vacuuming. Cleaning is performed three months after construction and then semiannually. Experience at the Danish Road Institute (DRI) has found that the pavement can become too clogged to clean effectively after two years if regular cleaning is not performed.

In the Netherlands, porous pavements are also cleaned semiannually with a captive hydrology cleaning machine. The Dutch have found that the noise reduction and drainage benefits are reduced immediately after cleaning since the clogging material is brought to the surface. However, after a short time these properties improve to an

unknown extent. Porous pavements are not used in urban areas because of the problem with clogging and questioned effectiveness of cleaning.

Porous pavements in France are not cleaned as the French have found cleaning to be ineffective. The mixes are designed to avoid clogging and the expected service life is greater than ten years.

Fog Sealing

Fog sealing is a process where asphalt is sprayed onto an existing pavement surface. Fog seals are used to replace asphalt that has deteriorated at the surface due to weathering (NCHRP, 2000). They can also be used to stop the pavement from raveling or reduce aggregate loss. Fog seals are applied by spraying dilute asphalt emulsion over the surface of the pavement. The fresh application of asphalt can lengthen the service life of the pavement and even seal small cracks in the pavement. However, applying too much asphalt can result in slick pavement surfaces and tracking of excess asphalt (Caltrans, 2003). Fog seals reduce the air void content of open-graded pavements. Some transportation authorities apply fog seals every 3-5 years as a part of surface maintenance. (NCHRP, 2000)

Winter Conditions

Winter maintenance is a commonly noted disadvantage of porous asphalt. A few studies on the performance of PFCs under winter conditions have been conducted. Bäckström and Bergstrom (2000) studied drainage through porous asphalt in freezing temperatures and snowmelt conditions. Laboratory experiments were performed in a climate room to

determine the infiltration rate through porous asphalt samples at cold temperatures. The results indicated that the infiltration rate decreased significantly at freezing temperatures and was nearly zero at -5ºC. To simulate snowmelt conditions, periods of freezing temperatures were combined with rainfall. After a few days of these conditions, the infiltration rate decreased to about 90% of the initial infiltration rate.

Shao et al. (1994) developed a model to predict the state of porous asphalt pavement surfaces. The thermal properties of the porous overlay depend on the porosity of the mixture. A higher porosity, or more air voids, creates a faster thermal response of the asphalt to the ambient air temperatures since it is an open structure. The air in the pores insulates the mixture from heat from the road sub-layer or ground. Water is retained in the pores of the pavement after wet conditions and incoming heat from the sub-layer is first consumed by evaporation of this water. Therefore, the surface of the pavement reaches freezing temperatures faster and stays below freezing longer than conventional pavements. Porous asphalt studies discussed by van der Zwan et al. (1990) also found similar results. Experience in France (FHWA, 2005) found that porous pavements reached freezing temperatures about 30 minutes before conventional pavements.

The “Icebreak Model” developed by Shao et al. (1994) was validated against actual temperature measurements at a site in England. The model successfully predicted 90% of the occurrences of below freezing temperatures at the pavement surface. Predicting freezing temperatures of the porous road surface would allow highway authorities to react in time and take appropriate actions. Therefore, road safety would not be compromised in winter conditions.

The pores in the pavement also affect the application of salt for de-icing in the wintertime since a portion of the salt will simply run into the pavement. This problem can be dealt with by increasing the frequency of salt applications on the roadway and also using wet salt instead of dry salt. (Van der Zwan et al., 1990)

A survey of DOT districts in Texas found that sand is the most commonly used material even though it causes clogging of the pavement. Anti-icing chemical agents, instead of de-icing agents, are the most effective winter maintenance procedure in these districts. Pre-wetted salts and chemicals are effective if they are applied at the right time. (Yildirim et al., 2006)

Pre-wetted salt is the most effective form of salt application for winter maintenance of porous asphalt in Europe. This type of salt application will stick to the porous surface instead of draining into the pavement and clogging the internal pores. This allows it to be useful for longer periods of time. Many users expect that the winter maintenance on the porous asphalt will require twice as much salt as the original dense-graded asphalt (Newcomb, 2004).

Camomilla et al. (1990) advise using almost three times the amount of salt used for conventional pavements to prevent icy conditions on roadways in Italy. Snowplow efforts are most effective shortly after snowfall before the snow penetrates the pores. Since the snowplows push some snow into the pores which can easily freeze, salt application is especially important following the snowplows. Experiences in Oregon also reveal that PFC should not be used in areas where snowplows are frequently used since it often damages the surface (Moore et al. 2001).

In Denmark, the DRI uses a wetted-salt solution with calcium-chloride to allow an even distribution of the solution. Experience has found that porous asphalt winter maintenance increases the salt use by 50%. The DRI also recommends avoiding short-sections of porous asphalt since the change in pavement type can startle drivers and make maintenance changes difficult. (FHWA, 2005)

In Italy, highway runoff of salt brine is an environmental concern, and therefore, a combination of magnesium and calcium is used for winter maintenance on the porous pavements (FHWA, 2005).

The Switzerland summary of porous asphalt performance in winter conditions by Isenring et al. (1990) found that porous asphalt did not behave worse than conventional pavements. They concluded that any disadvantages of porous asphalt in the winter can be avoided by intensive winter maintenance. The same conclusions were draw from porous asphalt use in Belgium (Van Heystraeten and Moraux, 1990).

The hydraulic properties as well as the maintenance of Porous Friction Course in literature were summarized in this chapter. The methods and fundamental equations of hydraulic conductivity and porosity were reported. Limitations of Darcy's law were also detailed. The next chapter deals with the air void content characterization of the extracted samples of porous asphalt.

3. LABORATORY MEASUREMENTS OF EFFECTIVE POROSITY AND RESULTS

3.1. INTRODUCTION

Evaluating the effective porosity of the samples is an important objective of the project because it quantifies the clogging phenomenon and verifies the homogeneous distribution of effective pores between the samples. Surface runoff can appear in the case of major clogging and both the safety for drivers and the water quality are impacted. Verifying the good effective porosity of the porous pavement was indeed necessary.

The first hydraulic parameter which was measured from the cylindrical samples of PFC is the porosity or air void content. The porosity can be seen as the water-holding potential of a porous media and is defined as the volume of voids per bulk volume (Charbeneau, 2000):

Equation 10

$$n = \frac{volume\,voids}{bulk\,volume} = \frac{V_v}{V_t}$$

Where V_v is the volume of voids and V_t is the total volume.

In our case, we were interested in characterizing the runoff within the pavement or the flow through the pores. The samples of porous asphalt are indeed susceptible to contain isolated air voids or clogged pores that do not contribute to the advection of water. The effective porosity describes this phenomenon and was determined in the experiments. Equation 11 defines the effective porosity:

Equation 11

$$n_e = \frac{volume\ \ of\ \ water\ \ able\ to\ circulate}{total\ volume\ of\ \ PFC\ sample}$$

The effective porosity was measured using two different methods:

- the water displacement method
- the image analysis method as verification

For each location, two samples A and B were analyzed using the water displacement method and one sample C was evaluated by the image analysis method. This chapter deals with the explanation of both methods in terms of procedure, equipment and mathematical solution. An interpretation of the results is given at the end.

3.2. WATER DISPLACEMENT METHOD

The method is commonly known and used in different asphalt laboratories as the Method of Test for determining the specific gravity and unit weight of compacted bituminous mixtures (Section 2.1). The water displacement method is accurate for open-graded pavements containing more than 2.0% of open or interconnected air voids. Two samples A & B for each location were investigated using the water displacement method on April 11, 2007.

Equipment required

The cylindrical cores were tested at the TxDOT asphalt laboratory in Cedar Park. The laboratory owns the required equipment:

- A specific gravity bench measures the volume of water displaced by the core plunged in water. More detail on this device is given in the procedure explanation (Appendix A: Permeameters & Measuring EAV Contents).
- A CoreLok apparatus, or automatic vacuum sealing apparatus for sealing the PFC sample in plastic bags,

- Plastic bag in conformity with the vacuum sealing device in order to enclose the PFC into them,
- An electronic ruler with a 1/100 millimeter precision,
- An electronic scale with a 1/10 gram precision.

Procedure and Mathematical Derivation

In a first step, the geometric characteristics of the cores were recorded using the electronic ruler:

- The minimum and maximum values of the diameter were measured. The average diameter was defined as D_{core}.
- The minimum and maximum values of the thickness were measured. The average thickness was defined as b_{core}.

The weight of the bag and core were recorded separately using the electronic scale as M_{bag} and M_{core}.

The plastic bags were of unique standardized dimensions: Length 30 cm and Width 22.5 cm. The assumption of a specific plastic density of $\rho_{plastic}$ = 1 g/cm^3 was taken and the volume of the plastic bag was determined as in Equation 12:

Equation 12

$$\left(V_{bag}\right) = \frac{M_{bag}}{\rho_{bag}}$$

In a second step, the CoreLok device and the specific gravity bench were successively used. The principle of the CoreLok is to vacuum up the air from inside the asphalt sample and seal this sample into a plastic bag. The plastic bag contours the shape of the sample after a 2 minute run of the device. A picture of the CoreLok device is presented in

Figure 15. The user is enclosing the asphalt sample into a yellow plastic bag, specific to the vacuum sealing device.

Figure 15 - Enclosing the Sample in the Plastic Bag – CoreLok device

The core sealed in the bag was then scaled on the specific gravity bench (Figure 16).

Figure 16 - Specific Gravity Bench

The specific gravity bench is composed of a tank filled with water at a standardized temperature of 68°F or 20°C, a basket immersed in the water which will contain the sample and a calibrated scale attached to the basket that weights the volume of water displaced by the specimen. In this step, the core in the bag was weighed and the displaced volume was recorded as $M_{1,\ measured}$.

Finally, the third step consisted in weighing the volume of water displaced by the core itself using the specific gravity bench. The displaced volume was recorded as: $M_{2,\ measured}$.

The mathematical derivation is based on Archimedes Principle, which states that a body immersed in a fluid experiences a buoyant force equal to the weight of the displaced fluid. In this case, the measures carried out with the specific gravity bench conform to the principle since samples were submerged.

The results of the second step (core sealed in plastic bag) are derived in the force balance (Equation 13):

Equation 13 $$\left(M_{bag} + M_{core}\right) \cdot g = \rho_{water} \cdot \left(V_{core} + V_{bag}\right) \cdot g + F_1 \quad where\ F_1 = M_{1,measured} \cdot g$$

We define ρ_{water} = 0.9981 g/cm^3 as the specific density of water at 20°C, F_1 as the force indirectly measured by the scale and g = 9.81 m/s^2 as the gravity acceleration. The right hand side is composed of the buoyant force and the force applied on the scale.

The results of the third step (core itself) are similarly derived in the following force balance (Equation 14):

Equation 14 $$M_{core} \cdot g = \rho_{water} \cdot V_{grains} \cdot g + F_2 \quad where\ F_2 = M_{2,measured} \cdot g$$

F_2 is the force indirectly measured by the scale and V_{grains} is the volume of the grains and binders composing the core. Taking into account the two force balances, the effective porosity is derived as in Equation 15:

Equation 15

$$n_e = 1 - \frac{V_{grains}}{V_{core}}$$

The same methodology was applied to the six investigated cores. This method was simple to use since the required devices were available at the asphalt laboratory.

3.3. IMAGE ANALYSIS METHOD

This method is specifically used by the Danish Road Institute in Europe (DRI, 2005) and allows looking at the air voids, grains and binders of a sample of porous asphalt at a microscopic level. The principle of the method is to examine a plane section of the core and analyze the void content of the surfacing, the size of the voids, their form and distribution. The cylindrical core was previously sliced in half and pores and other porosities in the matrix were filled by a fluorescent epoxy. A more detailed description of the device is available in the literature review (Section 2.1).

In order to illustrate the procedure, the example of RM 620 is detailed. Looking at the following pictures, it is interesting to note that binders have been removed from the plane section.

Procedure and Analysis

The cores were sent to the National Petrographic Service laboratory located in Houston, specialized in sample analysis and preparation of thin and polished sections for

petrographic studies. A first core from RM 620 was sent in May 2007 and the two others from Loop 360 and RM 1431 in August 2007.

A core was sliced and pores and other porosities in the matrix were filled by a fluorescent epoxy. A picture was taken with a camera in a dark room; a black light illuminated the cores.

Using an image editor such as Image J or Adobe Photoshop, the picture was cropped to the effective pores boundaries. In this example, Image J was used since it is freeware intended for research purposes. The cropped Figure 17 shows how the plane section appears: grains and binder connections are in dark colors and air voids come out in light green color.

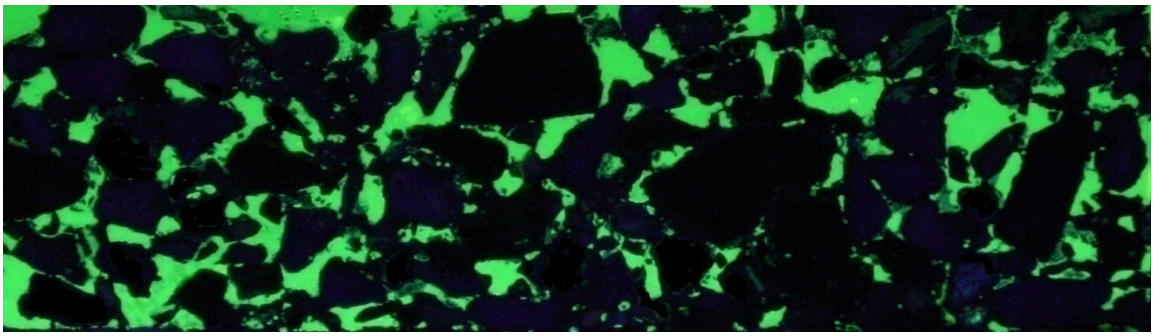

Figure 17 - Plane Section with Pores filled with Green Fluorescent Epoxy – RM 620

Further analysis was done with Image J such as the red color distribution. Image editors provide the histogram of basic colors for a RGB (Red-Green-Blue) Standard picture. On the red color histogram (Figure 18), the first peak corresponds to the grains and binders of the pavement. The second peak mostly corresponds to the effective voids and other porosities.

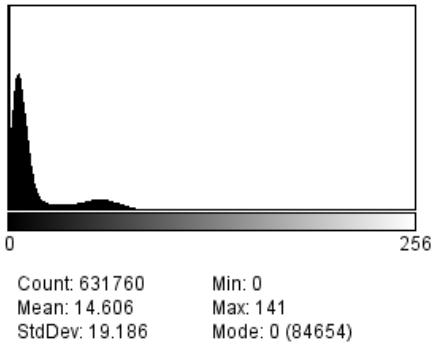

Figure 18 - Red Color Distribution with Image J – RM 620

Looking at the color distribution of the picture and at the contours of the pores on a grayscale basis, a threshold was calibrated to delineate grains, binders and pores. Considering that grains and binders are represented by the first 43 colors of the 256 composing the RGB system, the image was transformed into a black/white representation using a threshold function. The result is shown in Figure 19; white areas correspond to pores while dark areas represent grains and binders.

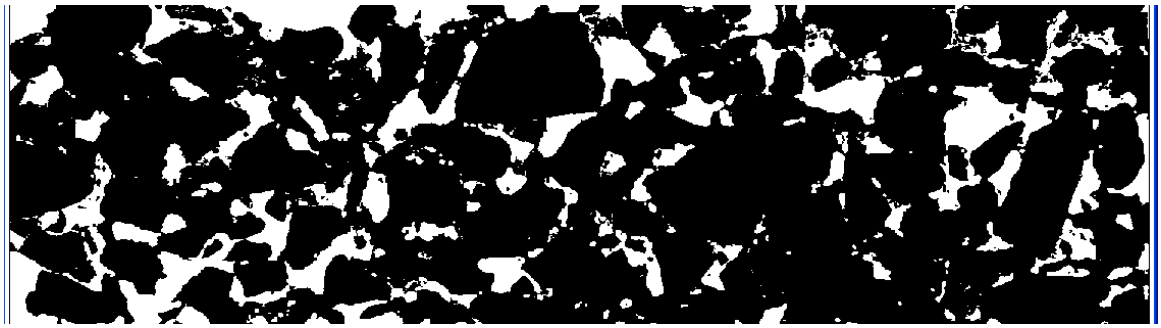

Figure 19 - Black and White Representation of the Plane Section – RM 620

The black and white picture was analyzed by its color histogram or distribution. The porosity was defined as the ratio of the total number of white pixels to the total number of pixels in the image. In the example, the figure has:

- 503504 black pixels,
- A total number of 631760 pixels.

The distribution of pixels is shown in Figure 20, the mode gives the number of black pixels and the count gives the total number of pixels:

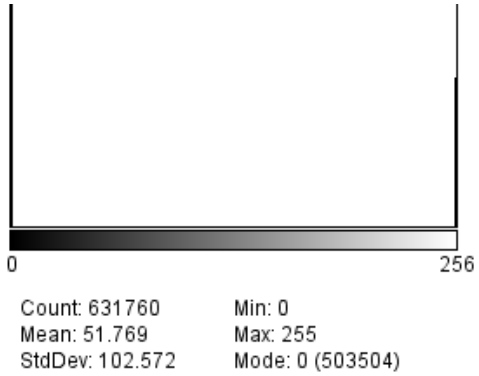

Figure 20 - Black and White Pixels Distribution – RM 620

The ratio of pixels implies an air void content of 20.30%. The same method was carried out on Adobe Photoshop for similar results; we obtained a porosity number of 20.34%

One core for each location was tested using the image analysis method. A summary of the results and their interpretation is in Section 3.4.

3.4. EFFECTIVE POROSITY RESULTS AND INTERPRETATION

When the PFC overlay was installed on the roads in 2004, the aggregate was designed to maintain a porosity specification of about 20%. The results obtained by both the water displacement and image analysis methods confirm the relative homogeneity of the cylindrical PFC samples in terms of air void contents. Table 5 summarizes the different calculated effective porosities.

Table 5 - Summary of Effective Porosity

Location	Core	Effective Porosity (%)	
		Specific Gravity	Image analysis
Loop 360	1A	22.78	
	1B	21.64	
	1C		20.36
RM 1431	2A	23.17	
	2B	20.51	
	2C		20.98
RM 620	3A		20.3
	3B	19.44	
	3C	19.55	

Basic statistical numbers are given at every location:

- On Loop 360, the average effective porosity equals 21.59% with a standard deviation of 1.21%.
- On RM 1431, the average effective porosity equals 21.55% with a standard deviation of 1.41%.
- On RM 620, the average effective porosity equals 19.76% with a standard deviation of 0.47%.

The weight and geometric characteristics of the cores are summarized in Appendix B: Weight & Characteristics of Cores. The method of water displacement determines accurately the effective porosity and is easy to realize as long as the required equipment is available.

The method of image analysis carries advantages but also weaknesses with it. The main advantage is the analysis of the plane section at the scale of a porous media. The structure of the aggregate is revealed such as the grain size, the binders and the voids and a description of the kinematical flow through the interconnected voids can be viewed.

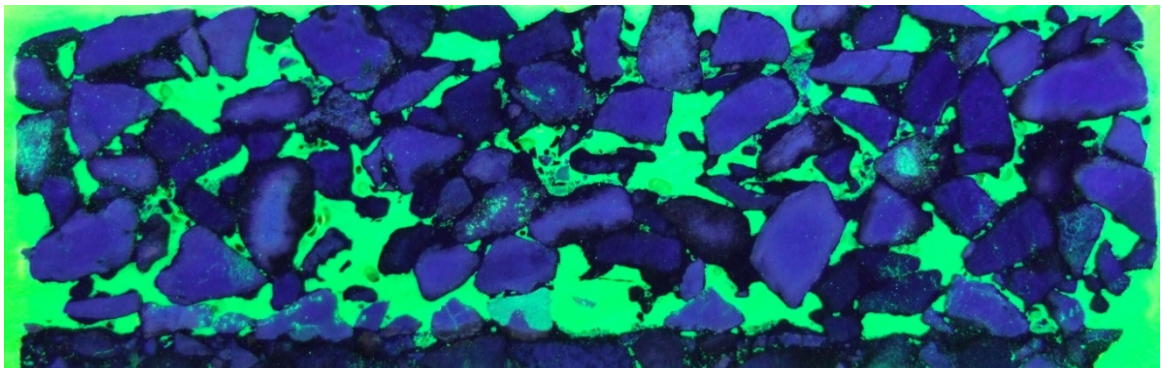

Figure 21 - Plane Section with Fluorescent Epoxy Filling Voids – RM1431

Observing Figure 21, the distributions of pores and grains are not homogeneous and the radial flow through pores might not be isotropic. The analysis of the other images leads to the same conclusions. In this image, the bottom layer corresponds to the impervious pavement and the size of the pores is heterogeneous being larger than the grains for some of them.

One main disadvantage is the technique of impregnating fluorescent epoxy through pores. The hot epoxy is vacuumed through the pavement for several hours before cooling down. Most of the binders are dissolved due to their hydrocarbon composition and the particles, which were supposed to clog the media, are flushed out. This method wasn't accurate to calculate the defined effective porosity.

Another disadvantage is the requirement of one core, which will be sliced in half sections just for the image analysis. The displacement method keeps the cores integral. Finally, the defined threshold of 43 colors remains a subjective value, even if experiments were coherent between the 3 cores examined.

The plane sections of the other pavement samples can be found in Appendix B: Weight & Characteristics of Cores.

For later studies on porosity calculations, it would be recommended to only carry out the water displacement method.

In this chapter, we have reviewed two different methods used to determine the effective porosity of the cores. The first method, or water displacement method, is based on Archimedes Principle and offers accurate results. The second one, or image analysis method, interprets the grains and voids composing a plane section. Results were mitigated by the drawbacks of the methods. Concerning the results, the aggregate specifications of porosity were respected with a porosity evaluated at 20-21% according to the site. The next chapter presents the laboratory experiments realized in order to determine the hydraulic conductivity of the PFC cylindrical samples.

4. LABORATORY MEASUREMENTS OF HYDRAULIC CONDUCTIVITY

In-situ rainwater drains down to the impervious surface and flows towards the edge of the pavement: the flow through porous media has both vertical and radial components. The design of the testing apparatus has attempted to comply with the in-situ flow characteristics. The objective of this chapter is to introduce the analytical and experimental methods carried out to determine the hydraulic conductivity from the cylindrical samples of PFC. A method for assessing the clogging phenomenon is also presented.

4.1. ANALYTICAL DESCRIPTION OF THE TESTING APPARATUS

The testing apparatus consists in an immersed sample of Porous Friction Course in a large tank of water. Two metallic plates as well as rubber gaskets ensure the impermeability of the top and bottom surfaces of the core. A peristaltic pump imposes a constant head gradient between the levels in the standpipe and in the tank. Heads are measured from measurement ports and lines by a manometer board and a bubbler respectively. The configuration of the testing system is observable in Figure 22.

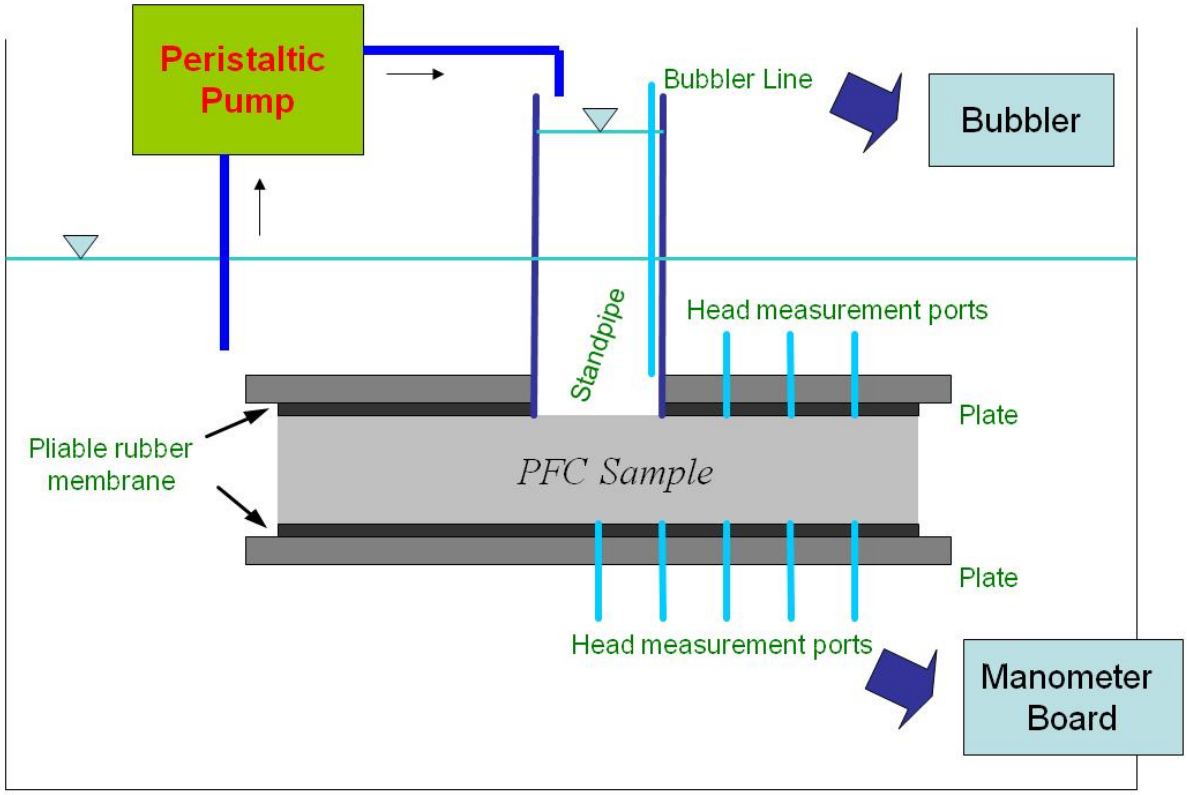

Figure 22 - Setup of the Testing Apparatus

The Porous Asphalt sample can be analytically interpreted as a cylindrical core with radius R and thickness b. The flow during the test has vertical flow from a standpipe of radius = *a* centered on the top of the sample and radial flow along the edges at radius R. The established head = h_A is uniform over the disk $0 < r < a$, $z = 0$. The established head = h_B is also uniform over the radial periphery of the sample, $r = R$, $0 < z < b$.

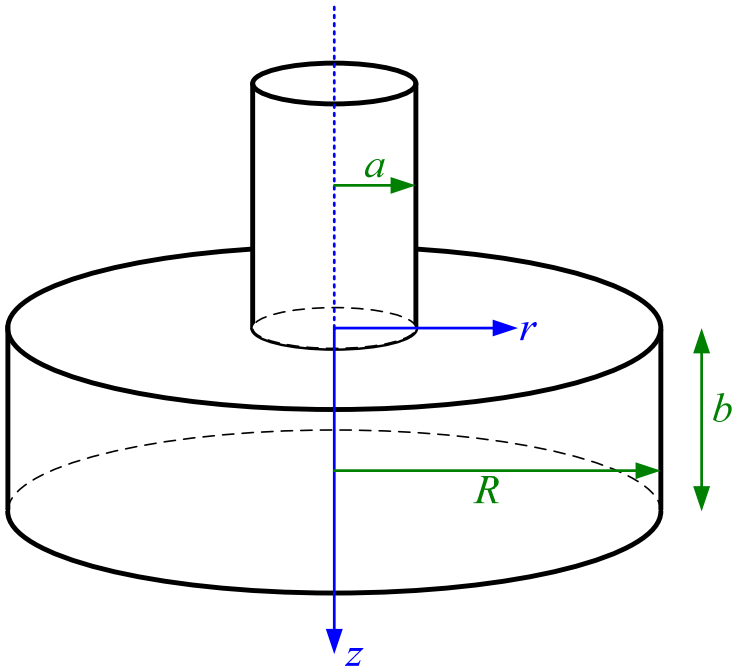

Figure 23 - Analytical View of the PFC Testing Apparatus

The goal is to derive an expression of the steady head in this porous media due to a constant head gradient applied over the circular area. The steady-state continuity equations along with associated boundary conditions are expressed as followed:

Equation 16
$$K_r\left(\frac{1}{r}\frac{\partial}{\partial r}\left(r\frac{\partial h}{\partial r}\right)\right)+K_z\frac{\partial^2 h}{\partial z^2}=0$$

Equation 17
$$h(r,z)=h_A \quad [0\le r\le a;\ z=0]$$

Equation 18
$$\frac{\partial h(r,z)}{\partial z}=0 \quad [a<r\le R;\ z=0]$$

Equation 19
$$h(r,z)=h_B \quad [r=R;\ 0\le z\le b]$$

Equation 20
$$\frac{\partial h(r,z)}{\partial z}=0 \quad [0\le r\le R;\ z=b]$$

Equation 16 – 20 present a well-posed boundary value problem whose solution h(r,z) exists. The solution to this problem is analogous to heat transfer through a finite medium due to heat supply over a circular area (Carslaw and Jaeger, 1959). The discharge through the porous media is derived from the known solution of head distribution (Equation 21).

Equation 21

$$Q = 2\pi K_z \int_0^a r \frac{\partial h(r,0)}{\partial z} dr = 2\pi R K_r \int_0^b \frac{\partial h(R,z)}{\partial r} dz$$

Due to the heterogeneous distribution of effective pores and the potential clogging of the pavement, the flow rate is not expected to be uniform over either the inflow or outflow surface.

We consider that the radial and vertical hydraulic conductivities are the same (for $K = K_r = K_z$) since one controls the other. If both R and b are considered infinite compared to a, the solution becomes (Equation 22):

Equation 22

$$h(r,z) = \frac{2(h_A - h_B)}{\pi} \sin^{-1}\left(\frac{2a}{\sqrt{(r-a)^2 + z^2} + \sqrt{(r+a)^2 + z^2}} \right)$$

The discharge calculated using the first of Equation 21 is

Equation 23

$$Q = 4K(h_A - h_B)a$$

Since R and b are not infinite, the effects of the finite vertical dimension are addressed using the method of images in Equation 24. This gives:

Equation 24

$$h(r,z) = \frac{2(h_A - h_B)}{\pi} \sum_{j=-\infty}^{\infty} \sin^{-1}\left(\frac{2a}{\sqrt{(r-a)^2 + (z+2jb)^2} + \sqrt{(r+a)^2 + (z+2jb)^2}} \right)$$

In Equation 24, the image j = 0 corresponds to the basic solution given by Equation 22. However the core has a thickness of b and the image j = -1 corresponds to a source disk located a distance z = 2b below the surface (z = 0) making the surface z = b a no flow boundary. The drawback of this image is the apparition of an upward gradient across the z = 0 surface because of the imaginary part. The conjugate j=-1 attempts to cancel this gradient. The same derivation happens infinitely between conjugate components at z = 4b, 6b…

The image solution satisfies Equation 16 and the boundary conditions from Equation 18 to Equation 20. The analogy with heat transfer doesn't take into account the non-uniform head on the disks 0 < r < a; z = 0 and r=R, 0<z<b disks because of the presence of grains and open pores. The boundary conditions (17) and (19) are not intrinsically verified nor mathematically satisfied.

The veracity of the images equation was tested and confirmed by quantitative measures (Charbeneau, 2006). Charbeneau found that the finite effects of Equation 24 $h(r,z)=\frac{2(h_A-h_B)}{\pi}\sum_{j=-\infty}^{\infty}\sin^{-1}\left(\frac{2a}{\sqrt{(r-a)^2+(z+2jb)^2}+\sqrt{(r+a)^2+(z+2jb)^2}}\right)$ can be represented using a shape factor. The shape factor corresponds to the geometric characteristics a, b and R of the sample (Equation 25).

Equation 25

$$F\left(\frac{a}{R},\frac{b}{R}\right)=\frac{\hat{Q}}{4a}$$

Q is the normalized discharge through the porous media. The magnitude of the shape factor is close to unity. The head gradient can be related to the flowrate through the shape factor (Equation 26).

Equation 26

$$Q = 4aK\Delta h\, F\left(\frac{a}{R}, \frac{b}{R}\right)$$

In the subsequent experiments, the shape factor will be determined by measuring the geometric characteristics of the sample. The hydraulic conductivity will be evaluated by monitoring the head gradient as well as the flowrate.

4.2. DESCRIPTION OF THE EQUIPMENT

In order to put in practice the analytical principle detailed in the last section, a measuring system was designed and assembled together. The equipment is listed according to the associated functionality and the purpose of the equipment is explained.

Tests

Different types of tests were carried out on the measuring device such as the importance of clogging and the isotropy of the radial flow. The radial flow was tested using a solution of potassium permanganate (KMnO4), coloring the water in the standpipe.

The clogging phenomenon was quantified by the mass extracted from the cores:

- Filter paper circles of characteristics: Ashless, Grade 40 and diameter 12.5cm. They were used to collect and dry the extracted mass.
- A scale “Scout Pro SP202” of maximum capacity 200g and precision 0.01g. The scale allowed weighing the extracted mass.

- A regular plunger of 4 inches diameter.

Measure of hydraulic heads

The hydraulic head was evaluated in the standpipe, at different radial positions and in the box. In order to address this purpose, two devices were used:

- A Bubbler Flow Meter (Isco Reference 4230). The flowmeter line was connected to the standpipe, converting the pressure necessary to force a bubble in the standpipe into a level reading.
- An inclined manometer board with measuring tubes connected to the different pressure tabs on the plates, the box and the standpipe. The manometer was built on a similar basis as the manometer board designed for the Rain Simulator at the Center for Research in Water Resources. Dimensions were changed to the purpose of our project: a slanted board of dimensions 34.5 x 16 inches and a frame offering different incline angles down to 5°. Blueprints and correspondence are available in Appendix C: Experimental System – Blueprints.

Measure of flowrate

The flowrate was measured from the discharge hose of the peristaltic pump in use with:

- Standard laboratory measuring glassware
- A standard stopwatch.

Testing system

Following the testing system described analytically (Section 4.1), several components were designed, built or ordered:

- Two boxes made with ½ inch thick Plexiglas plates. Both dimensions are of 23 inches by side and 18 inches of height. There are two threaded holes where a faucet and a pressure barb are attached. One box was used.
- Two metallic squared plates of side 12 inches side and thickness ½ inches. The plates were designed to analyze 12 inches diameter cylindrical cores and ¼ inch holes were threaded at 0, 1.375, 2, 2.625, 3.75 and 5.25 inches radius positions for pressure measurements. On the top plate, a 2" diameter open hole was drilled in order to insert the acrylic standpipe within the plate. Figure 24 depicts the design of the top plates. The locking system of the cylindrical PFC core was constructed with 3/8 inch holes on the sides.

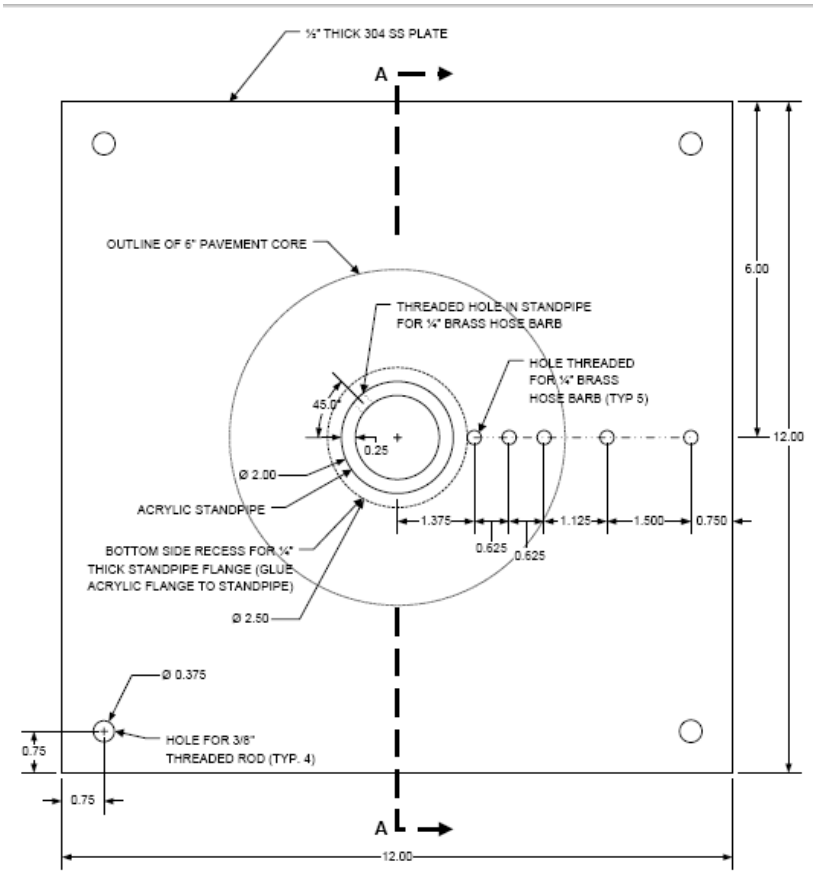

Figure 24 - Blueprint of the top plate.

- Two pieces of wood of dimensions L12x H 6x W1.5 inches constituting the support of the system. The two pieces were waterproof treated. 3/8 inch holes were drilled at the extremities and threaded rods were mounted in these holes. The locking system would use bolts on the four corners, squeezing the material between the 2 plates.
- An acrylic standpipe of characteristics 2.50 OD x 2.00 ID inches.
- Several pieces of rubber gaskets maintaining the impermeability of the top and bottom surfaces of the cylindrical cores. The rubber gaskets were ½ inch thick, and supple. Holes were drilled at the pressure tabs radial positions and also for the standpipe.

- Two peristaltic pumps working at different flowrates. The first peristaltic pump, Heidolph PD5106, was acquired with a Single Channel pump Head and silicone tubing (ID.250xOD.438 inches) according to technical criteria: low pressure, no particle matter, self-priming, high-accuracy dispensing, flowrates fluctuating between 100 mL to 2 L/min. This pump was primarily used for higher flowrates. Another pump, VWR peristaltic pump, was used for more accuracy within the low flow measurements.

All the blueprints of the testing apparatus are presented in Appendix C: Experimental System – Blueprints.

4.3. PROCEDURE OF THE CONSTANT HEAD TEST

This section summarizes the methodology followed when experiments were carried out.

Preparation of the measuring system

Tested cores were immersed in water overnight and shaken before being placed between two pieces of rubber gaskets. The whole assembling was locked between the two metallic plates using the locking bolts. The tank was completely filled with water and the peristaltic pump was turned on for 30 minutes to evacuate the last air voids from the core. The air in the connection between the manometer tubes and the devices was flushed out using a hose. When ready, the tank was drained until the water level was about 5cm above the top plate. Note: the torque applied on the system was as high as possible, consistent with the structure of the porous asphalt core.

Run of the experiment

The hydraulic conductivity was measured by decreasing the flowrate. Between two measures, the level on the bubbler was calibrated and set to zero. A hydraulic gradient was imposed on top of the open core surface by turning on one of the pumps. The levels were read on the manometer or bubbler once the levels were stabilized. The flowrate delivered by the pump was then measured using the stopwatch and the laboratory glassware. High flowrate measures were carried out with the Heidolph pump whereas low flowrates were delivered by the VWR peristaltic pump. 12 to 18 different head difference measures were reported for each core.

4.4. VERIFICATION TEST

Porous asphalt is subject to clogging. The main measure for hydraulic conductivity considers that the vertical and radial hydraulic conductivities are equivalent since the slowest velocity drives the behavior of the other velocity inside the pavement. Since the cylindrical samples were extracted from pavement installed in 2004, the pavement might be clogged on surface. An experiment was carried out in order to verify the veracity of the results. Experimented cores were drilled on their center by a core pin of 1.25 inches (1.59 cm) outer diameter at the TxDOT asphalt laboratory.

Comparing the situation to the one in (Section 4.1), we have a uniform established head H_1 imposed on the inner area of the cylinder at $R= R_1$. The established head H_2 is uniform over the radial periphery of the sample at $R= R_2$.

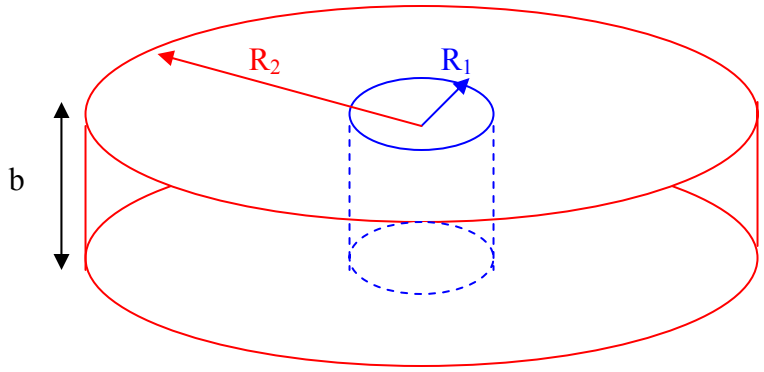

Figure 25 - Verification of the hydraulic conductivity results

At steady state, we consider that the continuity equation is independent of the vertical position and constrained to the following potentials (Equation 27):

Equation 27

$$\begin{cases} \dfrac{\partial}{\partial r}\left(r \cdot \dfrac{\partial h}{\partial r} \right) = 0 \\ h(r = R_1) = H_1 \\ h(r = R_2) = H_2 \end{cases}$$

From the velocity of the flow $q = K_r \cdot \dfrac{\partial h}{\partial r}$ and the cross-section of the cylindrical sample $A = 2 \cdot \pi \cdot r \cdot b$, we can derive the flow rate, which is considered uniform over the inflow and outflow surfaces this time:

Equation 28

$$-Q = 2 \cdot \pi \cdot r \cdot b \cdot K_r \cdot \frac{dh}{dr}$$

Or

Equation 29

$$-dh = \frac{Q}{2 \cdot \pi \cdot b \cdot K_r} \cdot \frac{dr}{r}$$

Integrating between the two boundaries of the cylindrical core, the hydraulic conductivity is derived as a function of the flowrate and the geometric characteristics of the core:

Equation 30

$$K_r = \frac{Q}{2 \cdot \pi \cdot b \cdot (H_1 - H_2)} \cdot \ln\left(\frac{R_2}{R_1}\right)$$

As described in Section 4.3, the same experimental procedure was followed during the verification tests.

4.5. CLEANING OF POROUS ASPHALT SAMPLES

Experiments were carried out in order to quantify the effects of clogging on the hydraulic conductivity. The comparison was done on the drilled cores using the same methodology.

The immersed cores were unclogged using a plunger on both top and bottom sides (Figure 26).

Figure 26 - Plunger unclogging a PFC core

Letting the particulate matter to decant for a few minutes, the sink was drained out with a high size cap. Accumulated sediments were gathered from the bottom of the tank using a filter paper (Figure 27).

Figure 27 - Sediments in sink

The sediments were then dried in the filter paper contained in glassware. The weight of collected sediments was obtained using the electronic scale after calibration.

Figure 28 - Sediments in filter paper

The hydraulic conductivity of the unclogged core was determined by running the PFC experimental apparatus.

In this chapter, the experimental apparatus employed for the determination of the hydraulic conductivity was presented. In both testing cases, simple equations of the hydraulic conductivity were derived. Results are summarized and interpreted in the next chapter, introducing the limitation of Darcy's law.

5. ANALYSIS OF THE CONSTANT HEAD EXPERIMENT RESULTS

Using the experimental system described in the previous chapter, the PFC samples were evaluated under different conditions and positions. Due to the high velocity of the radial flow within the pavement, the system operating region deals with the limitation of Darcy's Law: inertial effects appear to be consequent and are characterized within this chapter. An estimate of the clogging phenomenon is also carried out.

It is also important to summarize the differences between run experiments in order to understand the overall analysis:

- An initial test was run on the core 1B from Loop 360
- The five other cores were sliced on the bottom and characteristics were evaluated from the standpipe sitting on top and upside down.
- The six cores were finally drilled on their center. Hydraulic conductivity was evaluated before and after being cleaned up.

5.1. INERTIAL EFFECTS AND FORCHHEIMER MODEL

Empirical studies have shown the limitations of Darcy's Law in characterizing the flow within porous media at large velocities (Ward, 1964). In literature, the transition between the laminar and turbulent flow through porous media is seen at low Reynolds numbers ($1<Re<10$), (Charbeneau, 2000). Due to the geometric characteristics of the experimental apparatus, the formulas derived in the literature for Re are not applicable. The Reynolds number is then calculated from a non-unique method, allowing the author to have an idea

of Darcy's velocity. An equivalent radius is defined as the radius at which the flow would have covered half the volume of the core (Equation 31).

Equation 31

$$\pi \cdot b \cdot (r^2 - a^2) = 2 \cdot \pi \cdot b \cdot r_e^2$$

This leads to (Equation 32):

Equation 32

$$r_e = \sqrt{\frac{r^2 - a^2}{2}}$$

Where b is the height of the cylinder, *r* and *a* are the radiuses of the core and the standpipe respectively.

Darcy's velocity was therefore calculated at the r_e radial position (Equation 33):

Equation 33

$$q = \frac{Q}{2 \cdot \pi \cdot r_e \cdot b}$$

Where Q is the flowrate in cm^3/s flowing through the PFC sample. Knowing Darcy's velocity, the associated Reynolds number is derived (Equation 34):

Equation 34

$$\mathrm{Re} = \frac{q \cdot d_{10}}{\nu}$$

Where d_{10} is the effective grain size of the aggregate, defined as the size at 10% of the size distribution and υ is the kinematic viscosity of water at the recorded temperature.

For every core, the value of the Reynolds number was determined at each flow rate condition. The equivalent radius was calculated according to (Equation 35):

Equation 35

$$r_e = \sqrt{\frac{r^2 - a^2}{2}} = \sqrt{\frac{7.53^2 - 1.52^2}{2}} = 5.15\,cm$$

The effective grain size was obtained from the aggregate grain size distribution and equals $d_{1\text{-}20\%}$ = 4.75 mm (Appendix D: Porous Friction Course Aggregate - Water Properties). Temperatures changed between experiments on a range of 17°C – 25°C and the kinematic viscosity was determined from the Water properties table (Appendix D: Porous Friction Course Aggregate - Water Properties). The geometric characteristics of the cores have slightly changed between experiments but the range of associated Darcy velocities and Reynolds number remain approximately the same:

- Darcy's velocity, computed from Equation 33, fluctuates from .017 cm/s to 0.35 cm/s.
- The Reynolds number, derived from Equation 34, varies from 0.7 to 16.9.

Before analyzing any results on hydraulic conductivity, the Reynolds number shows that the range of flows within the porous asphalt samples might be characterized as transitional to turbulent.

At higher Reynolds numbers, the inertial effects are not negligible compared to the viscous forces (Rumer, 1969). These patterns were observed on the following Gradient (Head Difference) – Flowrate graph. Examples are focused on the sample 1B from Loop 360, representative of the observed trends.

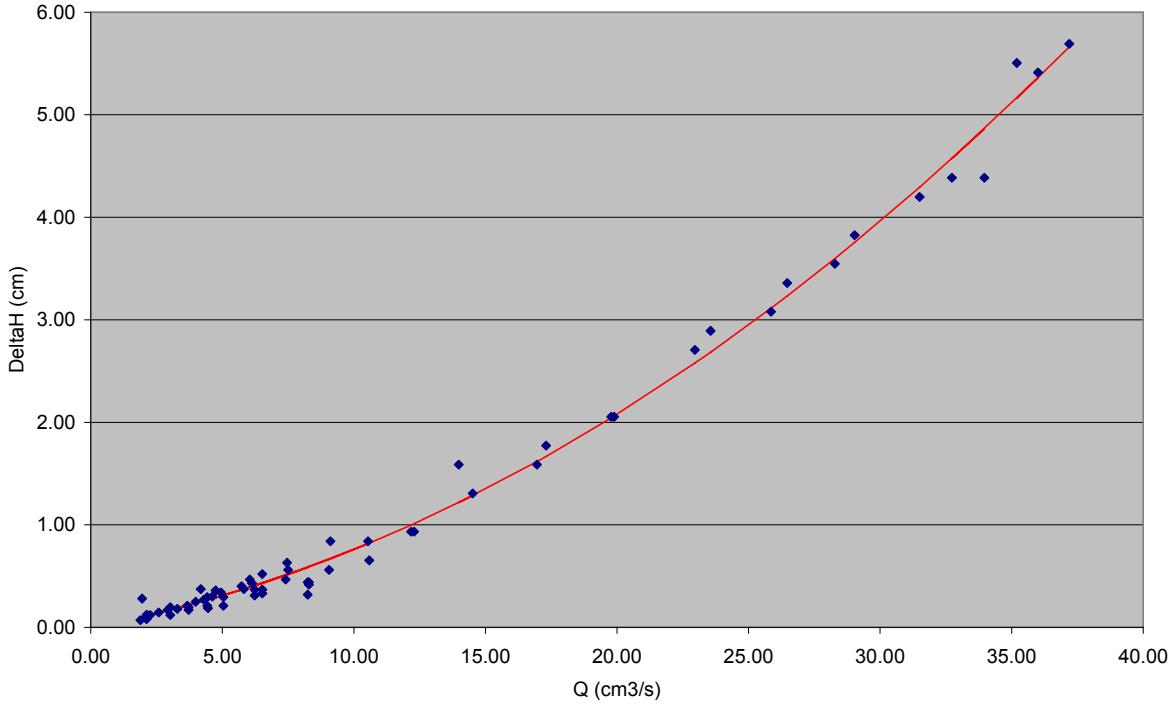

Figure 29 - Core 1B – Relationship between Hydraulic Gradient and Flowrate

As the discharge of water through the PFC sample increases, the hydraulic gradient increases more than proportionally to Darcy' law. A quadratic model was applied in order to describe the observed inertial effects (Forchheimer, 1901):

Equation 36 $$\Delta H = \alpha \cdot Q + \beta \cdot Q^2$$

Where α and β are parameters defined by the quadratic model. In this case, the following parameter values were determined: α = 0.0477 and β = 0.00281.

The hydraulic conductivity was computed from Darcy's law:

Equation 26 $$Q = 4aK\Delta h\, F\left(\frac{a}{R}, \frac{b}{R}\right)$$

The effects of the convective terms in Navier-Stokes equation are also viewable on the hydraulic conductivity versus head difference graphs (Figure 30). The higher the head difference is, the lower the hydraulic conductivity is since the inertial effects increase the rate of head loss along the characteristic flow line.

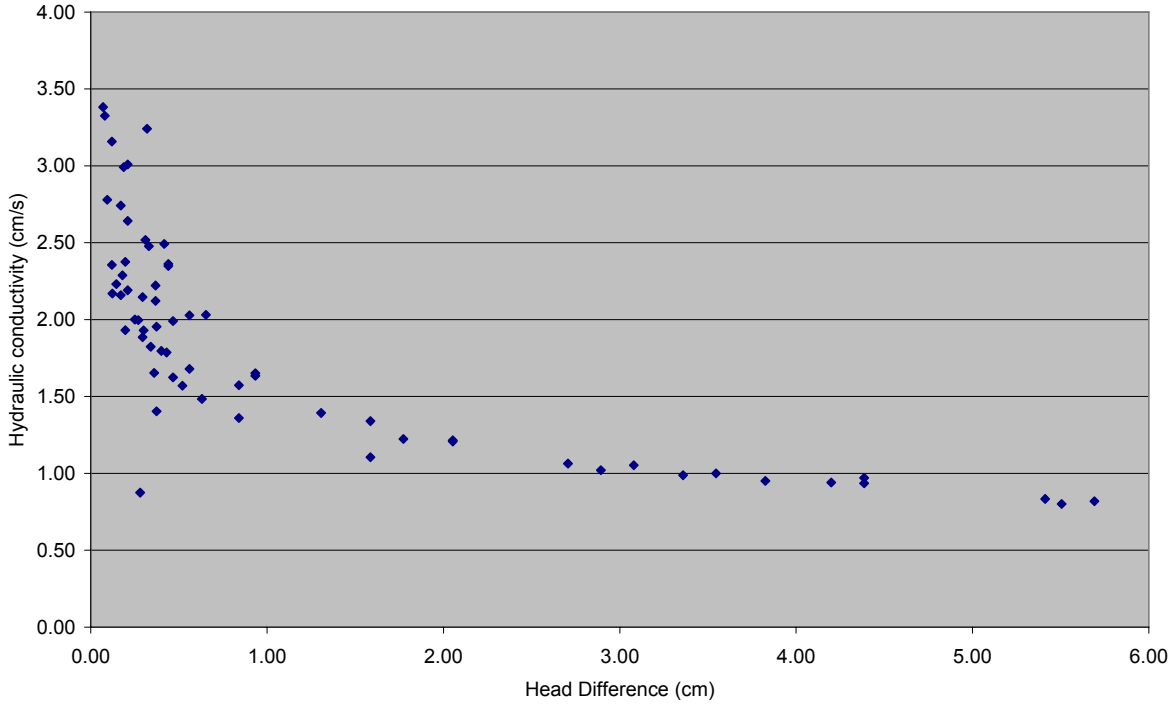

Figure 30 - Core 1B – Comparison of Hydraulic Conductivity and Head Gradient

The standard error of the model was determined from Equation 37 and appeared to be very small in this case: 0.125 cm.

Equation 37

$$SE = \sqrt{\frac{1}{N-2}\sum_{j=1}^{N}\left(\Delta H_{meaured} - \Delta H_{quadratic}\right)^2}$$

Where $\Delta H_{measured}$ and $\Delta H_{quadratic}$ are respectively the measured head gradient and the head derived by the quadratic model. According to Ward's approach (2.3), the first term of our quadratic model corresponds to the Darcy's linear law and one would anticipate:

Equation 38

$$\alpha = \frac{1}{4\,aKF\left(\frac{a}{R},\frac{b}{R}\right)}$$

This gives:

Equation 39

$$K = \frac{1}{4aF\left(\frac{a}{R},\frac{b}{R}\right)\alpha} = 2.63\ cm/s$$

The value K = 2.63 cm/s seems reasonable, especially given the scatter for small head difference values seen on figure. One benefit from using a Forchheimer model remains in the characterization of the deviation from Darcy's linear law.

Equation 40

$$\Delta H = \alpha \cdot Q\left(1 + \frac{\beta}{\alpha}Q\right) = 0.0477Q\left(1 + 0.0589\,Q\right)$$

This suggests that the model equation departs from the linear equation (Darcy's law) by a factor of 11 percent when the minimal discharge is Q = 1.89 cm^3/s. Deviations are of course much higher when the flowrate increases so that measurements within the linear range would be extremely difficult to make.

The other five cores presented lower hydraulic conductivity and their bottoms were sliced up in order to determine their degree of clogging. The same procedure was carried out with the hydraulic gradient imposed either on the top or bottom surfaces.

There were fewer experimental points which induced discrepancies into the fit of a Forchheimer model at low flow values. This trend can be seen in Figure 31, the plot corresponding to the relationship between the hydraulic head gradient and the flowrate.

One can observe in blue the experimental points and the quadratic model is represented by a red curve. The applied model doesn't fit the experimental points as well for flow rates lower than 4 cm^3/s.

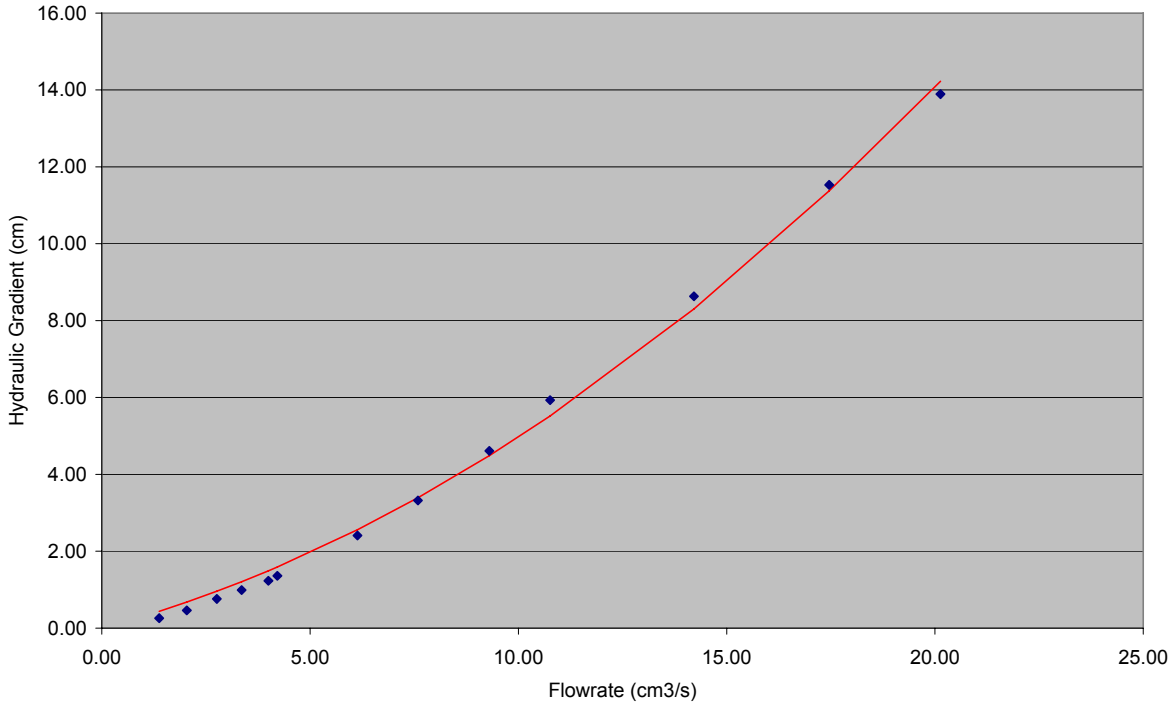

Figure 31 - Core 3C – Limitations of the Quadratic Model at Low Flow Measurements

The hydraulic conductivity was calculated from the coefficient α and the geometric characteristics of the different cores. Table 6 summarizes the results. "Top" corresponds to the tests where the standpipe was sitting on the top surface of the pavement. "Bottom" corresponds to the case where the sample was tested upside down.

Table 6 - Forchheimer Model - Hydraulic Conductivity and Standard Error

Forchheimer Model				
Core	Top		Bottom	
	K (cm/s)	SE (cm)	K (cm/s)	SE (cm)
1A	0.19	0.63	0.18	0.49
1B	2.63	0.13		
2A	0.7	0.22	0.58	0.19
2B	0.32	0.37	0.64	0.29
3B	0.49	0.51	0.1	0.36
3C	0.49	0.36	0.48	0.26

Results are globally homogeneous within the samples extracted from RM 1431 (Index 2) and RM 620 (Index 3). Hydraulic conductivities on RM 1431 range approximately from 0.5 to 0.6 cm/s; on RM 620 a typical value is 0.49 cm/s. Results between the two cores from Loop 360 are disparate: one averaging 0.19 cm/s of hydraulic conductivity, the other 2.63 cm/s. The difference can be interpreted as the importance of clogging in some samples.

Disparities between the top and bottom are also observed but are examined in the clogging phenomenon section. Parameters of the Forchheimer model are available in Appendix E: Hydraulic Conductivity Model Parameters. Due to the discrepancies of the quadratic model, the standard errors are higher for the five sliced cores, ranging from 0.19 cm to 0.63 cm. The same comment is made on the minimal deviation, ranging from 2% to 15.5%.

The advantage of a Forchheimer equation is the distinction of the linear terms (Darcy's law) and the inertial effects. In the next section, a linear model is applied to the low flux experimental points and a comparison is carried out.

5.2. LINEAR MODEL: DARCY'S LAW

Scatter was consequent at low flow measurements but a linear relationship between the hydraulic gradient and the flux of water seemed to be graphically consistent to these points. The linear regression was computed on the subjectively chosen low flow points. Figure 32 shows the linear relationship for the core 2B, tested upside down.

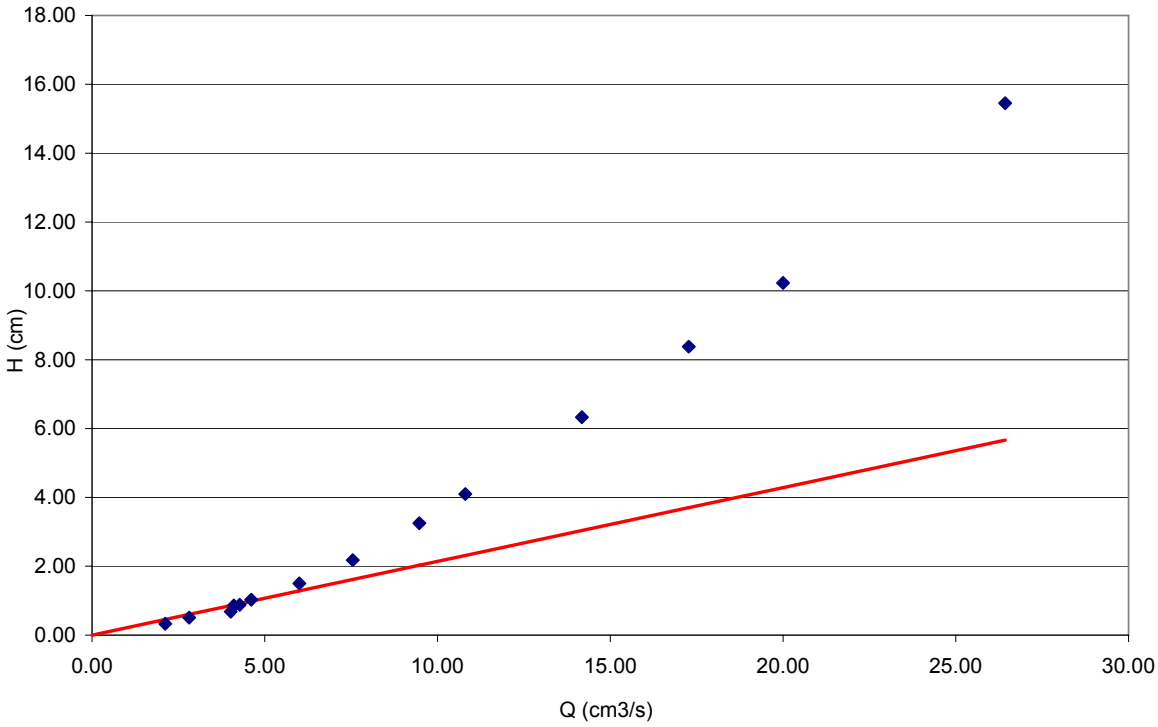

Figure 32 - Core 2B Upside Down – Linear Relationship between Head Gradient and Flux

The linear correlation is derived with a correlation factor γ:

Equation 41

$$\Delta H = \gamma \cdot Q$$

In this example, the coefficient γ = 0.2143 leads to a hydraulic conductivity of 0.61 cm/s.

Equation 42

$$K = \frac{1}{4aF\left(\frac{a}{R}, \frac{b}{R}\right)\gamma} = 0.606\, cm/s$$

The associated regression coefficient (R^2) was 0.981 and the associated standard error 0.61cm appeared to be reasonable. The scatter of points was taken into account by computing 95% confidence intervals of hydraulic conductivity. Results are summarized in Table 7.

Table 7 - Summary of 95% Confidence Intervals of Hydraulic Conductivity

Darcy's Law -Hydraulic Conductivity - 95% Confidence Interval						
	Initial		Top		Upside Down	
Core	Min	Max	Min	Max	Min	Max
1A			0.21	0.27	0.2	0.24
1B	1.88	2.22				
2A			0.57	0.7	0.49	0.6
2B			0.33	0.47	0.51	0.68
3B			0.3	0.37	0.08	0.09
3C			0.45	0.58	0.41	0.52

The 95% confidence intervals are still precise; the bandwidth of the confidence intervals doesn't go over 29% of the average hydraulic conductivity. The comparison of the hydraulic conductivities obtained either by application of quadratic model or from Darcy's linear law is graphed in Figure 33.

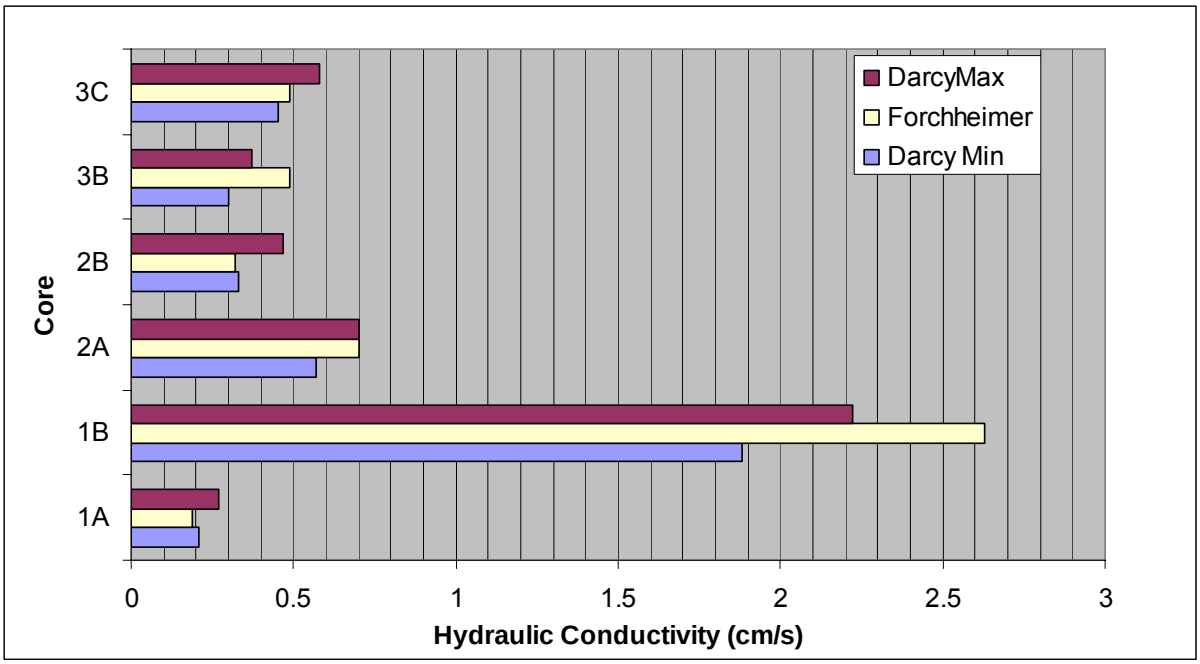

Figure 33 - Comparison of Quadratic and Linear model

The hydraulic conductivity computed from Forchheimer's model is represented by bright yellow bars bordered by the low and high values of the intervals. Results of the quadratic model globally fall within the range of values from the linear regression. However two exceptions subsist in cores 1B and 3B where the quadratic model goes over the upper value of the linear model respectively by 18% and 28%.

Until now, experiments were run on original cores, providing us the actual hydraulic potential of the porous asphalt of the three different roadways. In the following section, the PFC samples were manipulated in order to characterize the clogging phenomenon.

5.3. CHARACTERIZING THE CLOGGING PHENOMENON

Clogging remains one of the main issues with porous asphalt, since rubber particles and sediments change the hydraulic characteristics of the pavement (Section 2.4). The goal of this section is to understand the effects of clogging in terms of hydraulics. Note that the hydraulic conductivity obtained from the quadratic model is used in the following cases. The variability of results between the top and bottom experiments can be associated with the distribution of the grain size and no consistent trend appears.

Actual Rate of Clogging

The six cores were drilled and cleaned using the technique described in the methods section (Section 4.5). The hydraulic conductivity of the drilled cores was determined using Equation 39 from Forchheimer's model. The computed value of K may be corresponding to the original hydraulic conductivity of the porous asphalt when the pavement was installed in 2004. This assumption is limited by the fact that porous asphalt can remain permanently clogged (Section 4.5).

A comparison of the original and actual values of K provides explanation for the rate of clogging that porous asphalt is subject to at the different studied locations.

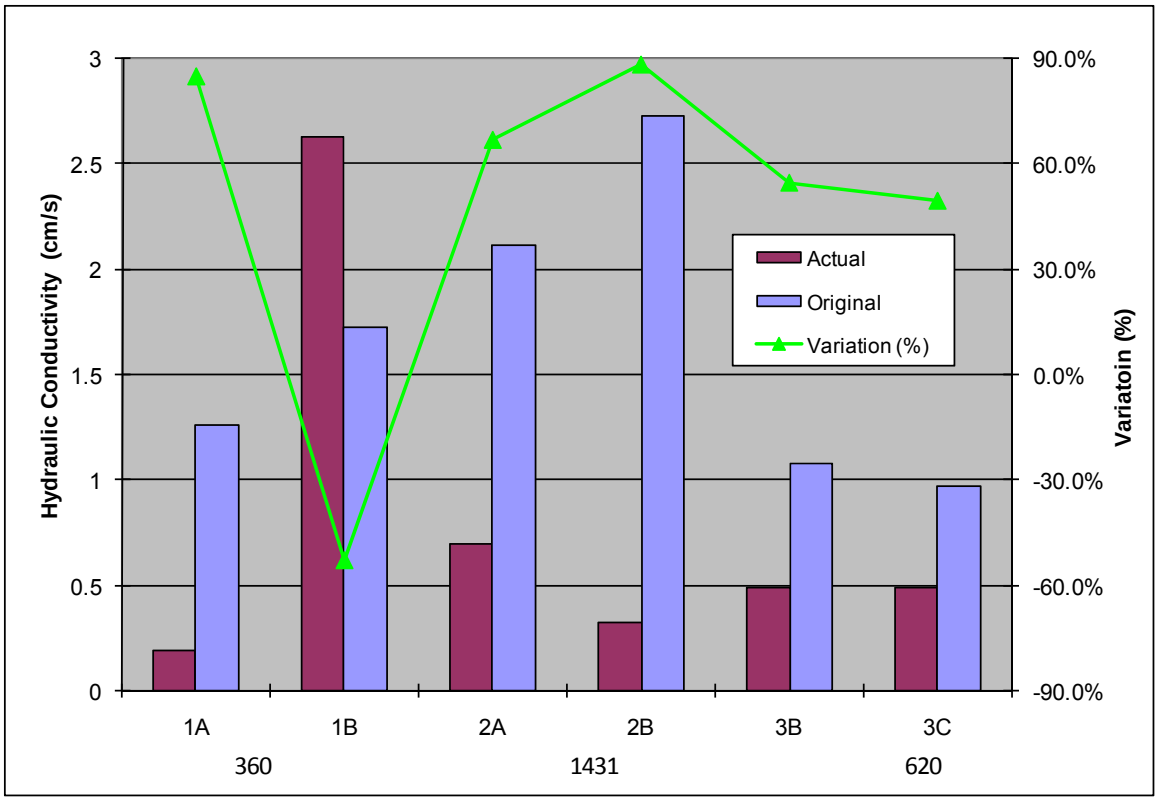

Figure 34 - Actual Decrease of Hydraulic Conductivity

Looking at Figure 34, the general trend is a higher hydraulic conductivity of the original cores. Only core 1B doesn't follow the tendency and observes a decrease from 2.6 cm/s to 1.7 cm/s. In the actual state, we have compared to the original hydraulic conductivities:

- A decrease of 50% in hydraulic conductivity on Loop 360; the original K value could be set as 1.5 cm/s, note that in this case one sample (1B) was not clogged.
- A decrease of 80% in hydraulic conductivity on RM 1431; the original K value could be set as 2.5 cm/s.
- A decrease of 50% in hydraulic conductivity on RM 620; the original K value could be set as 1.0 cm/s.

In general, the decrease in hydraulic conductivity reaches approximately 50% after 3 years of utilization besides on RM 1431 where particular conditions, such as the proximity to a large construction site, have contributed to a decrease estimated in average at 80%.

The pattern of 1B could also be explained by the fact that the core has been tested more than twelve times since it was the pilot core. The structure of the core could have been stressed by the torque applied by the measuring system: this would have led to the deformation of the matrix of grains and de facto to a change in hydraulic properties.

The actual decrease in hydraulic conductivity is induced by the presence of material clogging the voids of the samples. The volume occupied by the material leads to a decrease in porosity of the sample. Fair and Hatch (1933) derived the hydraulic conductivity as a function of the fluid properties and the size and packing of the porous medium (Equation 43).

Equation 43

$$K = \frac{g}{\upsilon} \cdot \frac{n^3}{(1-n)^2} \cdot \left[n \cdot \left(\alpha \sum_i \frac{f_i}{d_m} \right)^2 \right]^{-1}$$

Where α is a shape factor describing the geometry of the grains, f_i the fraction of sediments held between adjacent sieves, and dm is the geometric mean of the rate size of adjacent sieves. Since the fluid properties and the grain size of the samples have not changed between the two experiments, the change in hydraulic conductivity is derived as a function of the original 1 and actual 2 porosity numbers (Equation 44).

Equation 44

$$\frac{K_1}{K_2} = \frac{{n_1}^3}{{n_2}^3} \cdot \frac{(1-n_2)^2}{(1-n_1)^2}$$

The original porosity number was computed from Equation 44 and results are summarized in Table 8. The original air void content was taken as the one calculated using the water displacement method (Table 5).

Table 8 - Extrapolated Air void content

Core	Extrapolated Actual		Original	
	K (cm/s)	n	K (cm/s)	n
1A	0.19	0.131	1.26	0.228
1B	2.63	0.243	1.72	0.216
2A	0.7	0.169	2.11	0.232
2B	0.32	0.108	2.73	0.205
3B	0.49	0.154	1.08	0.194
3C	0.49	0.160	0.97	0.196

Porosity has sensibly increased for all the samples except 1B. The pattern of 1B was explained above and corresponds to the deformation of the grain matrix. The porosity has decreased by 0.07 in average in comparison to the 50% average decrease in hydraulic conductivity. The removed grains have a major effect on the increase of hydraulic conductivity since sand clogs critical throats of the porous medium. In the actual state, the porosity has decreased by:

- 0.04 on Loop 360 corresponding to a 15% clogging of the air void content
- 0.08 on RM 1431 corresponding to a 37% clogging of the air void content
- 0.04 on RM 620 corresponding to a 19% clogging of the air void content

The decrease in porosity is also in correlation with the amount of sediments extracted from the cores during the cleaning operation (Table 9). The decrease of hydraulic conductivity can also be associated with the effect of drilling as well as the potential deformation of the samples.

Factors & Consequences of clogging

During the cleaning operation, the extracted mass was conserved and weighed. The residual was principally composed of sediments such as sand grains. This section focuses on the extracted sediments and their impact on hydraulic conductivity, as well as the effect of traffic on the volume of sediments.

The extracted mass was recorded for all cores besides one from Loop 360 (1B). Results are reported in Table 9:

Table 9 - Mass of Extracted Sediments

Core	Mass extracted (g)
1A	13.79
1B	
2A	9.45
2B	27.82
3B	4.31
3C	2.86

The mass of sediments ranges from 2.9 g to 13.8 g except for core 2B whose extracted mass reached 27.2 g.

In the following development, the extracted mass was normalized by the volume of the core in question. The first focus was on quantifying the increase in hydraulic conductivity induced by extracted mass. The K value was determined for each drilled core before and after the cleaning operation. The increase of K value was reported as a percentage of K value associated to the non-cleaned drilled core (Figure 35).

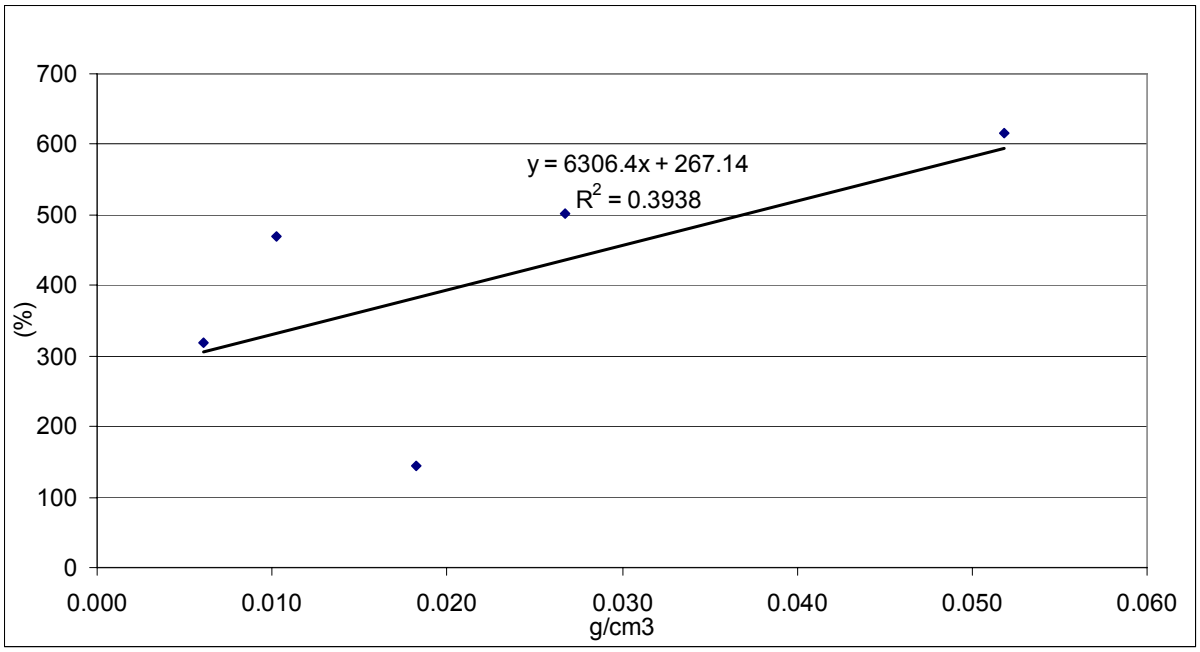

Figure 35 - Increase of Hydraulic Conductivity versus Normalized Extracted Mass

The scatter of points is important and no specific relationship can be established from the experimental data. One could at least note that the more sediment removed, the higher the increase in hydraulic conductivity.

The second interest is the impact of traffic density on the mass recovered from the PFC samples. Once again in Figure 36, the extracted mass was normalized by volume and the daily traffic was reported in thousand of cars.

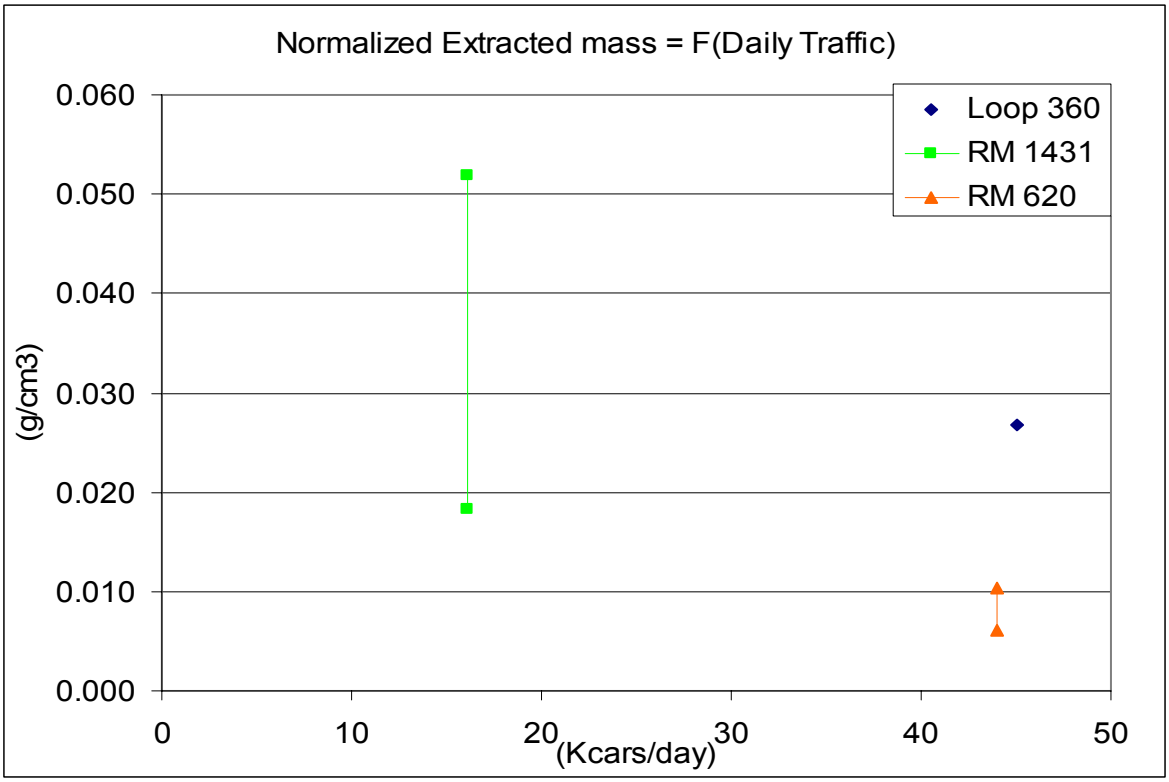

Figure 36 - Influence of Daily Traffic on Normalized Extracted Mass

The highest normalized mass was removed from RM 1431 even if the daily traffic (17,000 cars/day) is lighter than on the two other highways. This pattern was explained earlier and could be attributed to the proximity of a large construction site. The porous asphalt texture is also damaged at some locations.

There is no general trend appearing from the traffic density. The discrepancy of results between Loop 360 and RM 620 might be explained by the type of traffic and not the load. The porous asphalt samples on RM 620 were extracted in proximity to a large shopping mall and a large intersection which may induce a permanent clogging of the pavement.

A first evaluation of influence of sediments on permeability was given in Section 2.2 (Fwa et al., 1999). Figure 11 described the deterioration of permeability versus the mass of clogging soil added. In a similar way, Figure 37 describes the decrease of hydraulic conductivity versus the normalized accumulated mass for the six experimented cores.

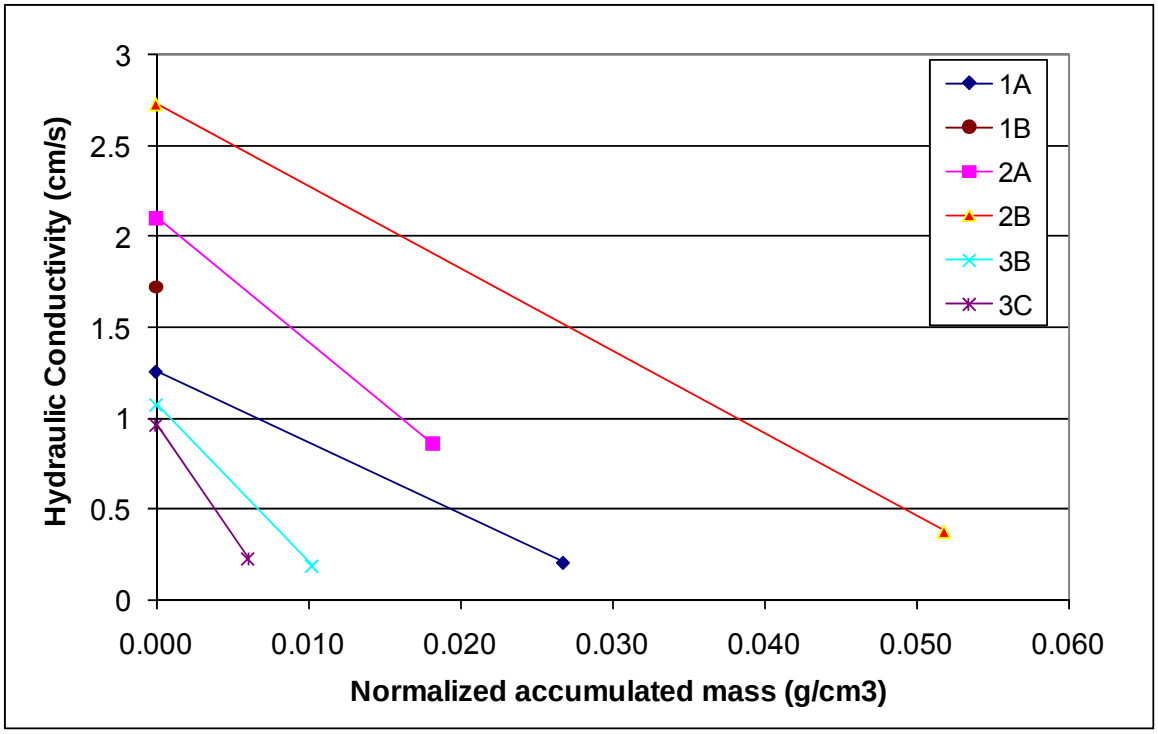

Figure 37 - Influence of Accumulated Sediments on K

At each location, the slopes of K reduction are subjects to variations but the trends between both cores of the same roadway concord. In analogy to Fwa (1999) and looking at the original (cleaned) hydraulic conductivity, the aggregate has a different matrix structure at the three locations. Results of Figure 37 will be implemented with a new set of experiments in the future. The implemented results will lead to the identification of a trend at the different locations.

Influence of Drilling

Experimental cores were successively drilled from the roadway, sliced up on their bottom and finally drilled on their center. This part studies the contribution of drilling to the change of hydraulic conductivity. Table 10 summarizes the hydraulic conductivities calculated initially from the plain cores and from the drilled cores before cleaning.

Table 10 - Hydraulic Conductivity of Initial and Non-Cleaned Drilled Cores

K (cm/s)	Top Initial	Drilled Initial
1A	0.19	0.21
1B	2.63	1.13
2A	0.7	0.86
2B	0.32	0.38
3B	0.49	0.19
3C	0.49	0.23

Thinner cores of volume lower than 470 cm^3, such as the ones from RM 620, were subject to a 30% decrease in hydraulic conductivity. However thicker cores with a higher volume (higher than 520 cm^3) were subject to a 10% increase in hydraulic conductivity. This pattern could be explained by the principle of testing apparatus: the flow is only radial in the drilled core experiment and doesn't have any vertical component. The fact that thinner cores get clogged could be related to the low number of effective pores participating to the radial flow.

Note that the trend of core 1B was not taken into account since the core could have endured a deformation of its structure. Since no particular mathematical trend has been discovered, it is unrealistic to differentiate the real contribution of clogging to the drilling effect.

5.4. RADIAL FLOW DISTRIBUTION

Characterizing the radial flow distribution was carried out at different levels. The first level was the use of a solution of Potassium Permanganate in order to verify the isotropy of the radial flow. Using a visual criterion, the dye seemed to flow out equally around the circumference of the core, as observed in Figure 38.

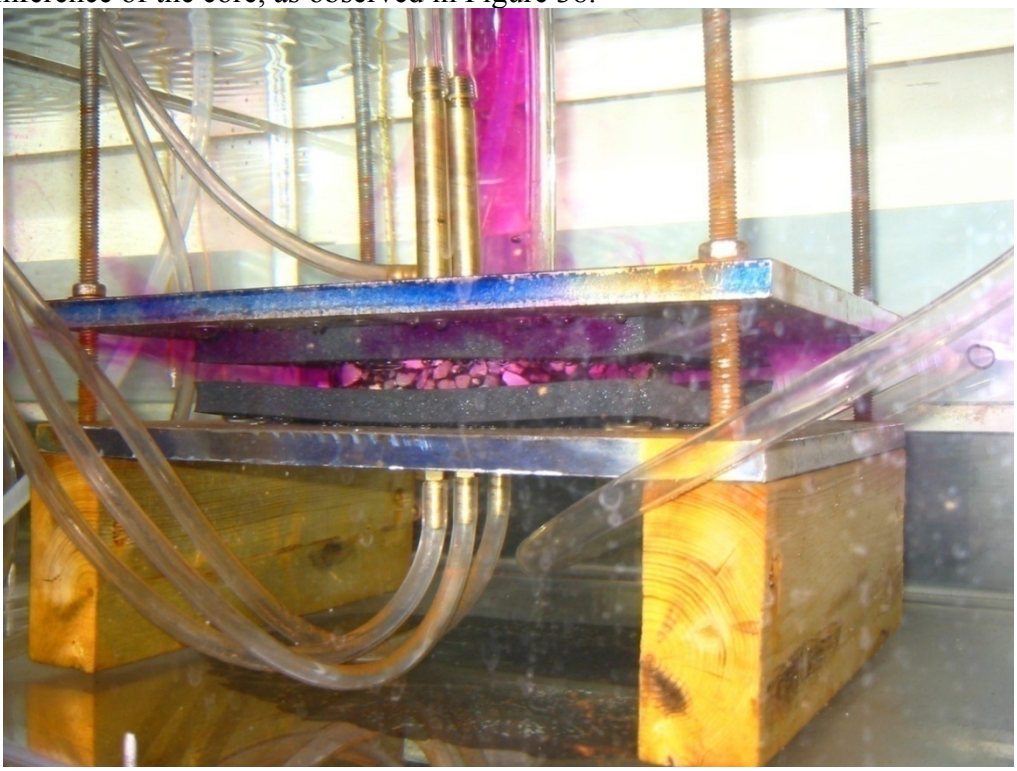

Figure 38 - Isotropy of the Radial Flow – Test with $KMnO_4$

The last level of study was the determination of head contours. The head was measured at different radial positions of the core by an inclined manometer whose inclination was set to 17° or 23°. Experimental runs were performed at different angular positions (0°, 20° and 180°) on core 1B, whose results are summarized in Figure 29. There is no significant discrepancy in head gradient between the experiments and proof is that the quadratic model has a small associated standard error (Equation 37).

Results of head contours were limited by the head gradients measured by the manometer: at some radial positions, the head gradient would be negative. The relatively low velocity of the flow through the pavement dismisses the theory of a Venturi effect. In order to keep the accuracy of the study, head contours are not reported in this thesis and possible improvements are discussed in Section 6.3.

The geometry of the experimental system induces a transitional to laminar flow through the tested asphalt core. Two models were used to describe the evolution of the head gradient as a function of the flux: a quadratic model taking into account the inertial effects and a Darcy's linear model on the low flow points. Results of hydraulic conductivity have revealed the importance of clogging and the influence of the highway environment. Hydraulic properties of the pavement at the three locations are summarized in the next chapter.

6. CONCLUSIONS

Different experiments and methods were used to determine the hydraulic properties of samples of porous asphalt. PFC cores were extracted on March 14, 2007. The porosity was evaluated either by analyzing the image of a half core filled with fluorescent epoxy or by the water displacement method. In addition, a testing apparatus was designed and built to determine the hydraulic conductivity of the samples.

6.1. GENERAL TREND

In terms of porosity, the aggregate was designed with an effective porosity of about 20%. The measured air void contents confirm the specifications after 3 years of utilization. Results were relatively homogeneous between samples. The image analysis method has to advantage of revealing the structure of the aggregate: grain and void sizes, interpretation of the kinematical flow through the interconnected voids can be observed. However it is recommended in the future to use the water displacement method for the following reasons:

- the water displacement method remains relatively accurate,
- the image analysis method monopolizes a core, unusable after operation,
- the preparation of the cores during the image analysis method requires the vacuum of hot epoxy through the pores: binders are dissolved and sediments flushed out.

In terms of hydraulic conductivity, results have shown an actual potential of about 0.5 – 0.6 cm/s besides on Loop 360 where results were disparate. Since the Reynolds numbers were high during the experiments, inertial effects were interfering with the viscous forces

and two models were fit to the experimental points. A quadratic model or Forchheimer model takes both effects into account; the standard errors associated to the models were reasonable fluctuating from 0.19 to 0.63 cm. A linear model or Darcy's model was fitted to the low flow points. The standard errors are acceptable (about 0.7cm) and the bandwidth of the confidence intervals didn't go over 29% of the hydraulic conductivity.

The clogging phenomenon is a reality and was observed and quantified during the experiments. The original hydraulic conductivity was not estimated since no data was available at this point but values are reported compared to the definitive clogging of the pavement. After three years of utilization, the decrease in hydraulic conductivity averages 50% and the decrease of air void content averages 0.04. These trends are of course subjects to variations according to the locations. The more sediment removed, the higher the hydraulic conductivity but no specific correlation of clogging versus traffic density was observed. Finally, the drilling operation influences the hydraulic conductivity according to the size of the cylindrical sample.

6.2. SPECIFIC LOCATIONS

On Loop 360, the air void content was reported to be 21.6% and the actual hydraulic conductivity fluctuating between 0.2 cm/s and 2.6 cm/s. There is indeed an important discrepancy between the two samples. Estimating the clogging, the highway seemed to have a decrease of 50% in hydraulic conductivity and 15% of the effective pores are clogged. Note that results from the pilot core have changed after the drilling operation, changes attributed to the deformation of the sample matrix.

On RM 1431, the porosity was evaluated to be 21.6% and the actual hydraulic conductivity fluctuating between 0.5 cm/s and 0.6 cm/s. The pavement has actually a reduction estimated at 80% of its hydraulic conductivity and at 37% of its porosity. The large percentage is tentatively explained by the presence of a large construction site at proximity of the extraction site: the sediments removed were much higher.

On RM 620, the effective porosity was reported to be 19.8% and the actual hydraulic conductivity 0.49 cm/s. The actual reduction in hydraulic conductivity was estimated at 50% and the clogged air void content was estimated at 19%. The highway seemed more clogged than the other roads since the maximum definitive hydraulic conductivity is estimated at 1.0 cm/s. The higher clogging of this road could be correlated with the proximity of a large intersection and a shopping mall inducing more debris in the pavement.

6.3. LIMITATIONS

The measure of air void content didn't encounter any major difficulties but the one of hydraulic conductivity did. The interpretation of hydraulic conductivity was limited at two levels.

The first limitation was the domain of operation of the testing apparatus. The dimensions of the standpipe and the cylindrical samples were respectively too large and too small inducing a high Darcy's velocity within the pavement. The inertial effects were consequent, associating variations to the determination of the hydraulic permeability. At this level, two actions are possible in the future in order to minimize the collateral effects of a turbulent flow through the samples: the inner radius of the standpipe a has to

decrease and the radius of the pavement R has to increase; a second set of cores should help us to determine accurately the intrinsic permeability of the pavement.

The second limitation was the measure of the head of water with the inclined manometer board. At some radial positions, the head gradient was reported to be negative. The radial measures would have helped to quantify and characterize the inertial effects within the pavement as well as the contours would have confirmed the developed theory. This pattern was observed with every core at low flow measurements. The manometer board was changed twice and rebuilt one time, the connectors were tested and the air was always flushed out. The problem seemed to occur at the interface between the core and the rubber gasket.

6.4. FUTURE WORK

A new set of 8 inches cores was extracted on February 27th, 2008. The same procedure will be carried out on these cores for determining their porosity and hydraulic conductivity. The larger radius will help to dampen the inertial effects within the cores. The comparison of results of this set with the present set will help to determine the evolution of clogging in time as well as status on the hydraulic properties of the pavement.

Another axis of the project on PFC is the correlation between laboratory results and in-situ measurements. An in-situ falling head permeameter is used on site and the hydraulic conductivity will be determined by comparison with the hydraulic characteristics evaluated in laboratory. This constitutes an easy and efficient way to determine directly the hydraulic properties of Porous Friction Course in Austin.

The final axis of the project is the development of a numerical model of flow within porous asphalt whose parameters will be based on the hydraulic properties evaluated through these experiments.

APPENDICES

APPENDIX A: PERMEAMETERS & MEASURING EAV CONTENTS

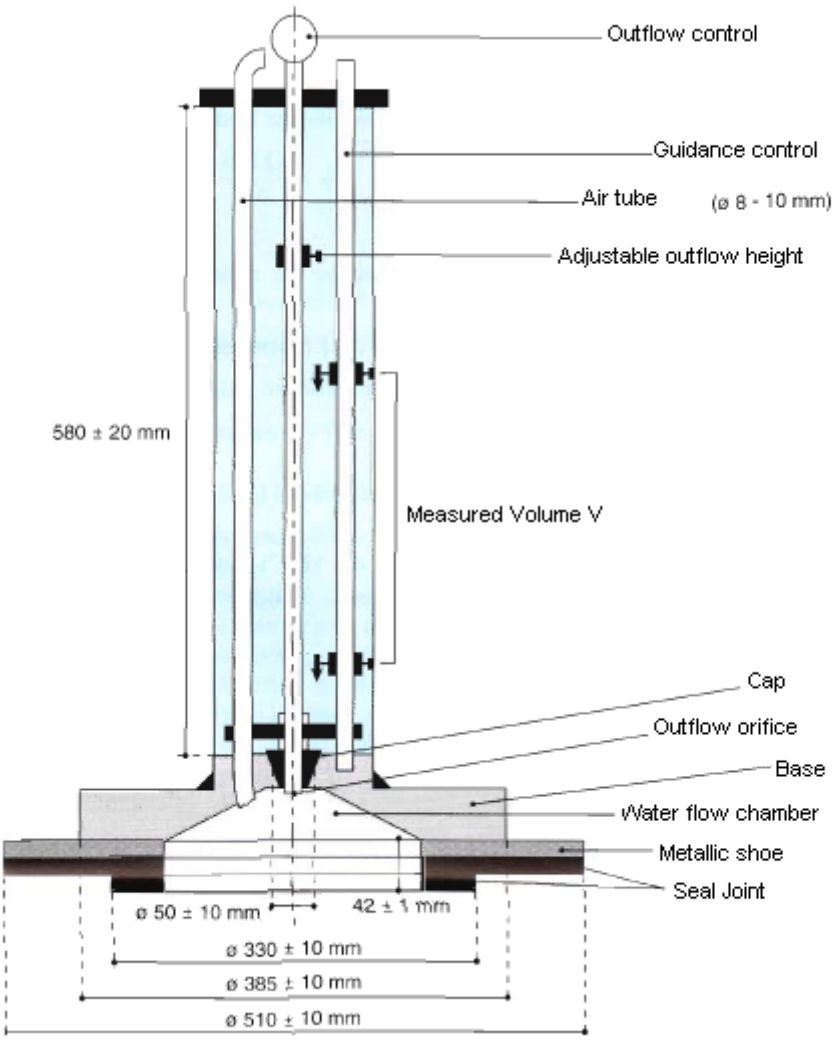

Figure 39 - In-Situ Field Permeameter (Di Benedetto et al., 1996)

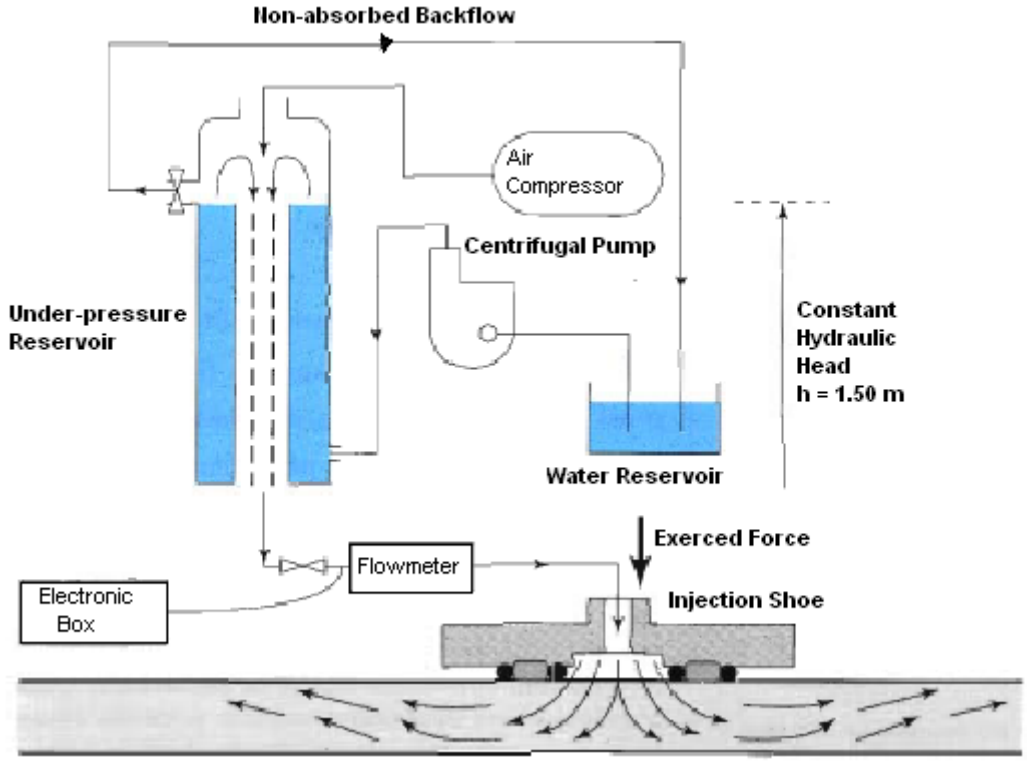

Figure 40 - Constant Head – Automatic Permeameter (Di Benedetto et al., 1996)

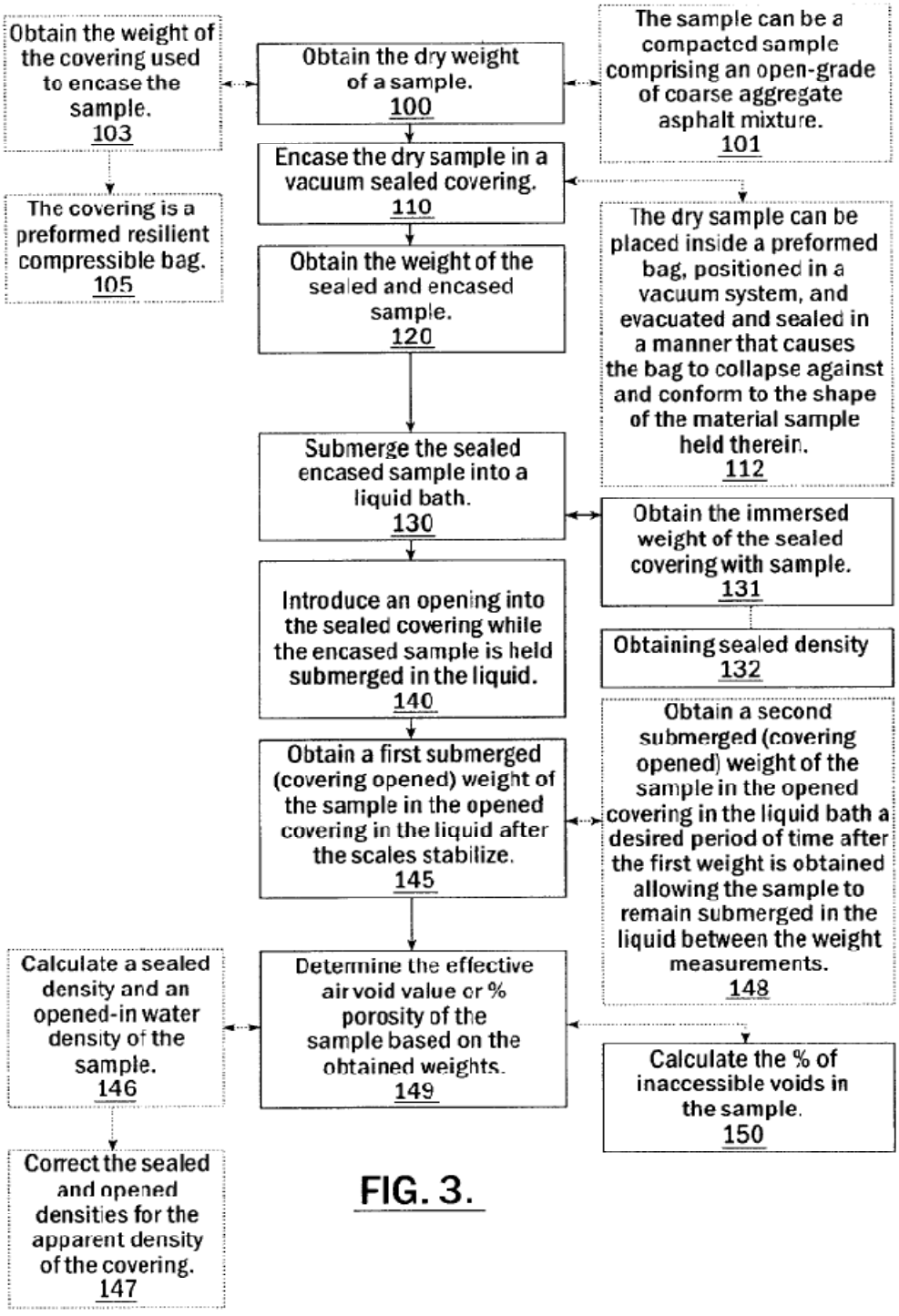

FIG. 3.

Figure 41 - Determination of the EAV content according to Regimand et al. (2003)

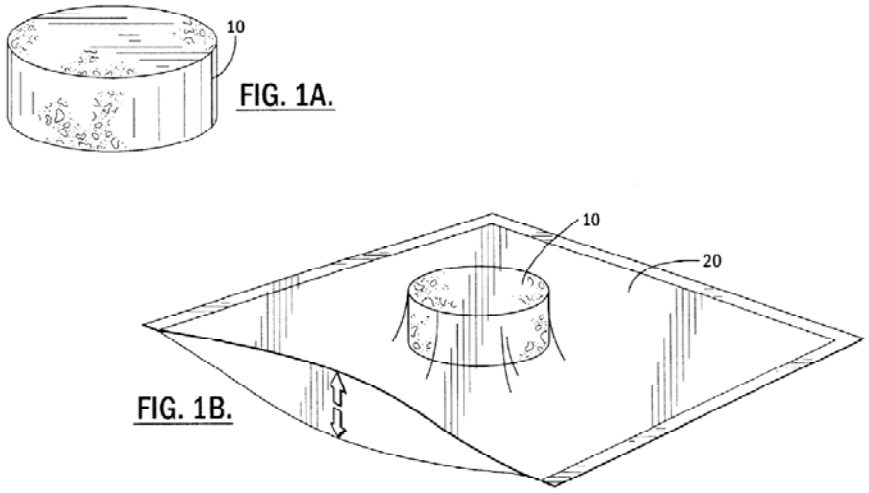

Figure 42 - Sample and its plastic bag (Regimand et al., 2004)

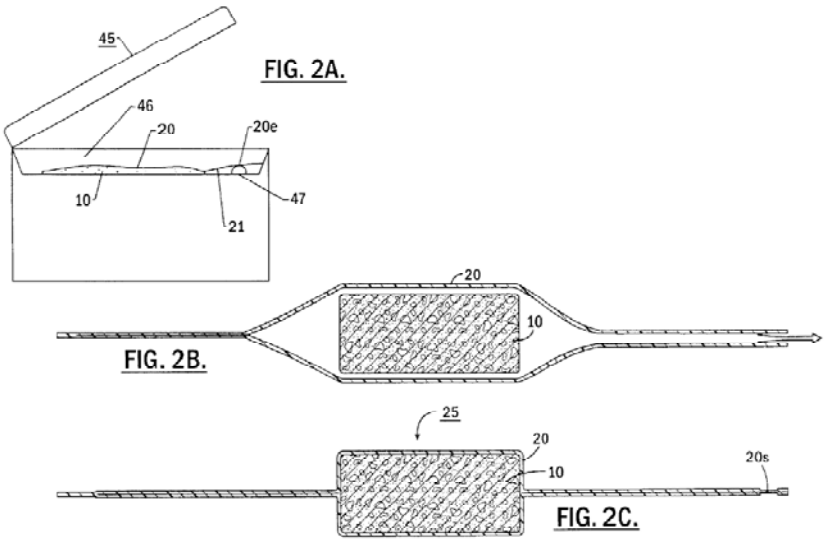

Figure 43 - Core-lock air vacuum and the core sealed in plastic bag (Regimand et al., 2004)

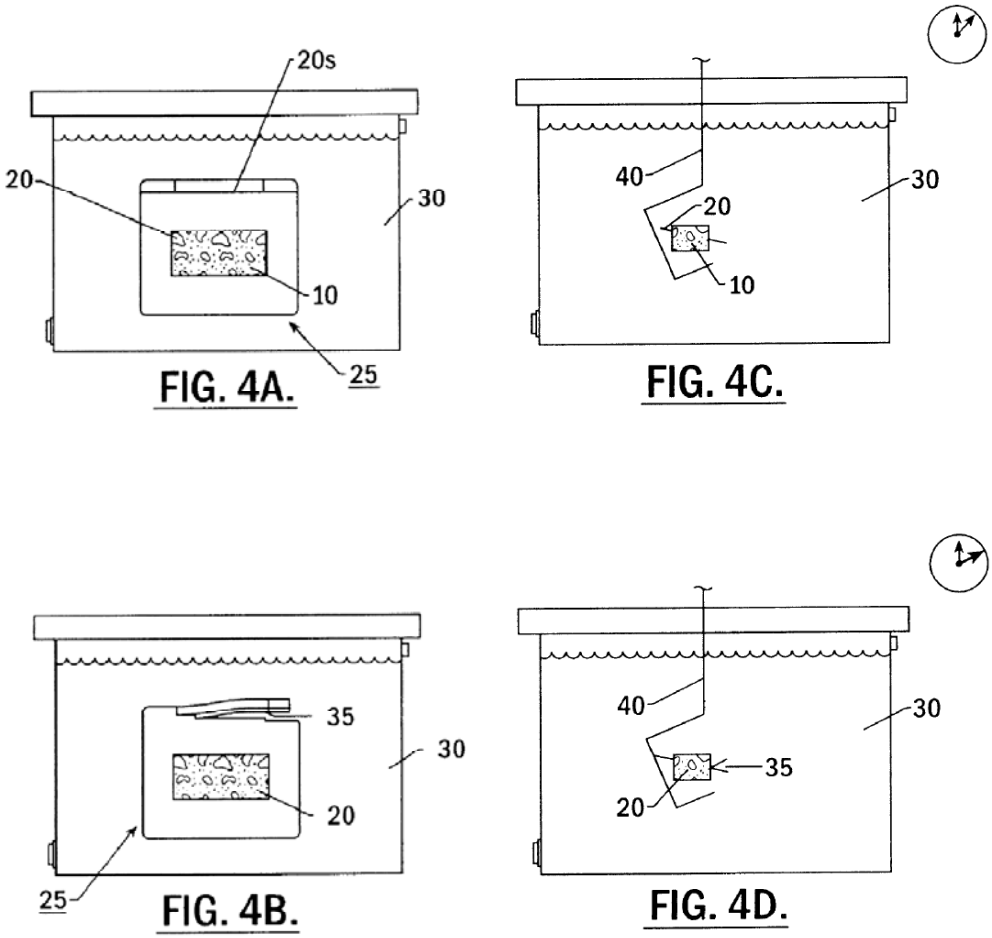

Figure 44 - Measuring the weights of the core with and without the plastic bag (Regimand et al., 2004)

APPENDIX B: WEIGHT & CHARACTERISTICS OF CORES

Table 11 - Weight & Geometric Characteristics of Cores – Sliced Cores

	Thickness (mm)			Diameter (mm)			Volume (cm3)	Shape Factor
Sample	min	max	avg	min	max	avg		
1A	22.58	35.24	**28.91**	150.34	151.01	**150.675**	515.5	0.992
2A	24.92	33.17	**29.045**	150.57	150.6	**150.585**	517.3	0.994
2B	28.46	31.95	**30.205**	150.35	150.41	**150.38**	536.5	1.01
3B	21.46	25.49	**23.475**	150.89	150.94	**150.915**	419.9	0.904
3C	27.66	24.29	**25.975**	151.69	151.69	**151.69**	469.4	0.946

Table 12 - Weight & Geometric Characteristics of Cores – Original Cores

	Thickness (mm)			Diameter (mm)			Bag Wt.	Dry Wt.	Water Wt. with Bag	Ga	Water Wt. without bag	Total Volume of the core	Volume of the grains	Porosity
Sample	min	max	avg	min	max	avg	(grams)	(grams)	(grams)	????	(grams)	(cm3)	(cm3)	
	43.4	45.6	**44.5**	150.21	150.31	**150.26**	30.1	1356.7	609.3	1.835	779.5	748.79	578.24	0.228
	35.25	39.52	**37.385**	150.72	150.85	**150.785**	30.4	1162.1	531.5	1.867	667.9	631.79	495.09	0.216
	31.1	40.02	**35.56**	150.14	150.52	**150.33**	30.1	1097.9	487.8	1.823	629.1	611.25	469.64	0.232
	39.66	41.93	**40.795**	150.15	150.71	**150.43**	30.4	1238.8	561.8	1.852	700.6	678.27	539.17	0.205
	37.88	42.44	**40.16**	150.27	151.17	**150.72**	30.2	1302.9	612.7	1.91	746.8	691.49	557.10	0.194
	38.26	40.79	**39.525**	150.69	151.08	**150.885**	30.9	1273.5	599.5	1.913	731.2	675.26	543.27	0.195

ϑ (˚C) 20

ter (g/cm3) 0.99821

nensions of bag	Bag Wt.(gr)	Length (cm)	Width (cm)	Thickness of one layer (mm)	Volume of the bag (cm3)
	30.1	30	22.5	0.223	30.1
	30.4	30	22.5	0.225	30.4
	30.1	30	22.5	0.223	30.1
	30.4	30	22.5	0.225	30.4
	30.2	30	22.5	0.224	30.2
	30.9	30	22.5	0.229	30.9

te : we consider that the plastic bag has a density of 1g/cm3.

Image Analysis Method – Cross Section of Cores Filled with Fluorescent Epoxy

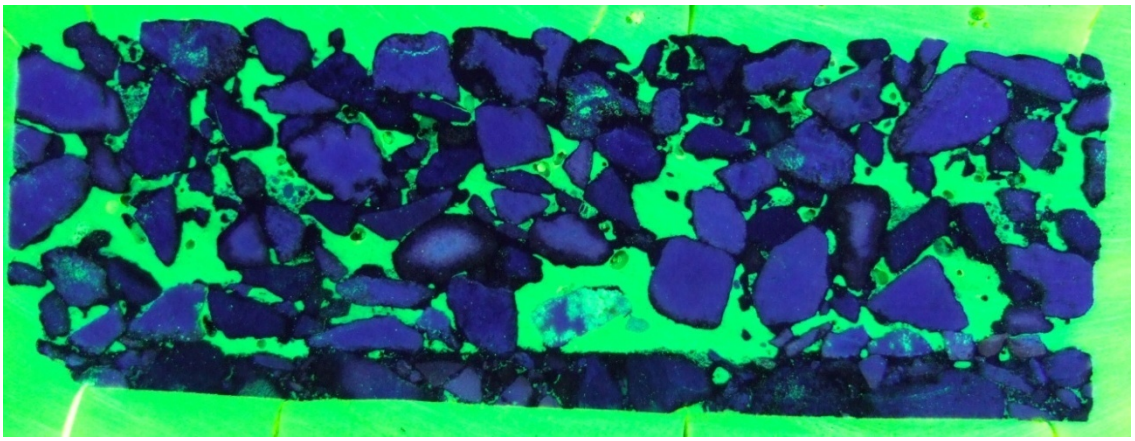

Figure 45 - Loop 360 – Core 1C – September 07 - Face A

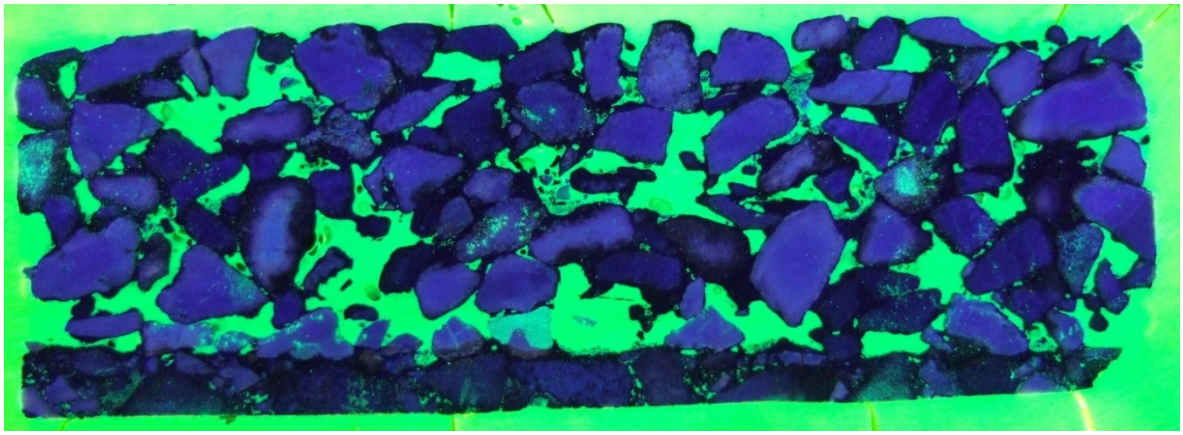

Figure 46 - Loop 360 – Core 1C – September 07 - Face B

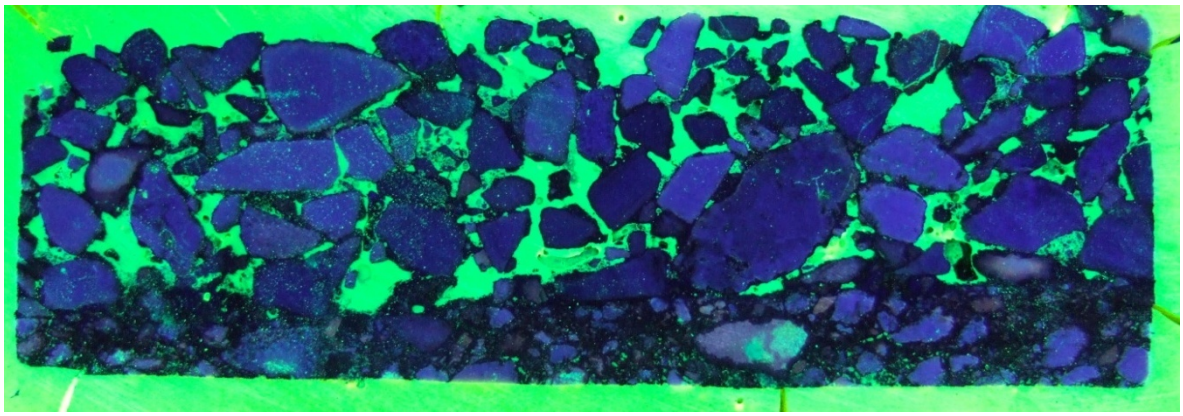

Figure 47 - RM 1431 – Core 2C – September 07 - Face A

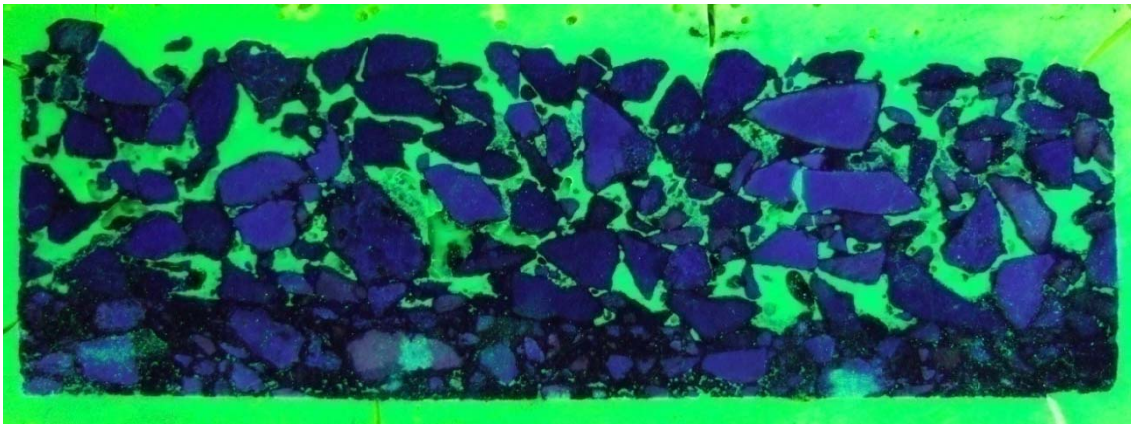

Figure 48 - RM 1431 – Core 2C – September 07 - Face B

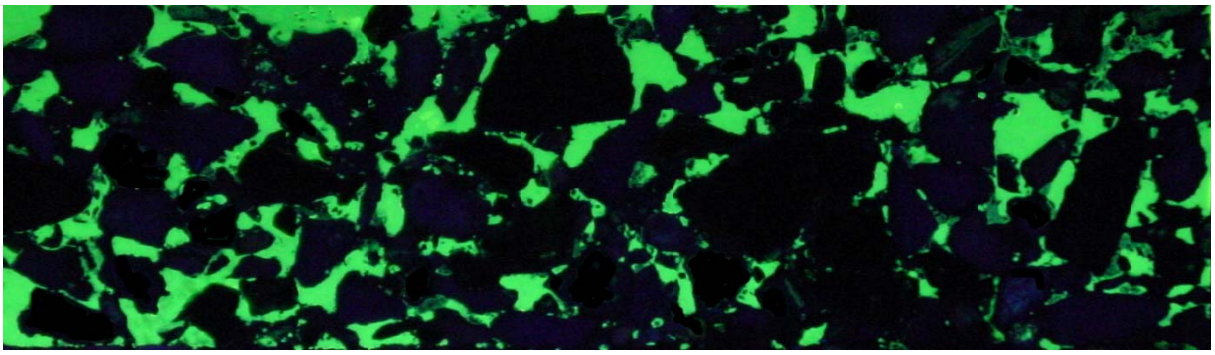

Figure 49 - RM 620 – Core 3A – June 07

APPENDIX C: EXPERIMENTAL SYSTEM – BLUEPRINTS

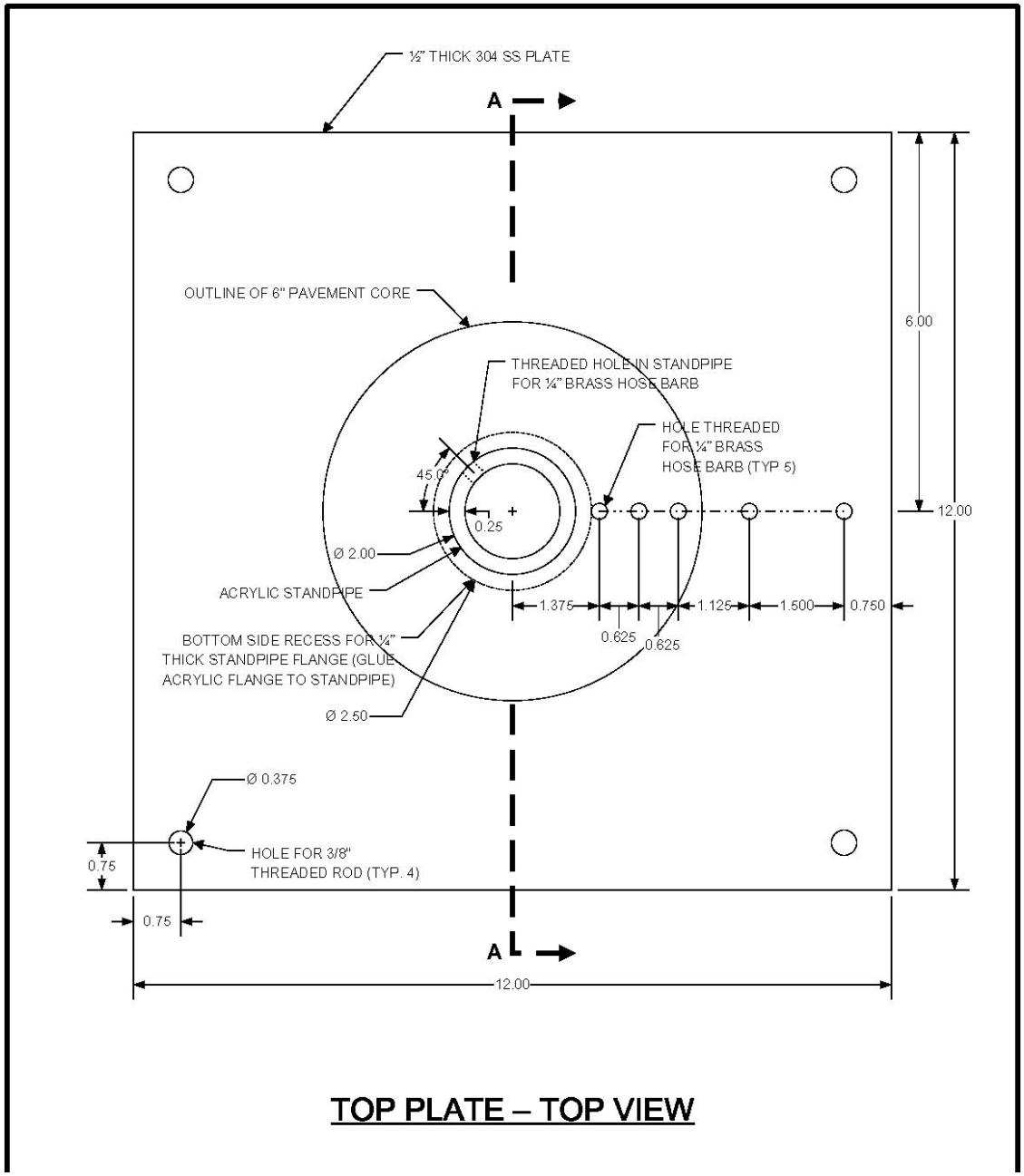

Figure 50 - Top Plate & Top View

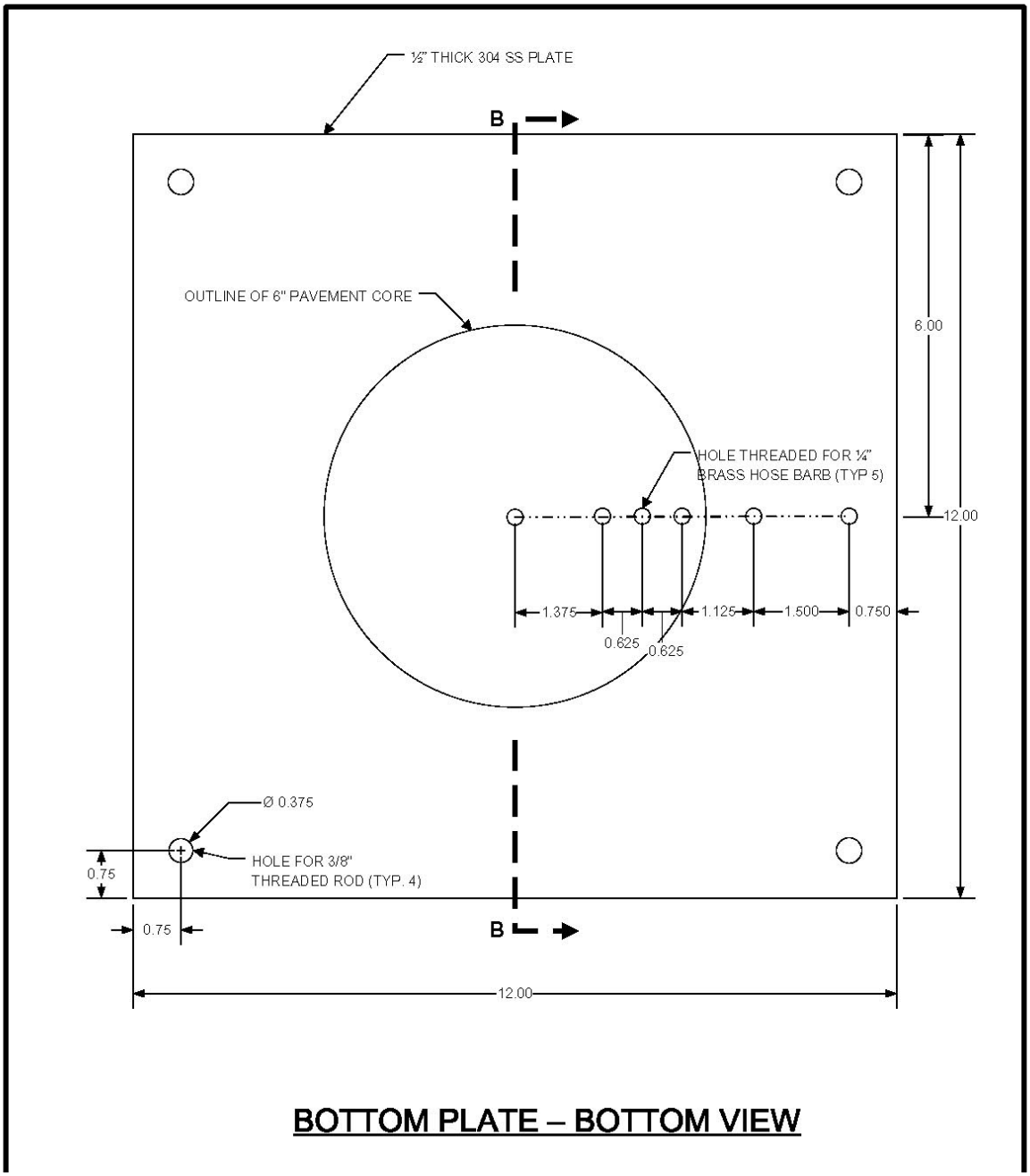

Figure 51 - Bottom Plate - Bottom View

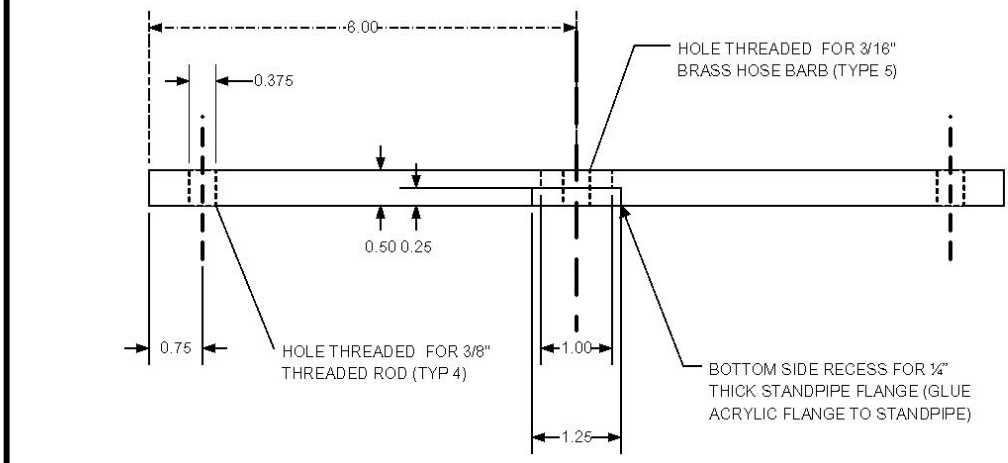

SECTION A-A

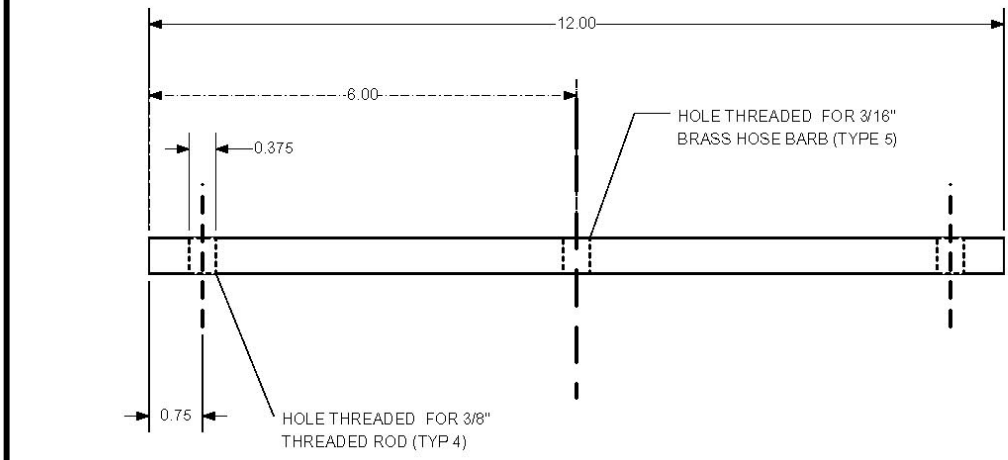

SECTION B-B

Figure 52 - Side View of Top and Bottom Plates

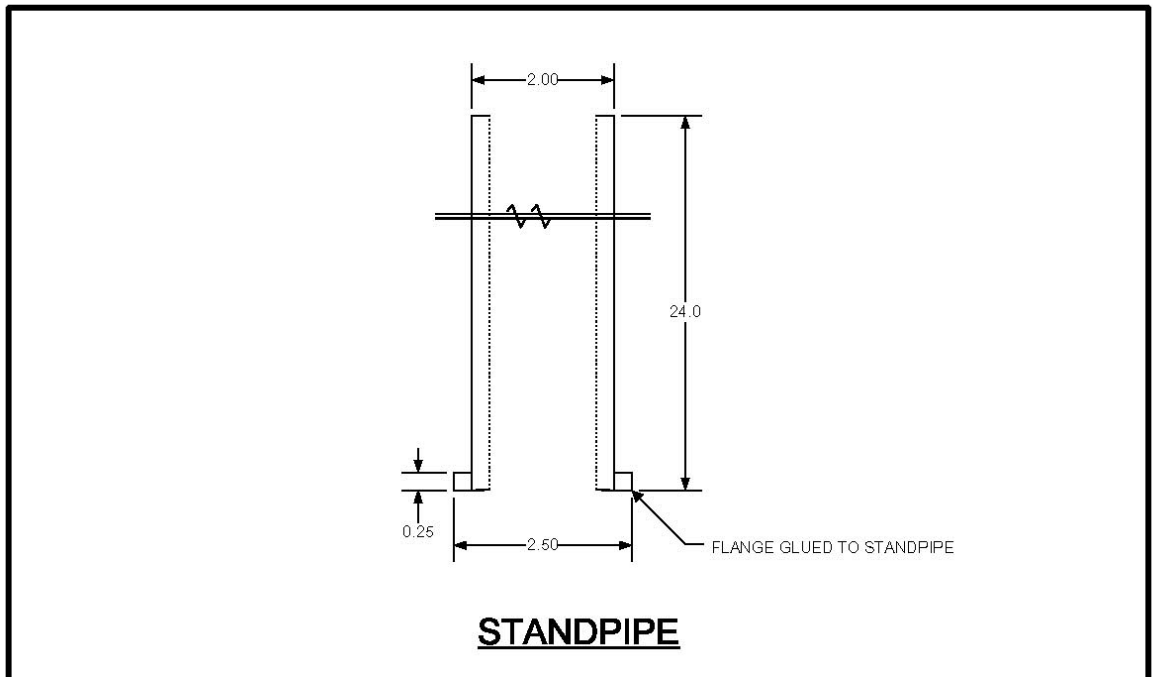

Figure 53 - Standpipe

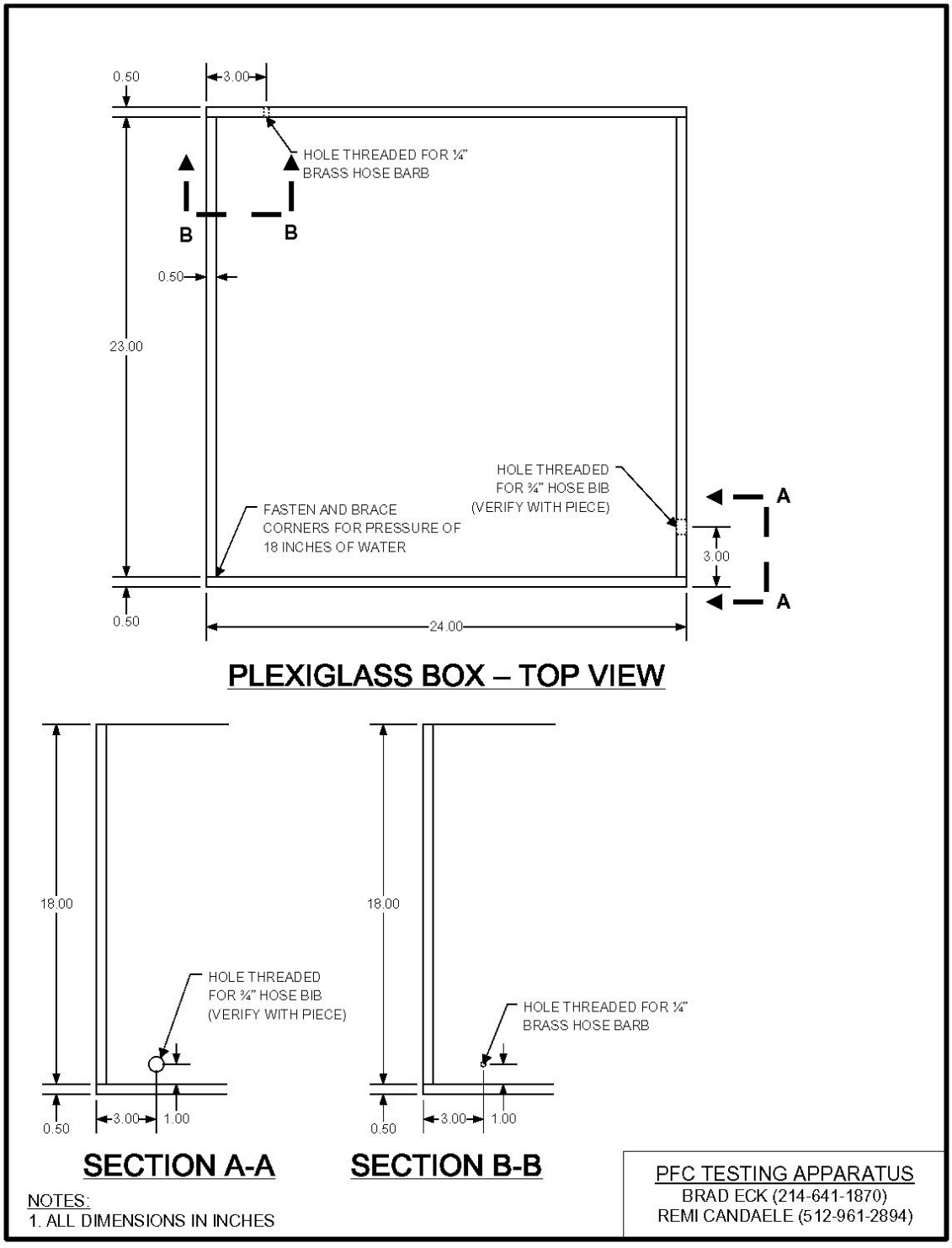

Figure 54 - Plexiglas Box

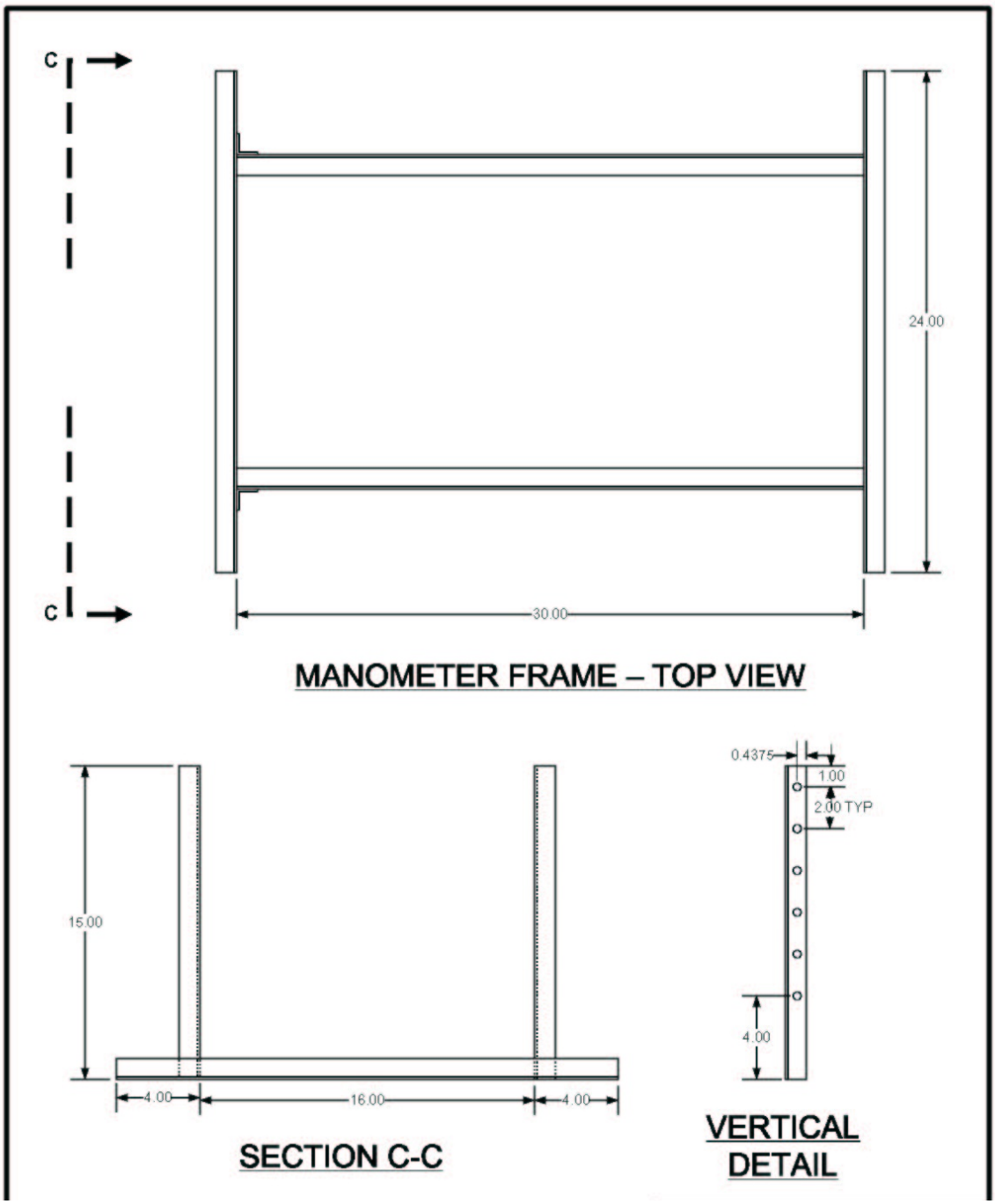

Figure 55 - Manometer Frame

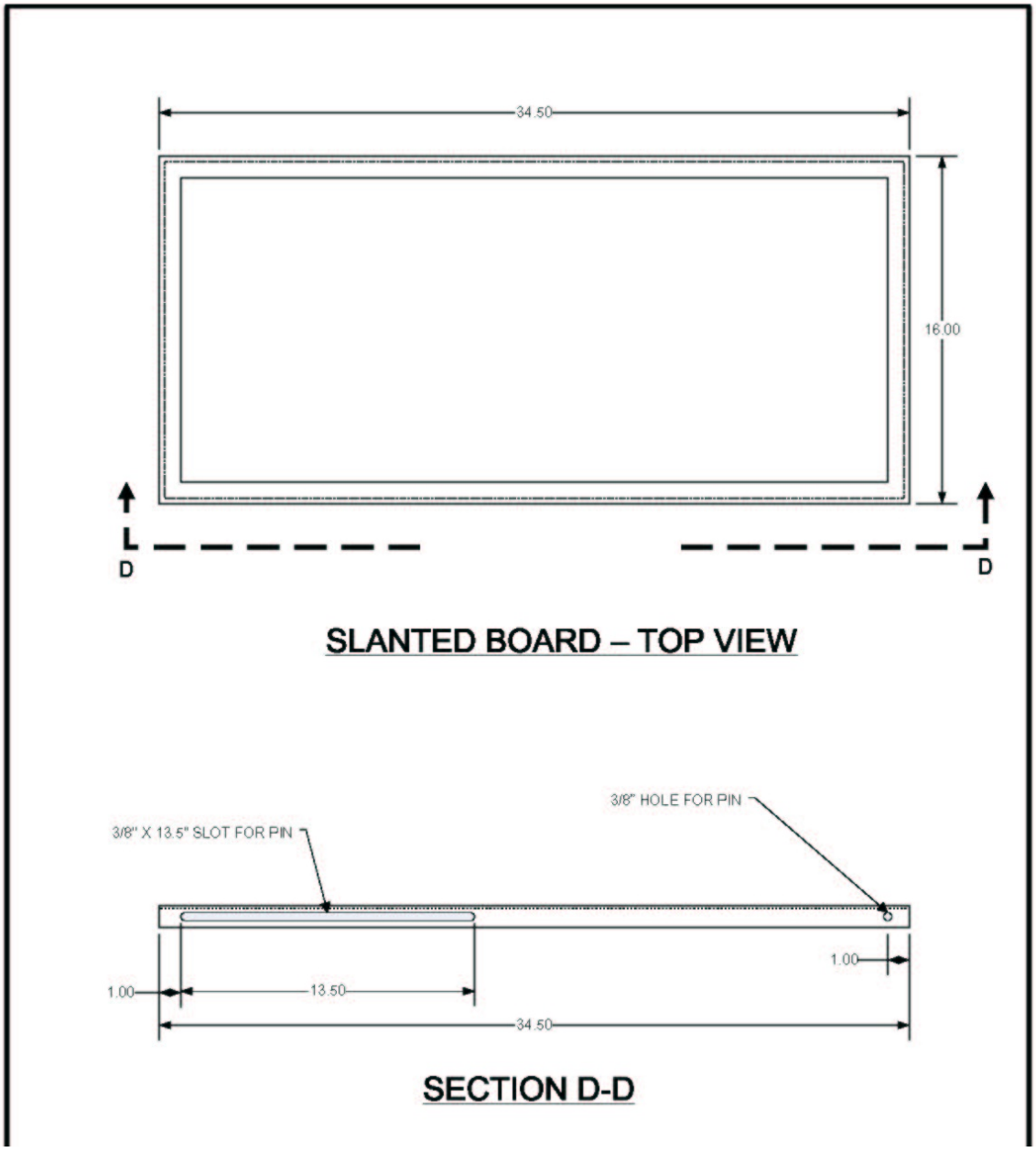

Figure 56 - Slanted Board

APPENDIX D: POROUS FRICTION COURSE AGGREGATE - WATER PROPERTIES

Table 13 - Water Properties (FHA, 2007)

Table A.6. Physical Properties of Water at Atmospheric Pressure in S1 Units

Temperature		Density[2]	Specific[2] Weight	Dynamic[3] Viscosity	Kinematic[4] Viscosity	Vapor Pressure	Surface[1] Tension	Bulk Modulus
Centigrade	Fahrenheit	Kg/m^3	N/m^3	$N\text{-}s/m^2$	M^2/s	N/m^2 abs.	N/m	GN/m^2
0°	32°	1,000	9,810	$1.79x10^{3}$	$1.79x10^{5}$	611	0.0756	1.99
5°	41°	1,000	9,810	$1.51x10^{-3}$	$1.51x10^{-6}$	872	0.0749	2.05
10°	50°	1,000	9,810	$1.31x10^{-3}$	$1.31x10^{-6}$	1,230	0.0742	2.11
15°	59°	999	9,800	$1.14x10^{-3}$	$1.14x10^{-6}$	1,700	0.0735	2.16
20°	68°	998	9,790	$1.00x10^{-3}$	$1.00x10^{-6}$	2,340	0.0728	2.20
25°	77°	997	9,781	$8.91x10^{-4}$	$8.94x10^{-7}$	3,170	0.0720	2.23
30°	86°	996	9,771	$7.97x10^{-4}$	$8.00x10^{-7}$	4,250	0.0712	2.25
35°	95°	994	9,751	$7.20x10^{-4}$	$7.24x10^{-7}$	5,630	0.0704	2.27
40°	104°	992	9,732	$6.53x10^{-4}$	$6.58x10^{-7}$	7,380	0.0696	2.28
50°	122°	988	9,693	$5.47x10^{-4}$	$5.53x10^{-7}$	12,300	0.0679	
60°	140°	983	9.643	$4.66x10^{-4}$	$4.74x10^{-7}$	20,000	0.0662	
70°	158°	978	9.594	$4.04x10^{-4}$	$4.13x10^{-7}$	31,200	0.0644	
80°	176°	972	9,535	$3.54x10^{-4}$	$3.64x10^{-7}$	47,400	0.0626	
90°	194°	965	9,467	$3.15x10^{-4}$	$3.26x10^{-7}$	70,100	0.0607	
100°	212°	958	9,398	$2.82x10^{-4}$	$2.94x10^{-7}$	101,300	0.0589	

[1]Surface tension of water in contact with air
[2]Typical values for sea water are approximately 3 percent higher
[3]Typical values for sea water are approximately 7 percent higher
[4]Typical values for sea water area approximately 4 percent higher

Table 14 - Aggregate Grain Size Distribution (Alvarez et al, 2006)

Table 11. Summary of Characteristics of American OGFC and Non-North American PA Mixtures (continued)

	Australia (26)				*South Africa (16)*		*NCAT (6, 21)*		*TxDOT (1)*			
	OG 10	OG 14	OG 20	Tolerance	Min.	Max.	OGFC Min.	OGFC Max.	PFC-PG 76 Min.	PFC-PG 76 Max.	PFC-A-R Min.	PFC-A-R Max.
Gradation, mm (inch)												
45 (1.77)												
31.5 (1.24)												
26.5 (1.04)			100									
22.4 (0.88)												
20 (0.79)					-							
19 (0.75)		100	95	±6	*100*	0	100		100		100	
16 (0.63)												
14 (0.55)					0	0						
13.2 (0.52)	100	95	55	±6	*90*	*100*						
12.5 (0.49)					-	-	80	100	80	100	95	100
11.2 (0.44)												
10 (0.39)					-	-						
9.5 (0.37)	90	50	30	±6	*25*	*65*	35	60	35	60	50	80
8 (0.31)					-	-						
6.7 (0.26)	40	27	20	±6								
6.3(0.25)					-	-						
5.6 (0.22)												
5 (0.20)					-	-						
4.75 (0.19)	20	11	10	±5	*10*	*15*	10	25	1	20	0	8
4 (0.16)					-	-						
2.36 (0.09)	12	9	8	±5	*8*	*15*	5	10	1	10	0	4
2 (0.08)					-	-						
1.18 (0.05)	8	8	6	±5								
1 (0.04)												
0.6 (0.024)	6	6.5	4	±5								
0.5 (0.02)					-	-						
0.25 (0.01)	5	5.5	3	±3								
0.15 (0.006)	4	4.5	3	±3								
0.075 (0.003)	3.5	3.5	2	±1	*2*	*8*	2	4	1	4	0	4
0.063 (0.002)					-	-						
Aggregate properties	Type I		Type II									
Los Angeles abrasion, %					*<21*		< 30		<30[f]			
Flakiness index, %					*<25*		<5 (5:1), <20% (3:1)		<10 (5:1)			
Sand equivalent, %					*>45*		-		-			
Fine aggregate Angularity					-		>45		-			
Crushed faces (2 faces), %					*100 (high traffic), 90 (low traffic)*		>90, one face: 100		>95			
Binder												
Asphalt binder grade												
Binder modifiers	Unmodified binders		PMB (SBS, SBR, EVA, crumb-rubber modified [CRM]), fibers (0.3% to 0.5%), hydrated lime		*Asphalt rubber-polymer modified*		PMB, cellulose (0.3%) or mineral fiber (0.4%)		PG 76 XX (PMB), lime (1% to 2%), and cellulose or mineral fibers (0.2% to 0.5%)		Type I or II asphalt rubber	
Binder content, %	OG 10: 4.5 to 5.5; OG 14: 4 to 5; OG 20: 3.5 to 4.5		OG 10: 5.5 to 6.5; OG 14: 5 to 6; OG 20: 4.5 to 5.5		*4.5 min.*				6 to 7		8 to 10	
Specimens compaction	AGC / 80 cycles				*Marshall 50 blows*		SGC/50 cycles		SGC/50 cycles			
Mixture properties												
Air voids content, %	>20		20-25		*>22: high volume, 18-22: low volume*		>18[h]		18-22			
Draindown test, %	<0.3[g]		<0.3[g]				<0.3		<0.2[g]			
Cantabro test, unconditioned (dry), %	<25		<20		*<25 (25°C)*		-		-			
Cantabro test, moisture Conditioned, %	<35		<30		*<30 (25°C)*		-		-			
Cantabro test, aged, %	-		-		*<30 (25°C)*		-		-			
Retained tensile strength Ratio, %	-		-		-		>80		-			
Permeability	-		-		-		Optional		-			

[g] Only the air voids content evaluation is used to define the maximum binder content.
[h] 18% when the dimensional method is used. 16% when the CoreLok® method (recommended) is applied.
[f] Deleterious material (<1%), decantation (<1.5%), and magnesium sulfate soundness (5 cycles) (<20%) are also required.
[f] Boil test is also required.

APPENDIX E: HYDRAULIC CONDUCTIVITY MODEL PARAMETERS

Plain Cores

Table 15 - Plain Cores - Darcy's linear Model

Darcy's Law -Hydraulic Conductivity - 95% Confidence Interval						
	Initial		Top		Upside Down	
Core	Min	Max	Min	Max	Min	Max
1A			0.21	0.27	0.2	0.24
1B	1.88	2.22				
2A			0.57	0.7	0.49	0.6
2B			0.33	0.47	0.51	0.68
3B			0.3	0.37	0.08	0.09
3C			0.45	0.58	0.41	0.52

Table 16 - Forchheimer Model Parameters

	Initial				
Core	K (cm/s)	alpha	beta	Deviation (cm)	Min. Deviation (%)
1A					
1B	2.63	0.477	0.0028	0.1253	11.1
2A					
2B					
3B					
3C					

	Top				
Core	K (cm/s)	alpha	beta	Deviation (cm)	Min. Deviation (%)
1A	0.19	0.7	0.0143	0.663	2.83
1B					
2A	0.7	0.19	0.0093	3.22	44
2B	0.32	0.403	0.015	6.26	5.2
3B	0.49	0.296	0.039	3.66	15.1
3C	0.49	0.286	0.014	4.99	6.9

	Upside Down				
Core	K (cm/s)	alpha	beta	Deviation (cm)	Min. Deviation (%)
1A	0.18	0.733	0.012	7.83	2
1B					
2A	0.58	0.229	0.009	3.46	11
2B	0.64	0.204	0.015	4.42	15.5
3B	0.1	1.437	0.023	7.128	2
3C	0.48	0.29	0.021	4.37	10

Drilled Cores

Table 17 - Drilled Cores - Darcy's linear Model

Darcy's Law -Hydraulic Conductivity - 95% Confidence Interval				
	Initial		Cleaned	
Core	Min	Max	Min	Max
1A	0.16	0.18	0.89	1.17
1B	0.94	1.28	1.52	1.88
2A	0.83	0.93	1.76	2.21
2B	0.34	0.39	2.68	3.53
3B	0.16	0.18	0.67	0.83
3C	0.19	0.21	0.81	0.88

Table 18 - Drilled Cores - Forchheimer Model Parameters

	Initial				
Core	K (cm/s)	alpha	beta	Deviation (cm)	Min. Deviation (%)
1A	0.21	0.409	0.016	2.61	9
1B	1.13	0.058	0.005	2.88	19
2A	0.86	0.099	0.005	2.39	12
2B	0.38	0.214	0.002	2.73	2
3B	0.19	0.559	0.012	1.92	4
3C	0.23	0.415	0.011	2.12	5

	Cleaned				
Core	K (cm/s)	alpha	beta	Deviation (cm)	Min. Deviation (%)
1A	1.26	0.068	0.006	2.41	18
1B	1.72	0.038	0.0015	1.05	9
2A	2.11	0.041	0.002	1.18	9
2B	2.73	0.03	0.0011	0.82	8
3B	1.08	0.098	0.009	0.95	25
3C	0.97	0.099	0.0035	1.46	10

APPENDIX F: HEAD GRADIENT VERSUS FLOWRATE CURVES

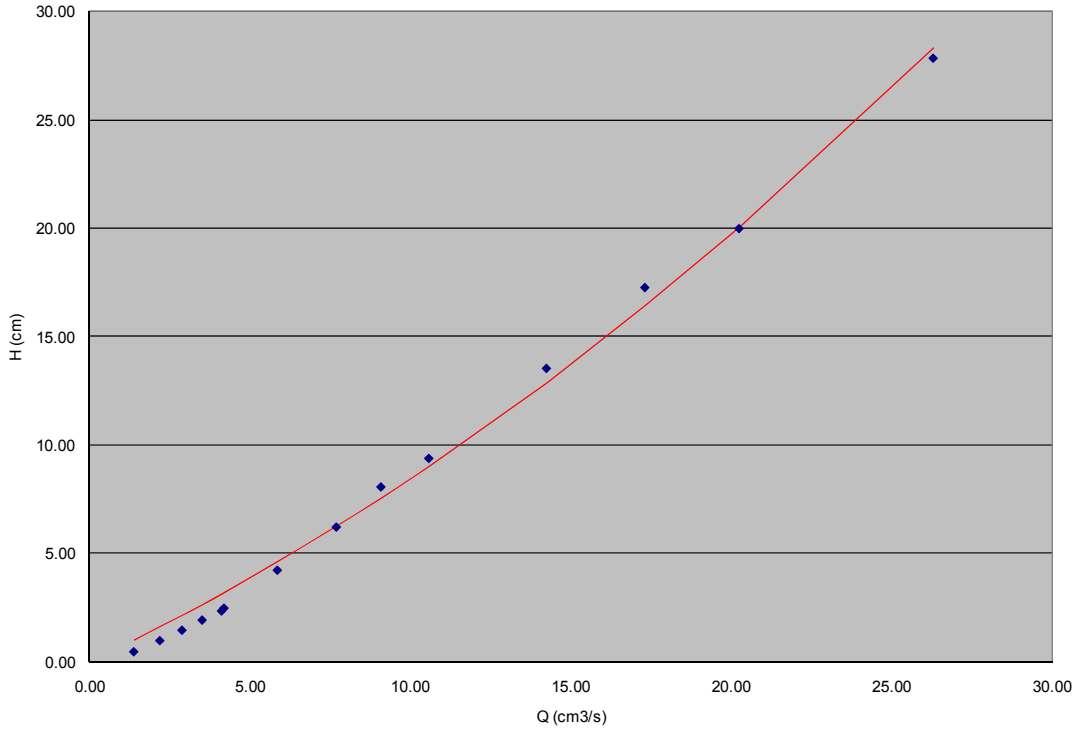

Figure 57 - Head Gradient vs. Flowrate - 1A Top

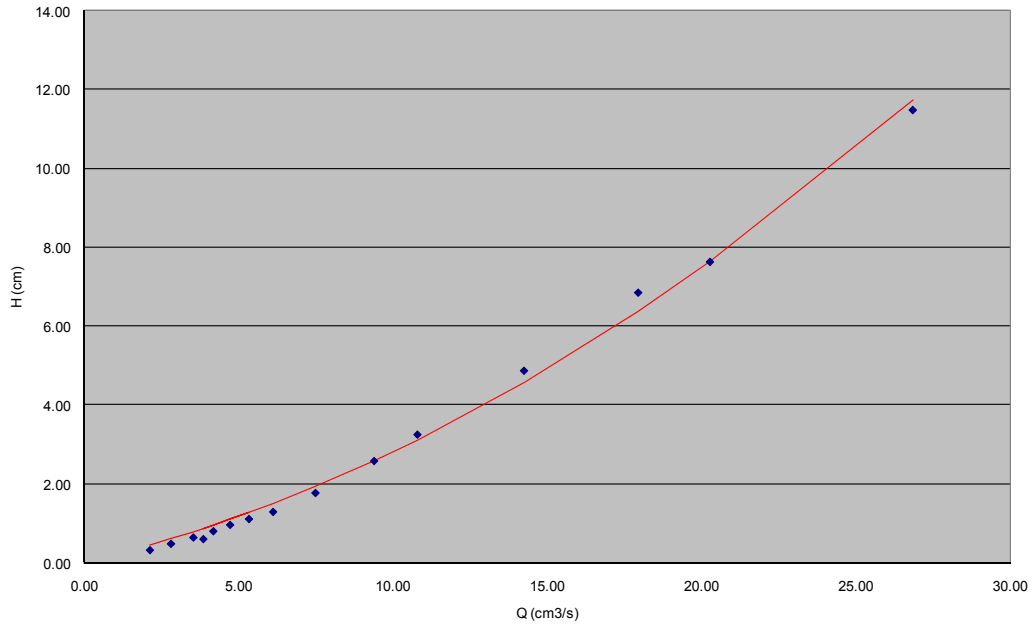

Figure 58 - Head Gradient vs. Flowrate - 2A Top

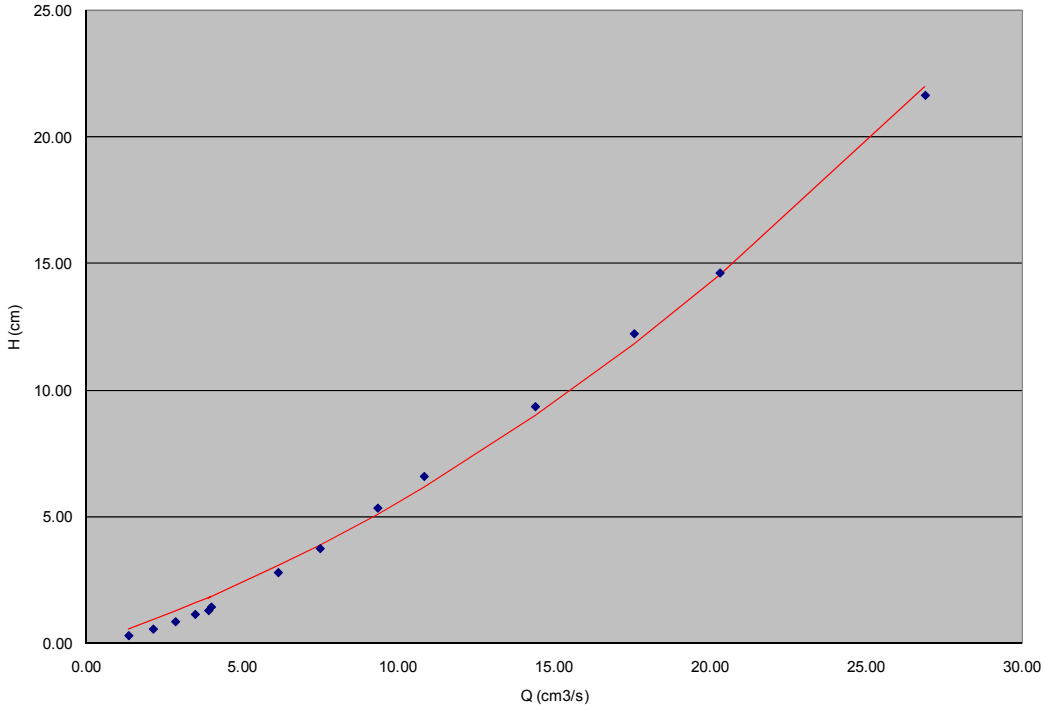

Figure 59 - Head Gradient vs. Flowrate - 2B Top

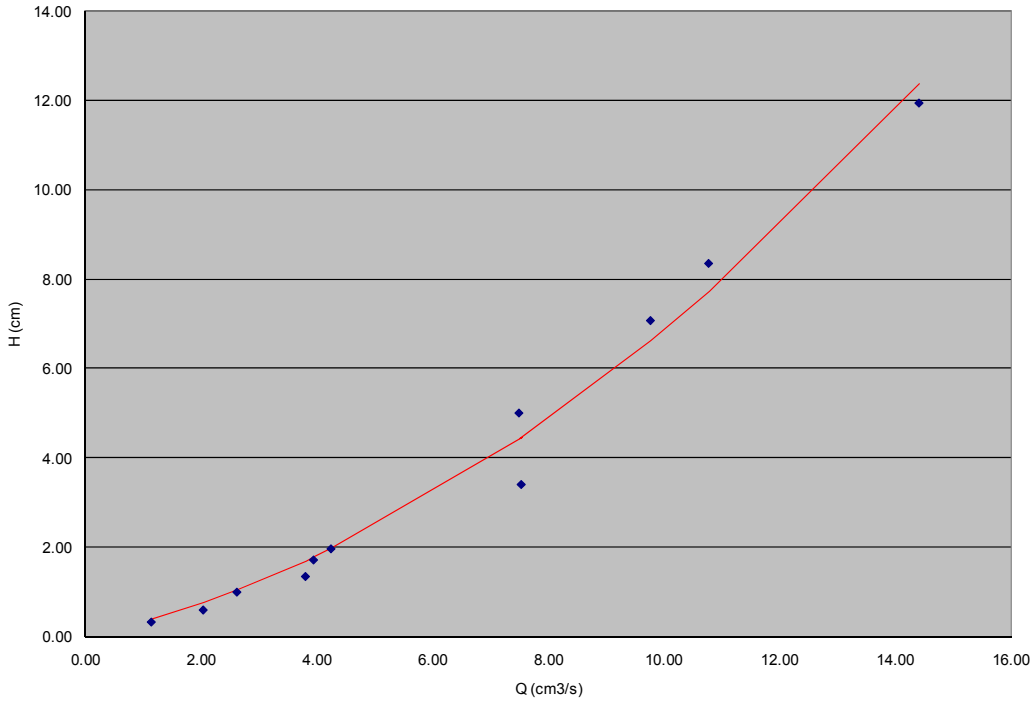

Figure 60 - Head Gradient vs. Flowrate - 3B Top

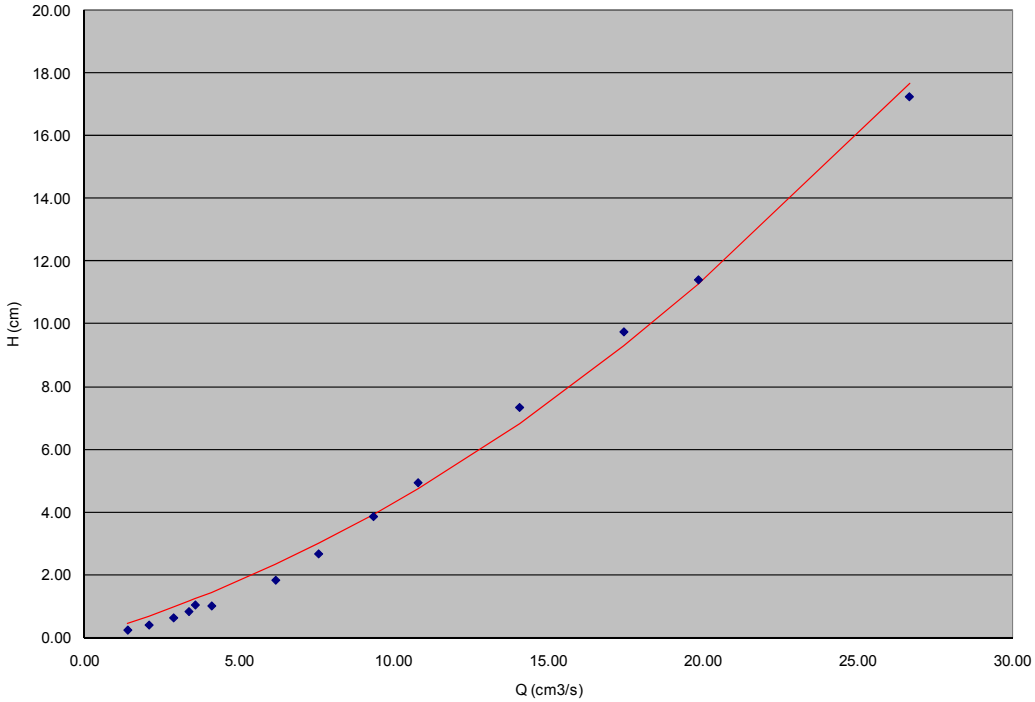

Figure 61 - Head Gradient vs. Flowrate - 3C Top

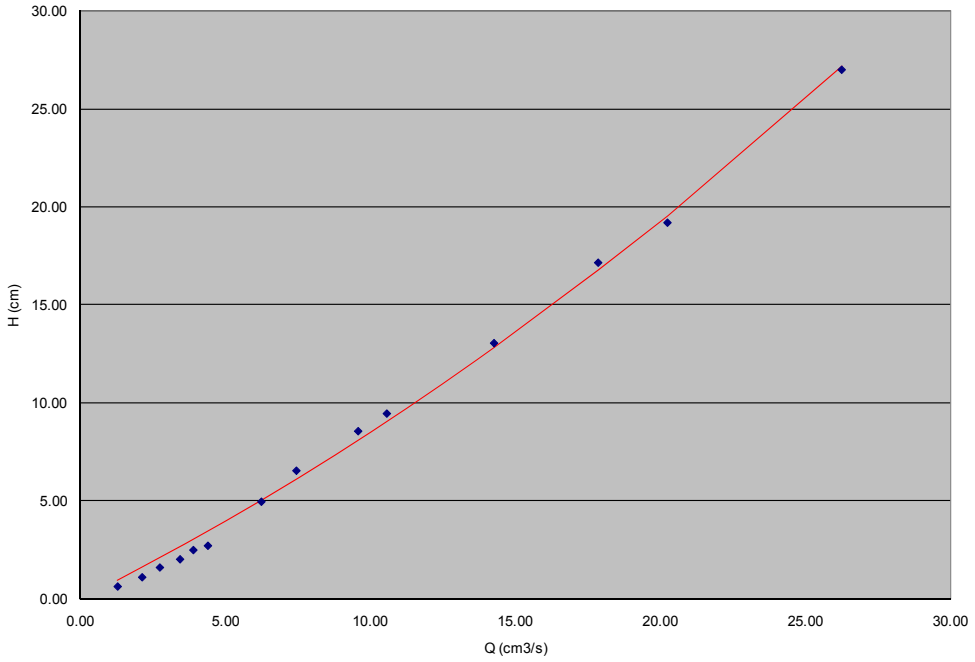

Figure 62 - Head Gradient vs. Flowrate - 1A Upside Down

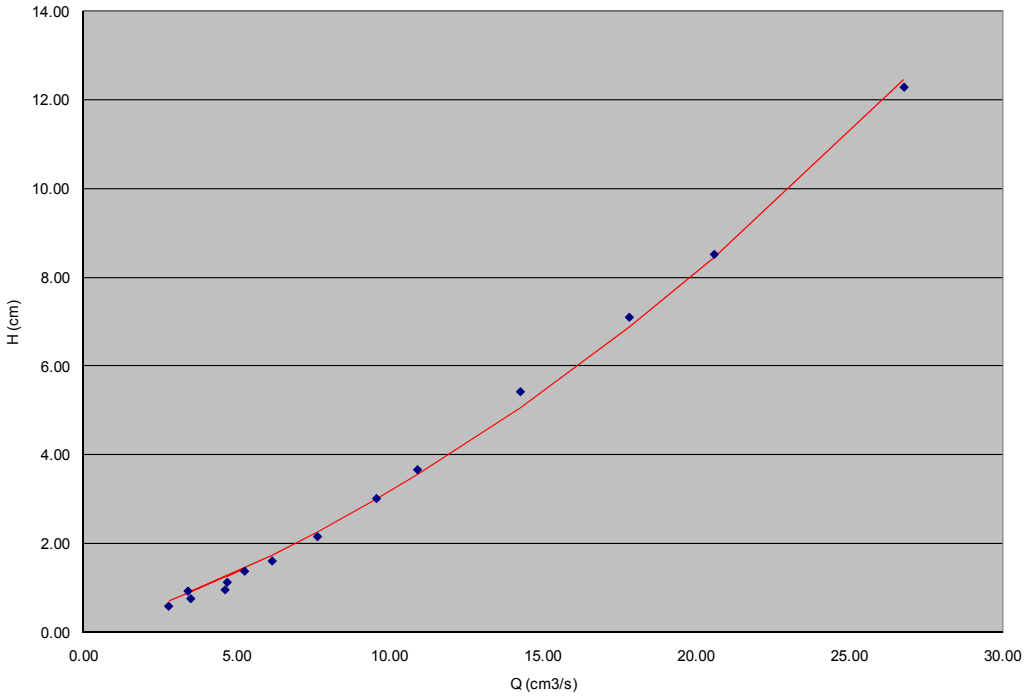

Figure 63 - Head Gradient vs. Flowrate - 2A Upside Down

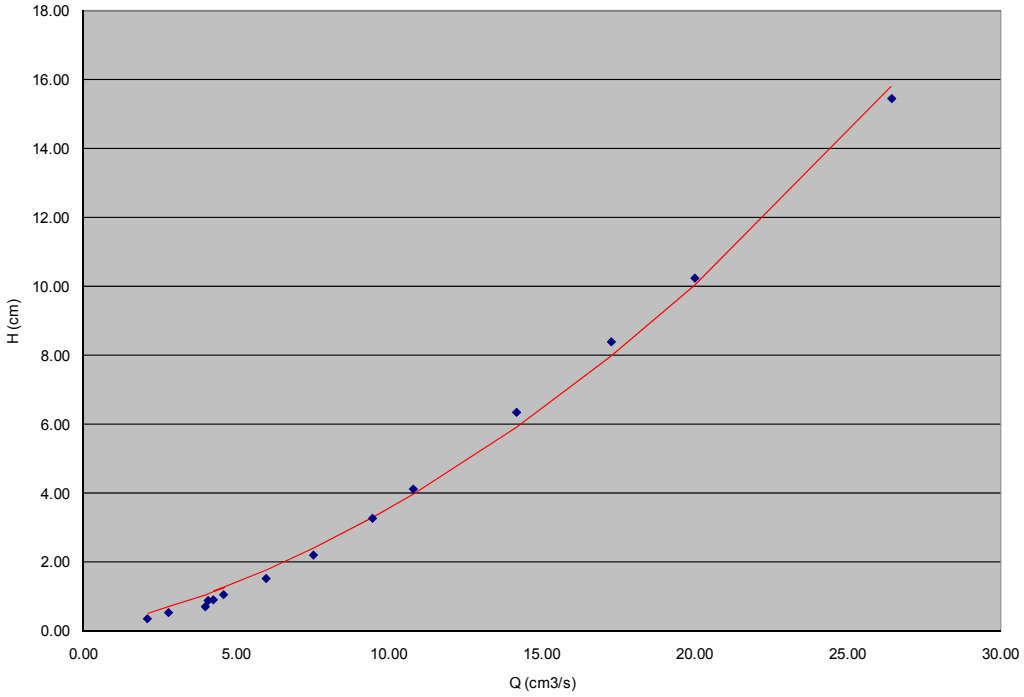

Figure 64 - Head Gradient vs. Flowrate - 2B Upside Down

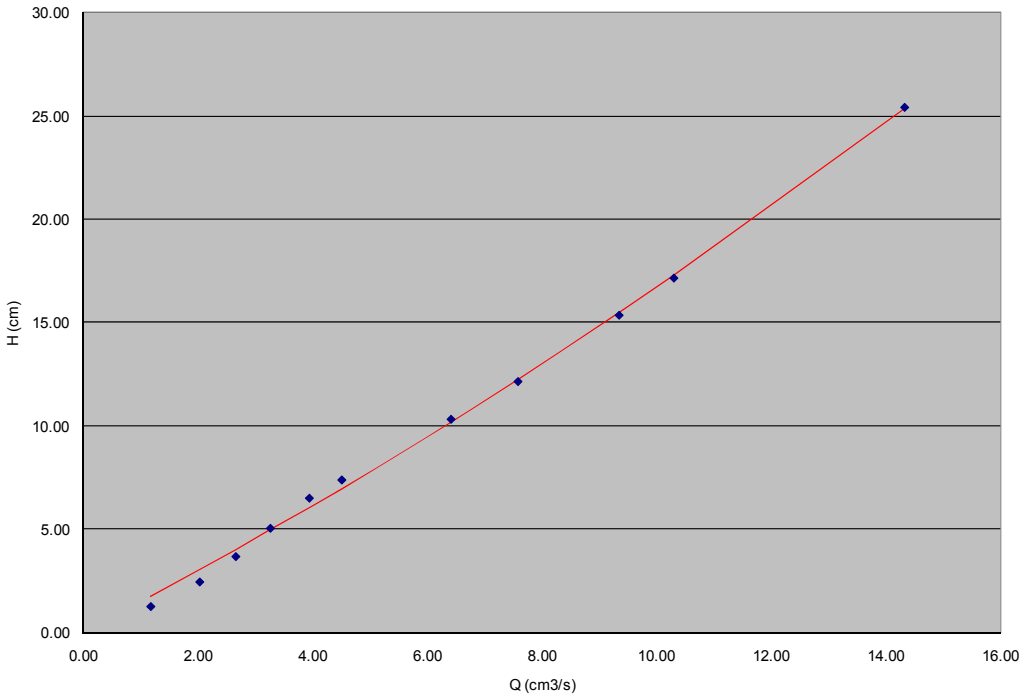

Figure 65 - Head Gradient vs. Flowrate - 3B Upside Down

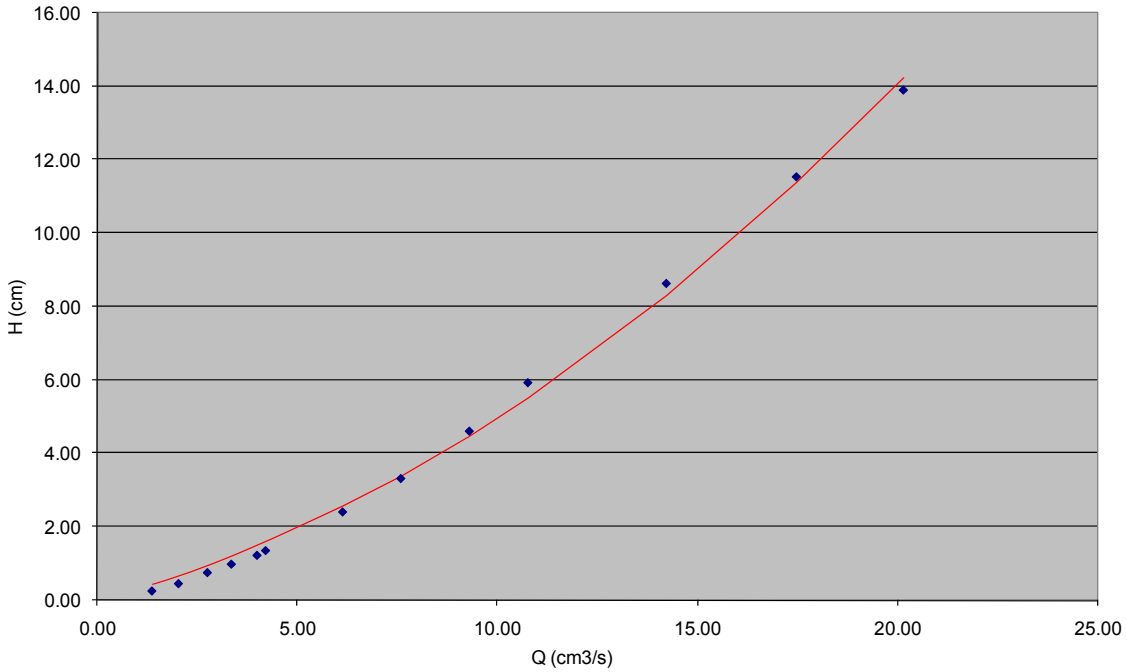

Figure 66 - Head Gradient vs. Flowrate - 3C Upside Down

REFERENCES

Alvarez, A., and Button, W. (2006). Synthesis of current practice on the design, construction, and maintenance of porous friction course, Texas Transportation Institute, pp. 28.

Bäckström, M., and Bergström, A. (2000) Draining function of porous asphalt during snowmelt and temporary freezing. Canadian Journal of Civil Engineering, Vol. 27, pp. 594-598.

Bear, Jacob (1972). Dynamics of Fluids in Porous Media, Dover editions, pp 125-171.

Bendtsen, H., Nielsen, C., Raaberg, J and Macdonald, R. (2002) Report 120: Clogging of porous bituminous surfacing – an investigation in Copenhagen. Road Directorate, Danish Road Institute.

Birgisson, B., Roque, R., Varadhan, A., Thai, T. and Lokendra, J. (2006) Evaluation of thick open graded and bonded friction courses for Florida. University of Florida.

California Department of Transportation (Caltrans) (2003) Fog Seal Guidelines.

Carslaw, H.S. and Jaeger, J.C. (1959). Conduction of Heat in Solids, Oxford University Ed., pp 214-231.

Charbeneau, R. (2000). Groundwater Hydraulics and Pollutant Transport, Waveland Press Editions, pp. 12-104.

Charbeneau, R. (2006). Analysis of CRWR PFC Testing Apparatus.

Di Benedetto, H., Jouni, M., Boillon, P. and Salhi, J. (1996) In situ and laboratory measurements of flows in porous bituminous concrete: modeling and validation, Bulletin des Laboratoires des Ponts et Chaussees, Vol 204.

Fair, G.H. and Hatch, L.P. (1933) Fundamentals Factors Governing the Streamline Flow of Water through Sand, Journal of American Water Works Association, Vol 25, pp. 1551-1565

Federal Highway Administration (FHWA) (2005) Quiet Pavement Systems in Europe, United States Department of Transportation, Federal Highway Administration, http://international.fhwa.dot.gov/quiet_pav/chapter_two_f.htm

Federal Highway Administration (FHWA) (2004) Tidal Hydrology, Hydraulics, and Scour at Bridges, Hydraulic Engineering Circular N°25, Appendix A, http://www.fhwa.dot.gov/engineering/hydraulics/hydrology/hec25appa.cfm

Forchheimer, P. (1901) Wasserbewegung dur Bodem, Z. Ver. Deutsch, Ing., Vol. 45, pp. 1782-1788.

Fwa, T., S. Tan, and Guwe, Y. (1999) Laboratory Evaluation of Clogging Potential of Porous Asphalt Mixtures. Transportation Research Record: Journal of the Transportation Research Board, No. 1681, TRB, National Research Council, Washington, D.C., pp. 43-49.

Graff, J. (2006) Asphalt Pavement Preservation, Lone Star Roads Magazine, Issue 1.

Isenring, T., Koster, H. and Scazziga, I. (1990) Experiences with Porous Asphalt in Switzerland. Transportation Research Record: Journal of the Transportation Research Board, No. 1265, TRB, National Research Council, Washington, D.C., pp. 41-53.

Kandhal, P. and Mallick, R. (1999) Design of New-Generation Open-Graded Friction Courses. NCAT Report No. 99-3.

Moore, L., Hicks, R. and Rogge, D. (2001) Design, Construction, and Maintenance Guidelines for Porous Asphalt Pavements. Transportation Research Record: Journal of the Transportation Research Board, No. 1778, TRB, National Research Council, Washington, D.C., pp. 91-99.

National Cooperative Highway Research program (NCHRP) (2000) Synthesis of Highway Practice 284: Performance Survey on Open-Graded Friction Course Mixes. Transportation Research Board, National Research Council, Washington, D.C.

Newcomb, D., and Scofield, L. (2004) Quiet Pavements Raise the Roof in Europe. Hot Mix Asphalt Technology, September-October, pp. 22-28.

http://www.quietpavement.com/hotmixasphalt/docs/Quiet_Pavements_Raise_the_Roof_in_Europe.pdf

Nutting, P.G. (1930). Physical analysis of oil sands, Bulletin of American Association in Petroleum and Geology, Vol. 14, pp. 1337-1349.

Pacific Water Resources, Inc. (2004) Cross Israel Highway Stormwater Quality Study Phase II Monitoring Report.

Pagotto, C., M. Legret and Le Cloirec, P. (2000) Comparison of the Hydraulic Behaviour and the Quality of Highway Runoff Water According to the Type of Pavement. *Water Resources*, Vol. 34, No. 18, pp. 4446-4454.

Public Works Reseach Institute (PWRI) (2005) Noise Reducing Pavement in Japan, Technical Note 31, Presentation on Function recovery and maintenance of porous pavements in Japan.
http://www.vejdirektoratet.dk/publikationer/VInot031/html/chapter06.htm

Regimand A. and Lawrence, J. (2004) Systems and methods for determining the porosity and/or effective air void content of compacted material, United States Patent 6684684.

Ruiz, A., Alberola, R., Pérez, F., and Sánchez, B. (1990) Porous Asphalt Mixtures in Spain. Transportation Research Record: Journal of the Transportation Research Board, No. 1265, TRB, National Research Council, Washington, D.C., pp. 87-94.

Rumer R.R. and Drinker P.A. (1966) Resistance to laminar flow through porous media. Journal of Hydraulic Division, American Society of Civil Engineers, V92, HY5, pp. 155-163.

Shao, J., Lister, P. and McDonald, A. (1994) A surface-temperature prediction model for porous asphalt pavement and its validation. Meteorological Applications, pp. 129-134.

Stotz, G. and Krauth, K. (1994) The pollution of effluents from pervious pavements of an experimental highway section: first results. The Science of the Total Environment, Vol. 146/147, pp. 465-470.

Terzaghi Karl, Peck Ralph B. and Mesri Gholanreza (1996). Soil Mechanics in Engineering Practice, Wiley-Interscience editions, pp. 78-80.

Texas Department of Transportation (2005), Capital Area Metropolitan Planning, Traffic Count. http://www.campotexas.org/programs_rd_traffic_counts.php

Van der Zwan, J., Goeman, T., Gruis, H., Swart, J. and Oldenburger, R. (1990) Porous Asphalt Wearing Courses in the Netherlands: State of the Art Review, Transportation Research Record: Journal of the Transportation Research Board, No. 1265, TRB, National Research Council, Washington D. C., pp.95-110.

Van Leest et al. 1997. Guidelines for determining the cleaning effect on porous asphalt. In the European Conference on Porous Asphalt; Proceedings, Madrid, 1997.

Van Heystraten, G., and Moraux, C. (1990) Ten Years' Experience of Porous Asphalt in Belgium. Transportation Research Record: Journal of the Transportation Research Board, No. 1265, TRB, National Research Council, Washington, D.C., pp. 34-40.

Venkataraman, P. and Rama, P. (1998). Darcian, Transitional, and Turbulent Flow Through Porous Media, American Society of Civil Engineers, Journal of Hydraulic Engineering, Vol. 125, pp. 63-71.

Ward, J. (1964) Turbulent flow in porous media. Journal of Hydraulic Division, V90, HY5, pp. 1-12.

Watson, D., Johnson, A., and Jared, D. (1998) Georgia Department of Transportation's Progress in Open-Graded Friction Course Development. Transportation Research Record: Journal of the Transportation Research Board, No. 1616, TRB, National Research Council, Washington, D.C., pp. 30-33.

Yildirim, Y., Dossey, T, Fults, K, and Trevino, M. (2006) Winter Maintenance Issues Associated with New Generation Open-Graded Friction Courses. Center for Transportation Research Technical Report 0-4834-1, The University of Texas at Austin.